

**NUMERICAL INVESTIGATIONS OF CONJUGATE POROUS
MEDIA: ON THE PERFORMANCE OF MINE VENTILATION AND
GEOHERMAL HEAT EXCHANGERS**

Putra Hanif Agson Gani

Department of Mining and Materials Engineering

McGill University, Montreal

August 2021

A THESIS SUBMITTED TO MCGILL UNIVERSITY IN PARTIAL
FULFILLMENT OF THE REQUIREMENTS OF THE DEGREE OF
MASTER OF ENGINEERING

©Putra Hanif Agson Gani 2021

Acknowledgements

First and foremost, I would like to express my sincere gratitude to my supervisor Prof. Agus P Sasmito, for the continuous support, encouragement, support, and guidance for the past two years. Thank you for your tolerance and patience when dealing with me and my frequent mistakes, while also keeps inspire me to improve as academia as well as a person. To my co-supervisor Prof. Ferri Hassani, thank you for your endless support and your constructive comments throughout this project. Your wisdom would not be forgotten and I have been truly fortunate.

To my colleagues, at Mine Multiphysics Lab, Ahmad Zueter and Dr. Leyla Amiri, who patiently mentor me and shares their knowledge in every discussion. Thank you for all those countless hours of meeting over the teams. Minghan Xu, who has always made himself available and only one call away for a discussion. I am going to miss our collaborative works in research and also in coursework. To Ika Rahayu and Abdurrasyid, who is, in particular, help me a lot during my remote working phase. And to all my colleagues, past and present, I am grateful to have the chance to meet you all.

To all my friends whom I met along the way, friends in McGill University, and my Indonesian friends and families, I am truly grateful to meet you during my journey as an international student, and thank you for being there for me.

I would also like to thank Indonesia Endowment Fund for Education (LPDP) for providing me with the financial support to finish my study. It is a privilege to be given such a chance and I will definitely aim to pay it forward.

Finally, for my parents and sister, thank you for the endless support and prayer. And last but not least to my wife, Atika Safitri, for her patience, support, affection that make this long-distance relationship, dealing with lockdown, and writing the thesis somehow bearable and surprisingly enjoyable. All the best for us.

Abstract

Predicting the conjugate heat transfer and fluid flow behavior in porous media is still a challenging research area in many applications due to the complex nature of the flow. This thesis is divided into three topics. The first two topics focus on the numerical modeling of conjugate porous media in the mine ventilation network and geothermal heat exchanger settings. The third topic solves the expensive computational cost of the previous topics by developing a reduced-order semi conjugate heat transfer model for a double-pipe heat exchanger.

In the first part of the thesis, conjugate porous media in mine ventilation network is discussed. The porous media is formed as a broken rock structure which is created due to the mining operations (e.g., blasting and hauling). In this thesis, a novel friction factor correlation which describes the effect of porous zone in the model is integrated into the mine ventilation network software which solves a one-dimensional model. The correlation accuracy is verified with three-dimensional computational fluid dynamic models.

In the second part of the thesis, conjugate porous media is applied to enhance the heat transfer performance of the closed-loop double-pipe geothermal heat exchanger. The porous zone was created at the bottom of the well with the hydraulic fracturing process, and fractal theory is implemented to emulate the tree-like porous structure. The results suggest that this novel geothermal heat exchanger design improves the heat extraction rate by 90%, which indicates the potential of the implementation of this design.

Both conjugate porous media applications in mine ventilation networks and geothermal heat exchangers are numerically investigated based on conservation equations of

mass, momentum, and energy in a three-dimensional (3D) model and two-dimensional (2D) axisymmetric model, respectively. However, numerical modeling of these systems could be computationally expensive due to its typical large domains and long operational time. Therefore, in the third part of the thesis, a novel computationally efficient one-plus-one-dimensional (1+1D) semi-conjugate heat transfer model is proposed. The proposed model solves the transient conservation equation of energy in radial coordinate coupled with the space marching algorithm to save computational time and cost. Lastly, thermal superposition theory is also implemented to expand the single borehole model into double boreholes and 3-by-3 boreholes.

Abrégé

L'action de prédire le transfert thermique conjugué et le comportement d'écoulement de fluide dans des milieux poreux est encore un domaine de recherche difficile dans plusieurs applications à cause du caractère complexe de l'écoulement. Cette thèse est donc divisée en trois sujets. Les deux premiers porteront sur la modélisation numérique de milieux poreux conjugués dans un réseau de ventilation de la mine et dans un domaine d'échangeur de chaleur géothermique. Le troisième sujet résoudra le coût énorme des calculs de deux sujets précédents en développant des modèles approximatifs du transfert thermique demi-conjugué aux tuyaux doubles.

Dans la première partie de cette thèse, on discutera les milieux poreux conjugués dans un réseau de ventilation de la mine. Le milieu poreux est formé de la destruction d'une structure rocheuse qui a été créée par l'exploitation minière (ex : le dynamitage et le creusement). Au cours de cette thèse, une corrélation du coefficient de frottement nouvelle, qui décrit l'effet de la zone poreuse dans le modèle, est intégrée dans le logiciel du réseau de ventilation de la mine et ceci résout le modèle à une dimension. La précision de la corrélation est vérifiée avec la modélisation de la dynamique des fluides computationnelles à trois dimensions.

Dans la deuxième partie, des milieux poreux conjugués est appliqués pour optimiser la performance du transfert thermique de l'échangeur de chaleur géothermique aux tuyaux doubles et circuit fermé. La zone poreuse est créée au fond du puits avec la méthode de la fracturation hydraulique, et la théorie fractale est appliquée pour imiter la structure poreuse et arborescente. Les résultats indiquent que la conception de ce nouveau modèle

de l'échangeur de chaleur géothermique améliore le taux de l'extraction de chaleur par 90%. Ceux-ci dénotent le potentiel de la réalisation de cette conception.

Les deux applications de milieux poreux conjugués, dans le contexte d'un réseau de ventilation de la mine et d'échangeur de chaleur géothermique, sont évalués numériquement basés sur l'équation de la conservation de masse, de la quantité de mouvement, et de l'énergie dans un modèle de trois dimensions et un modèle axisymétrique de deux dimensions, respectivement. Par contre, la modélisation numérique de ces systèmes peut être coûteuse en ressources informatiques à cause de leurs larges domaines et de longues durées opérationnelles. Donc, dans la troisième partie de cette thèse, on a proposé un nouveau modèle de transfert thermique demi-conjugué et 1+1D qui est efficace sur le plan des calculs. Ce modèle proposé résout l'équation de la conservation de l'énergie transitoire dans la coordonnée radiale, ainsi qu'avec l'algorithme de marches-espaces et en utilisant une correction thermique dans le sens axial, pour réduire le coût et temps de calcul. Pour finir, la théorie de la superposition thermique a été aussi appliquée pour élargir le modèle de forage seul à un forage double et 3-par-3.

Contribution of Authors

Putra Hanif Agson Gani, as the principal author of this work, performed all numerical works, data analysis and completed the manuscripts. This thesis also made possible with the contribution of fellow co-authors. Dr. Leyla Amiri (Université de Sherbrooke) defined the concept, involved in the data analysis and provided scientific guidance throughout the article in Chapter 3. Ahmad F. Zueter and Minghan Xu (McGill University) helped extensively with the numerical and analytical works in Chapter 4 and 5. Prof. Ferri Hasani (McGill University), Dr. Jundika Kurnia (Universiti Teknologi PETRONAS), Prof. Ali Madiseh (University of British Columbia), and Prof. Sebastian Poncet (Université de Sherbrooke) were involved in defining the concept in the mine ventilation project (Chapter 3) or the geothermal heat exchanger project (Chapter 4 and 5). Finally, my supervisor Prof. Agus Sasmito who guided me throughout the entirety of my program in McGill University.

Table of Contents

| | |
|---|----------|
| Acknowledgements | i |
| Abstract | iii |
| Abrégé | v |
| Contribution of Authors | vii |
| List of Figures | xiii |
| List of Tables | xiv |
| 1 Introduction | 1 |
| 1.1 Background and motivation | 2 |
| 1.2 Objectives | 2 |
| 1.3 Thesis outline | 3 |
| 2 Literature Review | 4 |
| 2.1 Introduction | 5 |
| 2.2 Numerical methods of heat transfer and fluid flow | 5 |
| 2.2.1 Generalized governing equations | 5 |
| 2.2.2 Reduced-order modeling in geothermal heat exchanger system | 6 |
| 2.2.3 Single borehole solution: Development of 1+1D model using a space marching algorithm | 8 |
| 2.3 Heat transfer and fluid flow in conjugate porous media | 10 |
| 2.3.1 Governing equations | 11 |
| 2.3.2 Applications of conjugate porous media in engineering practices | 14 |

| | | |
|----------|---|-----------|
| 3 | Integration of Conjugate Porous Media Model into Mine Ventilation Network | |
| | Software | 19 |
| 3.1 | Introduction | 21 |
| 3.2 | Model Description | 25 |
| 3.2.1 | Analytical solutions | 25 |
| 3.2.2 | Initial and boundary Conditions | 30 |
| 3.2.3 | Model development | 30 |
| 3.3 | Results and Discussion | 31 |
| 3.3.1 | Verification between Ansys Fluent and Ventsim results | 31 |
| 3.3.2 | Analysis of the air leakage and the pressure drop | 33 |
| 3.3.3 | Sensitivity analyses | 34 |
| 3.3.4 | Analysis of the computational time | 35 |
| 3.4 | Conclusion | 35 |
| 4 | Thermal and Hydraulic Analysis of a Novel Double-Pipe Geothermal Heat Exchanger with a Controlled Fractured Zone at the Bottom of the Well | 41 |
| 4.1 | Introduction | 43 |
| 4.2 | Model Description | 47 |
| 4.2.1 | Governing equations | 50 |
| 4.2.2 | Initial and boundary conditions | 55 |
| 4.2.3 | Numerical simulations | 58 |
| 4.3 | Results and Discussion | 58 |
| 4.3.1 | Model validation | 58 |
| 4.3.2 | Comparison of the closed-loop heat exchanger and the semi closed-loop heat exchanger | 60 |
| 4.3.3 | Influence of the physical and geometrical properties of the controlled fractured zone | 62 |
| 4.4 | Conclusion | 64 |

| | | |
|----------|--|-----------|
| 5 | Development of a 1+1D Reduced-Order Model in Double-Pipe Geothermal Heat Exchanger Systems: From Single to Multiple Boreholes | 73 |
| 5.1 | Introduction | 75 |
| 5.2 | Model Description | 78 |
| 5.2.1 | Governing equations | 80 |
| 5.2.2 | Initial and boundary conditions | 81 |
| 5.3 | Solution Algorithms | 82 |
| 5.3.1 | Single borehole solution: Development of 1+1D model using space marching algorithm | 82 |
| 5.3.2 | Multiple boreholes solution: Incorporating the use of symmetry with thermal superpositions algorithm | 85 |
| 5.3.3 | Three-dimensional numerical simulations | 86 |
| 5.4 | Results and Discussion | 87 |
| 5.4.1 | Development of Reduced-Order Model of GHE | 87 |
| 5.4.2 | Thermal analysis on the 1+1D models | 89 |
| 5.5 | Conclusion | 90 |
| 6 | Concluding Remarks | 98 |
| 6.1 | Final conclusion | 99 |
| 6.2 | Recommendations for future work | 100 |

List of Figures

| | | |
|-----|--|----|
| 2.1 | Computational domain of the 1+1D model of the DPGHE | 9 |
| 3.1 | Illustration of the haulage drift with a broken rocks-filled drawpoint as a simulated model: (a) schematic; (b) Ansys Fluent; and (c) Ventsim models. . | 26 |
| 3.2 | Flowchart for the integration of the Ansys Fluent and Ventsim to model the flow through porous media. | 27 |
| 3.3 | The airflow quantity values which seeped through the porous zone in the drawpoint Q_{leak} within different range of broken rock diameter d_p : (a) 0.04 m; (b) 0.1 m; (c) 0.3 m; and (d) 0.55 m [29]. | 32 |
| 3.4 | Flowchart for the integration of the Ansys Fluent and Ventsim to model the flow through porous media [29]. | 33 |
| 3.5 | Sensitivity analyses based on different operating conditions: height of the drawpoint h_1 , airflow rate Q_{in} gap between the duct inlet and drawpoint l_1 , and the porosity ε | 35 |
| 4.1 | Not-to-scale side view illustrations of: (a) closed-loop DPGHE; (b) semi closed-loop model DPGHE. | 48 |
| 4.2 | Not-to-scale semi closed loop DPGHE: (a) computational domain (rotated 90°); (b) A-A cross-cut; (c) isometric view. | 49 |
| 4.3 | Temperature dependent thermophysical properties of the water: (a) density; (b) thermal conductivity (data from [42]). | 50 |

| | | |
|-----|---|----|
| 4.4 | Temperature contour of semi closed-loop DPGHE at: (a) initial contion (Day 0); (b) transition phase (Day 1); (c) steady phase (Year 5). | 56 |
| 4.5 | Validation of the numerical model against the experimental measurement [3, 4]: (a) temperature difference between inlet and outlet; (b) pressure drop; (c) thermal power. | 59 |
| 4.6 | Comparison of the closed-loop heat exchanger and the proposed semi closed-loop heat exchanger, in terms of: (a) temperature difference between inlet and outlet; (b) pressure drop; (c) thermal power and pumping power. | 61 |
| 4.7 | Comparison of thermal power and pumping power based on the parametric analysis of semi-closed loop heat exchanger varying the geometrical and physical properties of the fractured zone based on the: (a) length of h_1 ; (b) length of h_2 ; (c) length of r_1 ; (d) damage. | 65 |
| 4.8 | The effect of contact area between the fractured zone and the ground ($A_{contact}$) to: (a) ΔT and the thermal power; and (b) ΔP and the pumping power. | 66 |
| 5.1 | Side view and top view of (not-to-scale) GHE with the following configurations: (a) a single borehole; (B) double boreholes; (C) 3-by-3 boreholes. | 79 |
| 5.2 | Flowchart of the development of the 1+1D semi-conjugate model, coupled with the thermal superpositions algorithm. | 83 |
| 5.3 | Computational domain of the 1+1D model of the DPGHE | 84 |
| 5.4 | Validation of the outlet temperature value of the single borehole solution (MATLAB) with the field data [3], and the 3D model (ANSYS Fluent) | 88 |
| 5.5 | Comparison of the outlet temperature at Year 1 as a dependency analysis of: (a) mesh count; and (b) the side boundary length. | 89 |
| 5.6 | Temperature profile of the single borehole solutions at: (a) 1 day; (b) 1 week; (c) 1 month; (d) 6 months; and (e) 1 year. | 92 |
| 5.7 | Temperature profile of the double boreholes solutions at: (a) 1 day; (b) 1 week; (c) 1 month; (d) 6 months; and (e) 1 year. | 93 |

5.8 Temperature profile of the 3-by-3 boreholes solutions at: (a) 1 day; (b) 1 week; (c) 1 month; (d) 6 months; and (e) 1 year. 94

List of Tables

| | | |
|-----|---|----|
| 3.1 | The twenty scenarios of the study based on the porosity ε and the diameters d_p of the broken rocks-filled drawpoint. | 31 |
| 4.1 | Thermophysical properties of the materials used in DPGHE. | 49 |
| 4.2 | Geometrical and physical properties for parametric analysis. | 63 |
| 4.3 | Tabulation of viscous α and inertia β resistances caused by the geometrical and physical properties of the controlled fractured zone. In addition, the thermal and pumping powers at the 10 th year are listed. | 63 |
| 5.1 | Thermophysical properties of the materials used in DPGHE | 78 |
| 5.2 | Computational time of the numerical simulations | 90 |

Chapter 1

Introduction

Contents

| | | |
|-----|-------------------------------------|---|
| 1.1 | Background and motivation | 2 |
| 1.2 | Objectives | 2 |
| 1.3 | Thesis outline | 3 |

1.1 Background and motivation

In engineering practice, porous media configuration is frequently formed, whether naturally or artificially. This configuration affects the fluid flow process and the heat transfer mechanism within the system. If these effects are well-studied, we can utilize the porous media configuration for our benefit. Therefore, this thesis presents the computational fluid dynamics studies of the application of conjugate porous media in an engineering context: mine ventilation network (MVN) and geothermal heat exchanger (GHE) systems.

Meanwhile, the requirement of substantial computational time in developing the numerical 2D or 3D models remains a problem due to its complexity of the structure, huge computational domain, and long operational time. Thus, it is important to propose a computationally efficient numerical model.

1.2 Objectives

The general objective of this thesis is to study the numerical model of heat transfer and fluid flow, especially in the conjugate porous media model. The specific objectives of this thesis are divided into three main topics, which are discussed separately in Chapters 3, 4, and 5, which are:

- Evaluate a novel friction factor correlation for flow through porous media to be used in one-dimensional simulation by verifying the results with a three-dimensional computational fluid dynamic model.
- Study the effect of conjugate porous media in enhancing the performance of a novel double-pipe geothermal heat exchanger with a fractured zone at the bottom of the well.

- Develop a reduced-order one-plus-one-dimensional model for a geothermal heat exchanger using a space marching algorithm. Later, implement a thermal superposition theory to extend the model into multiple boreholes further.

1.3 Thesis outline

This thesis is structured as a manuscript-based master thesis and is organized into the following chapters. Chapter 1 briefly discuss the introduction and summarizes the background and objectives of the research. Chapter 2 provides a literature review in the application of conjugate porous media in the mine ventilation and geothermal heat exchanger system. The numerical method is also discussed. Chapter 3 presents the conjugate porous media model in the mine ventilation. This model, then, is integrated into popular mine ventilation network software as a friction factor correlation. Chapter 4 comprises the applied conjugate porous media to improve the thermal performance of the geothermal heat exchanger. The sensitivity analysis is done to understand the effect of different configurations in the fractured zone. Chapter 5 presents a reduced-order numerical model to be implemented in the geothermal heat exchanger system. Then, the model is extended using the thermal superposition concept from one borehole into multiple boreholes. Finally, the last chapter provides the conclusion of the work and offers suggestions for future works.

Chapter 2

Literature Review

Contents

| | | |
|-----|--|----|
| 2.1 | Introduction | 5 |
| 2.2 | Numerical methods of heat transfer and fluid flow | 5 |
| 2.3 | Heat transfer and fluid flow in conjugate porous media | 10 |

2.1 Introduction

The overall purpose of this section is to give the reader context on the thesis structure, from discussing numerical models on fluid flow and heat transfer in the application of mine ventilation and geothermal heat exchanger to the development of a more efficient numerical model algorithm. The implementation of all three chapters is seemingly different; however, the basic foundation is the same: numerical heat transfer and fluid flow.

2.2 Numerical methods of heat transfer and fluid flow

This section is benefited a lot by Patankar's book [5]. Heat transfer and fluid flow processes play a vital role in several practical applications, such as the mine ventilation network and geothermal heat exchanger. The methods to predict these processes can be done in several ways: (a) experimental investigation, which is given by actual measurement; and (b) theoretical calculation, which consists of consequences of a mathematical model, mainly as a set of differential equations. Each method has its own merits and demerits, but both methods are working mutually. In this thesis, we focus on implementing numerical methods which utilize theoretical calculation processes computationally.

The principle in developing a numerical model is to implement mathematical formulation in differential equations to describe physical properties in the subject of interest. We briefly discuss the mathematical formulation and its implementation in the reduced-order numerical model in the following two sections.

2.2.1 Generalized governing equations

The general differential equation, with a dependent variable ϕ , can be written as:

$$\frac{\partial}{\partial t}(\rho\phi) + \nabla \cdot (\rho v\phi) = \nabla \cdot (\theta\nabla\phi) + S \quad (2.1)$$

where θ is the diffusion coefficient. The dependent variable ϕ can represent a variety of different quantities, such as enthalpy, temperature and velocity. The first term of the equation describes the rate-of-change of the dependent variable, the second term is the convective term, the third term is the diffusive term, and S is the source term. Based on variable ϕ , an appropriate meaning is given to the diffusive coefficient θ and the source term S [5].

The generalized governing equations let us construct various physical properties by adjusting the dependent variable ϕ and applying those in the numerical simulation.

2.2.2 Reduced-order modeling in geothermal heat exchanger system

According to the Sixth Assessment Report (AR6) of the Intergovernmental Panel on Climate Change (IPCC) [6], the temperature of the earth's surface is getting warmer and does not show the sign of stopping. Currently, with the increase of 1.1°C in temperature, several climate disasters are happening all over the world (i.e., floods, wildfire, heat waves, and intense drought.) The increase of the temperature is predicted to reach 1.5°C in the next two decades, and 3.3-5.7°C at the end of the century. Thus, climate legislation has to be implemented as massive as possible to tackle the climate crisis. One of the approaches is the energy transition. The need for alternative low-cost and environmentally-friendly energy makes geothermal heat an attractive option to replace fossil-fuel-based energy. The geothermal heat could be extracted by the ground source heat pump (GSHP) system, coupled with a geothermal heat exchanger (GHE). Then the extracted energy could be utilized for space heating/cooling, direct use applications, or power generation.

Typically, GHE configuration is installed by sinking a single or multiple vertical boreholes until a certain depth. By incorporating GSHP, water is pumped through the borehole from the inlet, and the heated water is extracted from the outlet. Installing this system is considered expensive due to the need of drilling a borehole up to 1000 m, therefore, a numerical study is widely used to analyze the GHE systems. Generally, the 2D or 3D numerical models are built by using commercial software, such as Ansys Fluent

[7, 8, 9], and COMSOL Multiphysics [10]. To fully capture the physics phenomenon of the GHE model, a fully conjugate CFD model is usually built. Consequently, the nature of the GHE system, which has a diverse spatial and temporal span when illustrating the system's heat transfer, causes the simulation of such model challenging and sometimes prohibitive.

Regarding the spatial span, the dimensions in the domain range from the order of millimeters (i.e., the pipes and coolant region) up to the order of meters in the ground region. In the case of the temporal span, the computation time has to be treated in the order of minutes to capture the physics in the flow, especially during the initial phase. At the same time, the GHE system has decades in its operating time. These conditions resulted in the huge number of nodes or elements required to simulate such a model adding to the difficulty of the numerical modeling. Therefore, the development of a computationally efficient numerical model is needed.

In order to develop the reduced-order model of the GHE system, a certain degree of information in the description of the model has to be accumulated. The computational domain of the GHE system is usually comprised of the coolant region, pipes, and the surrounding ground. Based on the working procedures, governing equations are working in these domains. Additionally, these domains are bounded by boundary conditions that affect the system while the work is progressing. Fang et al. [11] presented a computationally efficient model of the double-pipe geothermal heat exchanger by incorporating the Finite Difference Method (FDM). In their model, a novel algorithm of the time step is employed, which resulted in high-speed computation. The supposedly complex simulation in the coolant region and the pipes are also greatly simplified by treating the flow and the convective heat transfer as one-dimensional. Yu et al. [12] also developed a novel 1D numerical model of the u-tube GHE with Finite Element Method (FEM) to simulate the heat transfer between the GHE and its surrounding ground. They simplified the u-tube heat exchanger into an equivalent single-tube heat exchanger. With this method, they verified the model and maintained accuracy when compared with the experimental data.

Apart from the GHE application, the reduced-order model is also explored in several other engineering applications. The notable contribution is given by Zueter et al. [13] who developed a novel reduced-order model in an artificial ground freezing system. In their paper, the AGF system configuration resembles the double-pipe GHE, which consists of the double-pipe where the coolant is flowing and the surrounding ground. To simulate such model, they developed several novel semi-conjugate 1+1D numerical models, coupled with the analytical model and the axial thermal correction. They simplified the model by only simulating the temperature of the ground with a space marching algorithm, which is an iterative method to solve algebraic equations. This method works by calculating the values of the variable by visiting each grid in series order. With their proposed models, the computational time is reduced by 99% compared with the fully conjugate CFD models.

2.2.3 Single borehole solution: Development of 1+1D model using a space marching algorithm

As previously mentioned, in order to build a 1+1D model, we have to describe the model thoroughly. Fig. 2.1 shows the typical 2D axisymmetric model of double-pipe GHE. By applying a space marching algorithm, the 2D axisymmetric model is reduced into a series of 1D gridlines. The detailed process to simulate such model is given as:

1. In the beginning, the temperature in the computational domain is set based on the initial condition. The initial condition is usually based on the temperature profile of the ground, which gets hotter as the depth got deeper.
2. The heat conduction along the 1D grid-lines are solved line-by-line and sweeps to the desired direction by incorporating the heat conduction equation:

$$\frac{\partial \rho c_p T}{\partial t} = \nabla \cdot (k \nabla T) \quad (2.2)$$

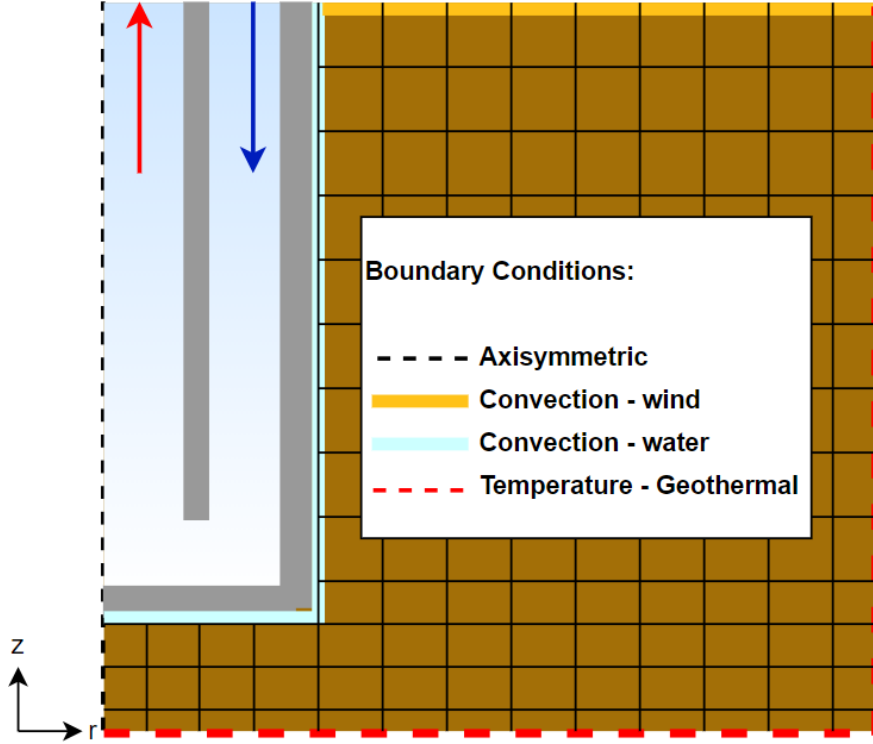


Figure 2.1: Computational domain of the 1+1D model of the DPGHE

where ρ is the density, c_p is the specific heat capacity, T is the temperature, and k is the thermal conductivity. At the same time, the fluid region is calculated by the 1st law of thermodynamics per unit area of the borehole, as follows:

$$\dot{m}c_{p,f}\Delta T_f = hA(T_s - T_f) \quad (2.3)$$

where h is the convection heat transfer coefficient. As shown in Fig. 2.1, the 1D gridlines are marching while bounded by the boundary conditions implemented in the domain. The gridlines are marching between the borehole pipes, which is calculated by the Eq. 2.3 and the side boundary, which is given by:

$$T = T_{geo}, \quad (2.4)$$

Additionally, an axisymmetric boundary condition is also applied to cut the computational process by half, which is given by:

$$\frac{\partial T_{axis}}{\partial r} = 0 \quad (2.5)$$

3. After all the grid-lines calculations are completed, the ground and coolant temperature profile of the present time step is set as an initial condition to solve for the temperature of the next time step.
4. Repeat steps (2-3) until the end of the simulation.

Once the simulation reaches convergence and the desirable time-steps, then the value of the temperature profile of the ground could be further utilized. Furthermore, by developing the reduced-order model, a design optimization that requires various parametric analyses could be done faster.

2.3 Heat transfer and fluid flow in conjugate porous media

The pioneering study of porous media was conducted by Henry Darcy in 1856 and resulted in an equation called Darcy's Law [14, 15]. After the publication of Darcy's Law, the development of fluid flow through porous media separated into two paths based on its applications [16]. The first path was based on the underground flow theory, which led to the discovery of the Forchheimer equation. And the following approach was based on the hydraulic radius theory, which is fundamental to the Ergun equation.

Porous media is a solid matrix with an interconnected void that allows the fluid to flow through it and is categorized as natural or artificial based on its forming method. The fluid flow through porous media has complex topology with high spatial variability in internal geometric features like porosity, permeability, and tortuosity [17, 18]. The study of the porous media is a challenging process due to its complex and multiscale natures, with length scales extending from the size of a pore until the size of the domain. The

following section describes an overview of the numerical study of porous media study in terms of its fluid flow and heat transfer mechanism, without the phase change.

2.3.1 Governing equations

In order to study the porous media numerically, the physical and theoretical length scales of the study have to be determined. In general, the length scales can be categorized in microscopic, macroscopic, and field-scale. In a microscopic or pore-scale model, the governing equations of mass, momentum, and energy are directly solved due to the complex flow is resolved around the matrix. On the other hand, on the macroscopic approach, a spatial averaged of the macroscopic properties is defined as a Representative Elementary Volume (REV) determined by volume averaging the microscopic properties over its REV. In this sense, the porosity ε is defined as the fraction of the total volume voids within a set volume of the porous media. At the same time, $1 - \varepsilon$ represents the fraction of the porous media occupied by the matrix. In the flow through porous media, the conservation equations could be formulated based on the Eq. 2.1 and special consideration of the velocity has to be taken. The mathematical model should consider Darcian or superficial velocity to describe the seepage flow through porous media, which could be illustrated by the Dupuit-Forchheimer relationship:

$$\mathbf{v} = \varepsilon \mathbf{v}_l \quad (2.6)$$

where \mathbf{v}_l is the actual liquid velocity.

Conservation of mass

The conservation of mass which solves for the accumulation and mass balance terms in porous media is as follows:

$$\varepsilon \frac{\partial \rho_f}{\partial t} + \nabla \cdot (\rho_f \mathbf{v}) = 0 \quad (2.7)$$

Conservation of momentum

To study the conservation of momentum, an approach based on hydraulic permeability has to be implemented. This approach takes the assumption of the water flow to satisfy Darcy's law as:

$$U = -\frac{K}{\mu}\nabla P \quad (2.8)$$

The permeability K is based on the geometry of the porous media, which is derived from the specific system configurations.

In order to create a more accurate calculation in the flow through porous media, Forchheimer arranged his equation by extending Darcy's linear equation by developing a non-linear relationship between the pressure gradient and the flow velocity [19, 20]. This empirical equation was created because of an understanding that the Forchheimer regime can describe a flow pattern, including the inertial effect, while the Darcy regime can describe a flow behavior when the viscous effect dominates the regime. The Forchheimer equation was developed by using the analogy with pipe flow [21], with coefficients as correction factors to account for viscosity and inertial terms [22, 23]:

$$\nabla P = -\frac{\mu\mathbf{v}}{K} - c_F \frac{\rho\mathbf{v}^2}{\sqrt{K}} \quad (2.9)$$

where c_F is the Forchheimer coefficient that accounts for inertia drag, Forchheimer non-linear equation also could be derived from the Navier-Stokes equation [24]. Forchheimer coefficient c_F and permeability K are highly dependent on the internal structure of the porous media.

The incorporation of the Darcy-Forchheimer term into the previous equation resulted in the momentum equation for the flow through porous media:

$$\rho_f \left[\frac{1}{\varepsilon} \frac{\partial \mathbf{v}}{\partial t} + \frac{1}{\varepsilon^2} (\nabla \cdot (\mathbf{v}\mathbf{v})) \right] = -\nabla P + \frac{\mu}{\varepsilon} \nabla^2 \mathbf{v} - \frac{\mu}{K} \mathbf{v} - \frac{c_F \rho_f}{K^{1/2}} |\mathbf{v}| \mathbf{v} \quad (2.10)$$

Conservation of energy

The Local Thermal Non-Equilibrium (LTNE) hypothesis is implemented to model a heat transfer within the porous media. The LTNE approach generates two-equation of energy inside the REV for each phase; solid and fluid. Hence, the conservation of energy for the solid phase is as follows:

$$(1 - \varepsilon)(\rho c_p)_s \frac{\partial T_s}{\partial t} = (1 - \varepsilon) \nabla \cdot (k_s \nabla T_s) + h_{sf} A_{sf} (T_s - T_f) \quad (2.11)$$

and the following describes the conservation of energy for the fluid phase:

$$\varepsilon(\rho c_p)_f \frac{\partial T_f}{\partial t} + (\rho c_p)_f \mathbf{v} \cdot \nabla T_f = \varepsilon \nabla \cdot (k_f \nabla T_f) + h_{sf} A_{sf} (T_f - T_s) \quad (2.12)$$

where s and f is the solid and fluid phases, respectively. The other approach to solve the energy equation in porous media is the Local Thermal Equilibrium (LTE) method. This hypothesis considers the local averaged temperature of the solid particle T_s and the fluid T_f as equal:

$$T_s = T_f = T \quad (2.13)$$

Based on these conditions, the LTE conservation equation of energy can be built by combining Eq. 2.11 and 2.12 as follows:

$$(\rho c_p)_e \frac{\partial T}{\partial t} + (\rho c_p)_e \mathbf{v} \cdot \nabla T = \nabla \cdot (k_e \nabla T) \quad (2.14)$$

where

$$(\rho c_p)_e = (1 - \varepsilon)(\rho c_p)_s + \varepsilon(\rho c_p)_f \quad (2.15)$$

$$k_e = \varepsilon k_f + (1 - \varepsilon)k_s \quad (2.16)$$

The LTE equation can be considered valid if the following time scale holds true:

$$\frac{\varepsilon(\rho c_p)_f l^2}{t} \left(\frac{1}{k_f} + \frac{1}{k_s} \right) \ll 1 \quad (2.17)$$

and

$$\frac{(1 - \varepsilon)(\rho c_p)_s l^2}{t} \left(\frac{1}{k_f} + \frac{1}{k_s} \right) \ll 1 \quad (2.18)$$

and the length scale satisfies:

$$\frac{\varepsilon k_f l}{A_{sf} L^2} \left(\frac{1}{k_f} + \frac{1}{k_s} \right) \ll 1 \quad (2.19)$$

and

$$\frac{(1 - \varepsilon) k_s l}{A_{sf} L^2} \left(\frac{1}{k_f} + \frac{1}{k_s} \right) \ll 1 \quad (2.20)$$

2.3.2 Applications of conjugate porous media in engineering practices

Extensive studies on the heat transfer mechanism and the fluid flow through porous media have been done [25, 26, 27]. Thus, a good understanding of the conjugate porous media could be implemented in engineering practices, such as mine ventilation networks and geothermal heat exchanger systems.

Applications in mine ventilation network

The underground mining operation is considered as an energy-intensive industry, and the mine ventilation network system as the lung of the underground mine may account for up to 40% of the total electricity used in the underground mine [28]. The necessity to supply a sufficient air quantity, maintain the air quality, and control temperature-humidity level inside the mine resulted in a high cost of this system, especially in a deep and huge underground mine [29]. Therefore, thorough planning is necessary when installing an MVN system.

In the mining cycle, the tunnel development progression in an underground mine is caused by hauling and blasting. These activities create a certain formation of porous

media inside the underground mine depending on the activities and the mining method. For example, during the drawbell blasting in block caving operation, which caves the rock on the upper level into the lower level, this process results in a broken rock formation in that zone. There is a possibility that the airflow dedicated to ventilate a certain airway is leaked into these porous zones, resulting in inefficient energy use. A similar condition is also applied when the rock is sent to the drawpoint, which made the drawpoint filled with the broken rock. Another example is in longwall mining operation when the longwall is advancing; the gob area is formed and acted as a porous zone that could accumulate methane gas inside the zone. Similar gob condition is also applied in the room and pillar mining operation [30]. In those cases, a possibility of methane explosion which results from a certain level of methane, air, and heat mixture has to be avoided [29, 31].

Other than the general mining activities effect to the formation of porous media in the underground mine, an implementation of a novel concept in ventilating the mine with the utilization of broken rock formation is done in Creighton and Kidd Creek mines Canada [32]. These mines created a natural heat exchanger which was made by dumping a massive number of waste rocks into their open pit to create seasonal thermal energy storage (SeTES). The method of utilizing such system is by flowing fresh air into the rock pit into the underground mine. The heat exchange between the broken rock formation in Summer and Winter leads to a significant reduction of ventilation cost by 50 to 80%. Ghoreishi-Madiseh et al. [33] developed a 3D transient model of large-scale SeTES to evaluate the performance of the system numerically. Later, they compared the effect of LTE and LTNE on the heat transfer performance and analyzed the effect of exhaust fan pressure.

Based on the literature thus far, the importance of the study of porous media in the MVN application is required to avoid energy loss, to prevent the methane explosion due to the leakage, and to be able to utilize the flow even further. Generally, mine ventilation engineers use the Atkinson equation to analyze the flow in underground mine, which is

given as:

$$\Delta p = RQ^2 \quad (2.21)$$

where Δp is the pressure drop, R is the resistance in the airway, and Q is the volumetric flow rate. The Atkinson equation is based on the Chezy-Darcy relationship and could be rewritten as:

$$\Delta p = kL \frac{per}{A^3} Q^2 \quad (2.22)$$

where L , per , and A are the airway's length, perimeter, and cross-sectional area. While k is the Atkinson's friction factor which is a function of the coefficient of friction, f , and the air density, ρ , given as:

$$k = \frac{f\rho}{2} \quad (2.23)$$

When defining the value of the friction factor, McPherson and Malcolm [29] compiled the friction factor list in their book in Table 5.1. This list is a compilation of numerous experiments and observations during ventilation surveys. However, a friction factor that describes the flow through porous media is not on this list. In an attempt to define the friction factor for the flow through porous media, Amiri et al. [34] proposed a novel friction factor correlation for broken rock with a large diameter. This correlation is derived from the Eq. 2.10 and assisted by the pressure-Reynolds database generated from the pore-scale computational model. The proposed correlation is a function of rock size and porosity, ranging from 0.04 m to 1.2 m and 0.2 to 0.7, respectively. Agson-Gani et al. [1] provided a proof of concept of the new friction factor correlation in MVN application by developing a 3D CFD model of a haulage drift with a drawpoint filled by broken rocks. Later, they incorporate the friction factor correlation into a 1D-MVN software (Ventsim).

Applications in geothermal heat exchanger system

As discussed in subsection 2.2.2, geothermal energy is one of the promising renewable energy sources due to its sustainable feature. Geothermal energy is abundant inside the

earth and can be utilized regardless of the meteorological conditions, unlike other renewable energy sources (e.g., tidal, solar, and wind). In order to exploit the geothermal heat, a geothermal heat exchanger is sunk into the ground. The extraction methods of the GHE employ two techniques, which are the open-loop and the closed-loop system. The open-loop GHE works by extracting the heated water from the aquifer with production well, and an injection well is also sunk to return the water into the ground. The closed-loop GHE circulates the water inside a closed-loop tube, usually in the shape of u-tube or coaxial pipes. The choice between both models is highly dependent on the availability of the groundwater resources.

By design, the process of geothermal heat extraction is related and sometimes affected by the porous media in the surrounding system. It is since the geothermal energy resides inside the earth, whether in the ground, subsurface rocks, or aquifer, which are considered as porous media. Particularly, in an open-loop system in which the coolant is directly in contact with the ground, the heat transfer rate of the water is affected by its surrounding. For example, the enhanced geothermal system (EGS) is an open-loop system that works by inserting an injection well with a depth within 3 to 10 km below the surface. A pressurized fluid is injected from this injection well to fracture the subsurface rock to create permeable channels underground. The channels act as an access for the water to circulate inside the porous ground. Finally, a production well is installed to extract the water from the ground. While the water is circulating the fractured ground, a heat transfer mechanism occurs and improves the heat performance of the system

In the closed-loop system, there is no direct contact between the coolant and the ground. However, by installing such a model in the porous geothermal system, the GHE could benefit from the effect of the natural convection, which may improve the heat performance of the system. Goreishi-Madiseh et al. [35] developed a heat transfer model for the simulation of the natural convection in a closed-loop geothermal system. Their study shows that if the hydraulic conductivity is increased from 10^{-5} to 10^{-3} , then the role of the natural convection is considered as effective. Additionally, by extending the system

into multiple boreholes, the buoyancy-driven natural convection becomes more significant. Later, in chapter 4, a semi closed-loop DPGHE model is proposed, which uses the fractured zone at the bottom of the well to improve the heat transfer rate of the system.

Chapter 3

Integration of Conjugate Porous Media Model into Mine Ventilation Network Software

Contents

| | | |
|-----|----------------------------------|----|
| 3.1 | Introduction | 21 |
| 3.2 | Model Description | 25 |
| 3.3 | Results and Discussion | 31 |
| 3.4 | Conclusion | 35 |

Preface (Linking Paragraphs)

The utilization of the applied conjugate porous media was implemented in this chapter. A model comprises a mine drift with a drawpoint in an underground mine was created and investigated numerically based on conservation of mass and momentum. The drawpoint is filled with broken rocks, which will obstruct the flow and increase the friction losses. This article was presented at the 18th North American Mine Ventilation Symposium, Virtual, 2021:

Agson-Gani, P. H., Amiri, L., Madiseh, S. G., Poncet, S., Hassani, F. P., & Sasmito, A. P. (2021). Integration of conjugate porous media model into mine ventilation network software. In *Mine Ventilation* (pp. 47-55). CRC Press.

Additionally, this paper was recommended and is in preparation for a submission to the CIM Journal.

Abstract

In underground mining operations, investigating the airflow through porous zones is typically arduous due to the flow's complex and dynamic nature. Despite the challenges of modelling the flow with the general mine ventilation network (MVN) software, it is essential to accurately measure such flow to satisfy the quantity, quality and temperature-humidity controls in the underground mine. This study integrated the computationally expensive conjugate porous media model into the versatile MVN software to analyze the airflow through the porous zone more efficiently. A novel friction factor coefficient was compiled into the broken rocks-filled drawpoint model in the MVN software, which later was verified against the 3D computational fluid dynamics model. Several simulations were conducted to ensure the reliability of the model by varying the porosity and broken rocks diameter of the porous zone. The results show that the novel friction factor coefficient could accurately predict the flow through porous media by using MVN software and drastically reduce the computational time by >99% compared with the usage of the 3D solver. In addition, sensitivity analyses were conducted to assess the effects of var-

ious factors on the system. This method enables mine ventilation engineers to plan the fast-changing natured underground mine ventilation network effectively.

3.1 Introduction

Due to the haulage and blasting processes, porous media formations are bound to be developed during underground mining operations. These porous zones are made up of broken rock or gob and affect the airflow circulating inside the mine. Moreover, the accumulation of methane inside these zones (i.e., gob and goaf) could result in an underground gas explosion if left untreated. Therefore, understanding the properties of these broken rocks is essential to create a safe mine ventilation design, which satisfies quantity, quality, and temperature-humidity controls [1].

The spontaneous combustion of coal mining has long been a significant problem that needs to be mitigated. A standard requirement for fire in a coal mine to occur is if oxygen and the fuel (i.e., coal) maintain their interaction and generate heat. If the accumulated heat rate exceeds the cooling rate provided by the mine ventilation, then it could lead to a fire, and an explosion [2]. Other attributes which affect the self-heating are the properties of the coal (i.e., rank, porosity, moisture content, and petrology) and external conditions around the coal, such as airflow velocities, pressure drops, and the mining methods [3]. In 2008, Karacan [4] analyzed the effect of seventeen principle components that affect ventilation emission in longwall mines across the U.S. The results show that the properties of the coalbed configuration and the mining method affect ventilation methane emissions due to their effect on the airflow through the system. Additionally, in regards to the effect on the airflow, Amiri et al. stated that the size and the porosity of the rocks, as well as the airflow velocity and the dimensions of the airway, are the key parameters that influence the friction factor and the flow resistance [1, 5].

Modelling flow through porous media in a huge model is especially challenging (i.e., porous zones in underground mine airways). To model the characteristics of the flow ac-

curately, direct in situ measurement of the airways is preferred. However, this measurement is sometimes prohibitive due to the inaccessible locations or the dangerous nature of the underground mine. Therefore, other methods such as the analytical approach or developing a pore-scale CFD model are preferred.

In a longwall mining operation, gob and goaf are two of the riskiest locations supporting spontaneous combustion occurrence, especially when air is leaked into them. One of the widely used methods to better understand airflow behaviour through those permeable locations is by conducting a computational fluid dynamics (CFD) simulation [6]. Several methods are used to model flow through gob or goaf, such as by implementing Darcy's law [7, 8], Forchheimer's equation [9, 10], and Carman-Kozeny equation [11, 12, 13]. For instance, Ren and Edwards [7] numerically investigated the flow through broken coal around the longwall face, which resulted in the understanding of the methane flow behaviour in various permeability. They simulated the porous zone by applying Darcy's law into the flow which flows through it. Zhang et al. [9] utilized Forchheimer's equation to simulate the air leakage through gob with uplink and downlink ventilations which the findings indicate that the usage of the downlink ventilation was better to reduce the accumulated gas inside the gob.

To date, several mitigations for spontaneous coal combustion are proposed; among them are goaf inertization. Goaf inertization was done by injecting inert gas (i.e., N_2 in most cases) into the gob or goaf to maintain the self-ignite coal. Zhang et al. [14] proposed the proactive inertization plan by developing 3D CFD models based on a coal mine in China. They employed the Carman-Kozeny to solve for the additional viscous term in the flow through the permeable gob. Several studies were conducted by Ren and Balusu to better utilize the goaf inertization by defining the optimum strategies to improve the safety in coal mines [15, 16, 17, 18]. They added a momentum sink which calculates the viscous and inertia resistances of the gases.

The other common method to minimize the risk of goaf/gob spontaneous combustion is by draining the methane from the goaf or gob to reduce its emission. In 2016, Liu

et al. [19] assessed the in-situ gob drainage with a gob gas ventholes by developing a 3D CFD model. The fractured gob is coupled with the expansion coefficient to emulate the "O-shaped" pathway in the gob. Later, the Blake-Kozeny equation is utilized as the analytical approach to calculate the relation of permeability and porosity of the gob. Li et al. [20] studied the gas drainage which was based on the 1262 working longwall faces in a coal mine in China. They developed a 3D CFD model, and modeled the porous zone by applying Darcy's law and momentum sink which was used by Ren et al. [21]

Understanding the flow through porous zone on mine ventilation is also useful to better plan the ventilation in the MVN. The popular utilization of such system was introduced in Creighton and Kidd Creak mines [22]. These mines turned their open-pit into a natural heat exchanger by filling it with a huge amount of waste rocks. By flowing fresh air through the natural heat exchanger into the underground mine, the mines could save up to 80% of ventilation cost based on the heat exchange between the rock formation in Summer and Winter. Later, Ghoreishi-Madiseh et al. [23] extended this study by developing the numerical model based on Creighton's mine condition. Ajayi et al. [24] studied the flow in a panel caving mine which was affected by the broken rocks formation created by the drawbell blasting. A transient CFD model was developed and the simulation was done by discrete and continuum methods.

From the literature presented thus far, it can be said that analyzing and simulating the flow through porous zones on mine ventilation application is essential for mine ventilation engineers to understand better and plan the mine ventilation network. However, the typical way to simulate such a complex model is by developing a CFD numerical model that is computationally expensive and long-running. On the other hand, in mining operations, the tunnels and airways are changing daily and rapidly based on their sequences, which requires the mine design adjusted based on the changes. Mine ventilation network (MVN) software such as Ventsim, VNetPC and VUMA are generally used to design, plan and analyze the performance of the mine ventilation in the mine. These 1D numerical software are popular due to their versatility and the ability to compute the

airways swiftly, which are suitable to model the fast-changing geometry of the underground mine. These software utilize the Atkinson equation and Kirchhoff's laws which are solved by the Hardy-Cross algorithm to simulate the behaviour of the flow inside the underground mine. However, it is still considered a challenge to simulate a flow through broken rocks or porous structures using MVN software due to the complex nature of the flow [25, 26, 27]. Inaccurate prediction of the airflow quantity and the resistances of flow through porous media in underground mines could lead to significant problems in designing the mine ventilation network, such as mistakes in defining the necessary airflow quantity, which leads to a higher mine ventilation cost or a dangerous gas leakage that could cause an explosion. Therefore, it is crucial to solving this knowledge gap by bridging the usage of a computationally expensive CFD solver and the versatile MVN software to model a flow through porous media on mine ventilation application.

In this paper, a simple haulage drift with a drawpoint filled with broken rocks is developed. Then, we utilize the novel analytical solution to estimate the friction factor and the resistances of the flow through porous zones reported in our previous study [1] to model the broken rocks inside the drawpoint. Parametric analysis on the configuration of the broken rocks was also conducted by considering the effect of wide range porosity (within 0.2 – 0.6) and broken rocks diameter (within 4 – 55 cm) in the drawpoint resulted in 20 different scenarios. Afterwards, the friction factor correlations of flow through broken rocks were compiled into the MVN software, Ventsim. At the same time, the inertia and viscous resistances values were used as an input in the CFD solver, which is Ansys Fluent. Finally, both results were quantitatively evaluated and verified with each other to determine the accuracy of both models. The results of this study could act as a convincing reference to simulate flow through porous zones accurately on mine ventilation application by using an MVN software which is incredibly faster to compute than the CFD solver.

3.2 Model Description

In block caving operation, the ground was caved from the undercut level to be extracted by the level below it, namely extraction level. Then, additional blasting was done to connect between the undercut and extraction levels. This process resulted in the development of a drawpoint which the broken rocks will be extracted by mine haulage equipment. For this study, a simplified haulage drift with a drawpoint at its end was chosen as the physical domain of the flow through porous media and developed by using two different software, Ansys Fluent and Ventsim. As shown in Figure 3.1.(a), a drawpoint was filled with broken rocks with certain diameter and porosity. These broken rocks acted as the porous zone in the airways and created resistances in the mine ventilation system. The ventilation started from the duct inlet where airflow was flowing in the direction of the drawpoint. When the air reached the broken rocks filled drawpoint, then a certain amount of air was seeping through the broken rock into the drawpoint's outlet, namely Q_{leak} , and some of it was reflected back to the opposite direction into the drift's outlet, namely Q_{out} . The airflow quantity as well as the pressure drop of the air which flow through the outlet were the parameters which were used to compare both models. The integration process of modelling a conjugate porous media model in the CFD solver into the MVN software is shown in Figure 3.2.

3.2.1 Analytical solutions

Governing equations

The simulated model comprises two zones, the haulage drift and the broken rocks-filled drawpoint. The airflow is considered a turbulent flow based on the calculated Reynolds number (89,000-295,000) in every scenario. In the haulage drift, where the flow has minimum obstruction, the conservation equation of mass and momentum is as follows:

$$\frac{\partial}{\partial t}(\rho_f) + \nabla \cdot (\rho_f \mathbf{U}) = 0 \quad (3.1)$$

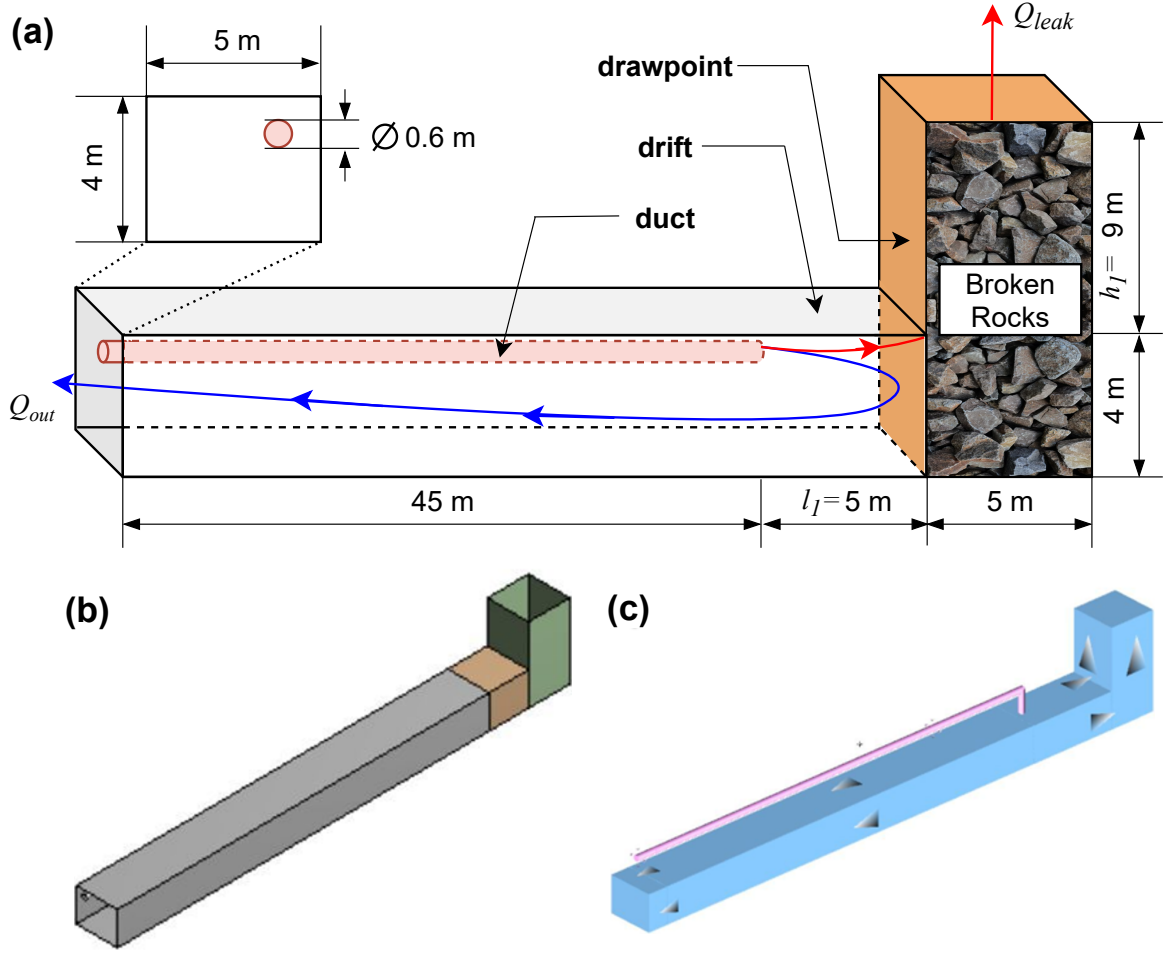


Figure 3.1: Illustration of the haulage drift with a broken rocks-filled drawpoint as a simulated model: (a) schematic; (b) Ansys Fluent; and (c) Ventsim models.

$$\frac{\partial}{\partial t}(\rho_f \mathbf{U}) + \nabla \cdot (\rho_f \mathbf{U} \mathbf{U}) = -\nabla P + \nabla \cdot [(\mu_f + \mu_{t,f})(\nabla \mathbf{U} + (\nabla \mathbf{U})^T)] + \rho_f \mathbf{g} \quad (3.2)$$

where ρ stands for the density, \mathbf{U} is the air velocity, P is the pressure, μ is the dynamic fluid viscosity, \mathbf{g} is the gravity, and subscripts f and t is fluid and turbulent, respectively.

Since the flow in the system is turbulent, the study was coupled with the k-epsilon turbulence model. To employ this model, two equations models are applied to solve for the turbulence kinetic energy κ and the rate of dissipation ϵ , which given by[28]:

$$\nabla \cdot (\rho \kappa \mathbf{U}) = \nabla \cdot \left[\left(\mu + \frac{\mu_t}{\sigma_\kappa} \right) \nabla \kappa \right] + G_\kappa - \rho \epsilon \quad (3.3)$$

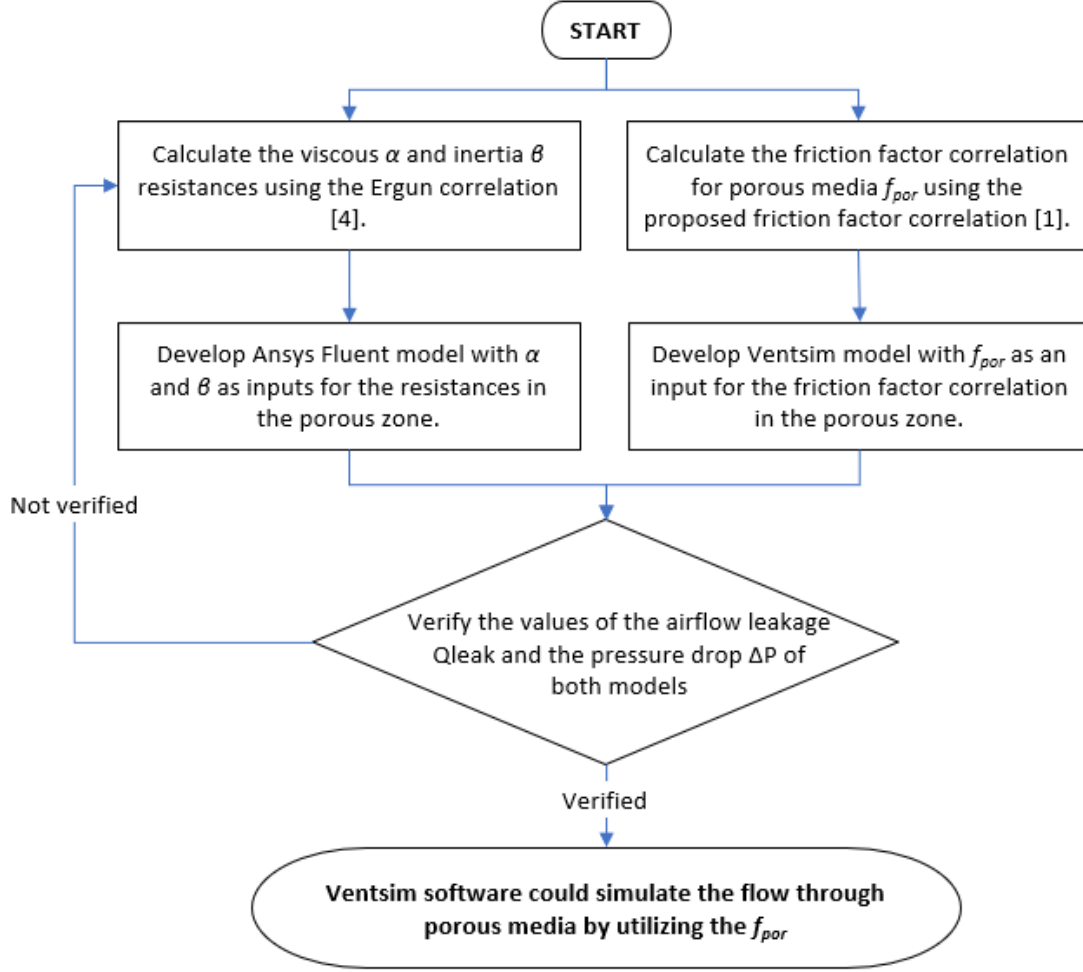


Figure 3.2: Flowchart for the integration of the Ansys Fluent and Ventsim to model the flow through porous media.

$$\nabla \cdot (\rho \epsilon \mathbf{U}) = \nabla \cdot \left[\left(\mu + \frac{\mu_t}{\sigma_\epsilon} \right) \nabla \epsilon \right] + C_{1\epsilon} G_\kappa - C_{2\epsilon} \rho \frac{\epsilon^2}{\kappa} \quad (3.4)$$

where G_κ is the turbulence kinetic energy, and σ_κ and σ_ϵ are expressing the Prandtl numbers of κ and ϵ , respectively. The turbulent viscosity μ_t is formulated by combining κ and ϵ as:

$$\mu_t = \rho C_\mu \frac{\kappa^2}{\epsilon} \quad (3.5)$$

where $C_{1\epsilon}$, $C_{2\epsilon}$, and C_μ are constants.

On the other hand, the airflow which seeped through the broken rocks filled draw-point is assumed to be laminar and steady. Therefore, the conservation equation of mass and momentum inside the drawpoint is given by:

$$\nabla \cdot (\rho_f \mathbf{u}) = 0 \quad (3.6)$$

$$\nabla \cdot (\rho_f \mathbf{u}\mathbf{u}) = -\nabla P + \nabla \cdot [(\mu_f)\nabla \mathbf{u}] + S_D + S_F + \rho_f \mathbf{g} \quad (3.7)$$

where \mathbf{u} is the superficial velocity and the S_D and S_F are the Darcy and Forchheimer terms, respectively, which are expressed as:

$$S_D = -\frac{\mu}{K} \mathbf{u} \quad (3.8)$$

$$S_F = -\beta \rho \mathbf{u}^2 \quad (3.9)$$

where K is the permeability which is also the inverse of viscous resistance coefficient α , and β stands for the inertia resistance coefficient. Both resistances are the function of broken rocks diameter d_p and its porosity ε , which are given by:

$$K = \frac{d_p^2 \times \varepsilon^3}{A \times (1 - \varepsilon)^2} \quad (3.10)$$

$$\beta = \frac{B \times (1 - \varepsilon)}{d_p \times \varepsilon^3} \quad (3.11)$$

where constants A and B are the Ergun coefficients which the values could be determined from the graphs developed by Amiri et al. [5].

Friction factor correlation of the flow through porous zone

Generally, mine ventilation engineers investigate the flow in an underground mine by utilizing the Atkinson equation, which is given by[2]:

$$\Delta P = RQ^2 \quad (3.12)$$

where ΔP is the pressure drop, R is the resistance and Q is the airflow quantity. This equation could be further extended by applying the Chezy-Darcy relationship and could be written as:

$$\Delta p = kL \frac{per}{A^3} Q^2 \quad (3.13)$$

where L , per , and A are the airway's length, perimeter, and cross-sectional area. k is the Atkinson's friction factor which calculated as:

$$k = \frac{f\rho}{2} \quad (3.14)$$

The coefficient of friction f is used to determine the rate of friction in a particular condition. When defining the value of f , mine ventilation engineers often refer to the Moody chart or the compilation of the friction factor based on the ventilation surveys compiled by McPherson and Malcolm [2]. In addition, a novel coefficient of friction for porous media f_{por} was developed and is a function of the local Reynolds number Re_k and the Forchheimer coefficient F [1]. The proposed friction factor could be used to model a porous zone with a porosity within 0.2 to 0.7 and the particle diameter within 0.04 to 1.2 m, which is the ideal size to simulate the broken rocks created by the blasting process. Then, the f_{por} correlation can be calculated as:

$$f_{por} = \frac{c_1}{Re_k} + (Re_k F)^{c_2}; \quad c_1 = 5.6; c_2 = 0.12 \quad (3.15)$$

In the MVN software, a general coefficient of friction f is an input to defining the friction in an airway. Therefore, f_{por} should be converted to f by applying the following equation:

$$f = f_{por} \frac{\xi}{\gamma} \quad (3.16)$$

where ξ is the specific surface area based on the solid volume, and γ is the geometric characteristics which can be calculated as $\frac{per}{A}$.

3.2.2 Initial and boundary Conditions

The duct inlet provided the air to ventilate the system throughout the simulation, and the flow rate is given by:

$$Q = Q_{in} = 20m^3/s \quad (3.17)$$

No-slip condition is applied at the drift and drawpoint walls, as well as the duct wall:

$$\mathbf{U} = 0 \quad (3.18)$$

Finally, at the outlet of the drift and the drawpoint, the pressure is set as 0:

$$P = P_{out} = P_{leak} = 0 \quad (3.19)$$

3.2.3 Model development

The development of the numerical models in Ansys Fluent and Ventsim were shown in Figure 3.1.(b) and Figure 3.1.(c), respectively. Parametric analysis was done by running twenty simulations with different porosity and broken rocks diameter of the broken rocks-filled drawpoint, as compiled in a matrix shown in Table 3.1. This analysis was done to better understand the effect of porosity and broken rocks diameter affecting the behaviour of the flow. These parameters were used to calculate the values of viscous and inertia resistances (Eq. 3.10 and 3.11, respectively) to be compiled in the Ansys Fluent solver. At the same time, the value of friction factor correlations for porous media were also calculated using the same parameters by Eq. 3.15 and 3.16 to be coupled into the Ventsim simulation.

Table 3.1: The twenty scenarios of the study based on the porosity ε and the diameters d_p of the broken rocks-filled drawpoint.

| | | ε | | | | |
|-------|------|---------------|-------|-------|-------|-------|
| | | 0.2 | 0.3 | 0.4 | 0.5 | 0.6 |
| d_p | 0.04 | ID:1 | ID:2 | ID:3 | ID:4 | ID:5 |
| | 0.1 | ID:6 | ID:7 | ID:8 | ID:9 | ID:10 |
| | 0.3 | ID:11 | ID:12 | ID:13 | ID:14 | ID:15 |
| | 0.55 | ID:16 | ID:17 | ID:18 | ID:19 | ID:20 |

In regards of the Ansys Fluent simulation, the computational domain was developed and meshed using Ansys Fluent 2020R1. A fully built three-dimensional (3D) model is verified by doing a mesh-independent analysis resulted in a final mesh size of 4×10^5 number of elements. The conservation equation of mass and momentum as well as the initial and boundary conditions were solved using the finite volume method. Also, the model was computed by the Semi-Implicit Pressure-Linked Equation (SIMPLE) algorithm and second-order upwind discretization. the residuals of all calculations were set as 10^{-6} to ensure the convergence of the simulation. At the same time, a similar model was built in Ventsim Design 5.2. The 1D numerical model was solved using the Hardy-Cross sequential solver by using iterative estimation method to analyse the behaviour of the airflow in the ventilation.

3.3 Results and Discussion

3.3.1 Verification between Ansys Fluent and Ventsim results

The main objective of the study is to ensure the usage of Ventsim software to model flow through porous media have a similar accuracy with the value provided by Ansys Fluent software. Therefore, the verification was made between the results provided by both software. The quantity of the air which seeped through the broken-rocks filled drawpoint Q_{leak} and the pressure drop ΔP are the main parameters which were observed to compare both models. Based on Figure 3.3 and 3.4., the difference between the Q_{leak} and ΔP are

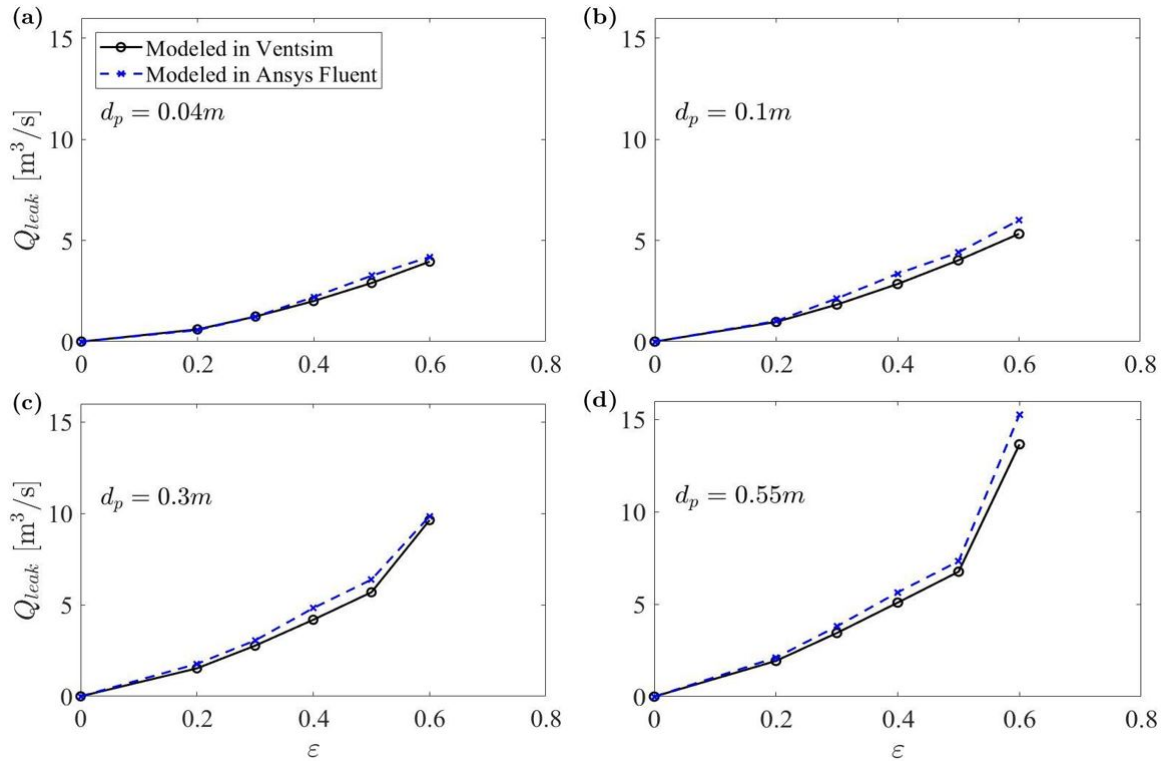


Figure 3.3: The airflow quantity values which seeped through the porous zone in the drawpoint Q_{leak} within different range of broken rock diameter d_p : (a) 0.04 m; (b) 0.1 m; (c) 0.3 m; and (d) 0.55 m [29].

less than 12% and 3%, respectively, with the results from the Ansys Fluent model are higher for both parameters.

These differences might result from the different approaches in developing the models in both software, which are listed below:

- The effect of the duct's placement. In Ansys Fluent, the duct is modelled precisely which affects the flow based on its position and geometry; while in Ventsim, less control is given regarding the placement. This duct's placement is also affecting the size of the outlet. Due to the precisely built duct in Ansys Fluent's model, the size of the duct took up some portion in the drift and outlet size in which added other resistances to the system. However, Ventsim does not simulate as precisely as the model given by Fluent.

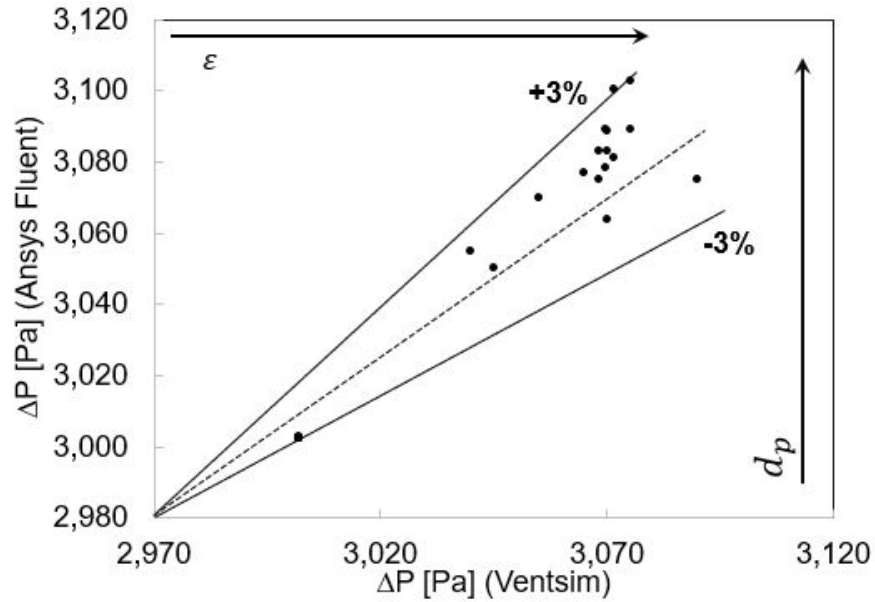


Figure 3.4: Flowchart for the integration of the Ansys Fluent and Ventsim to model the flow through porous media [29].

- The effect of the bending between the drift and the drawpoint. Ansys Fluent numerically investigates the resistance affected by the bending, compared to the utilization of shock loss which is the user-input in Ventsim usage. In addition, in Ventsim, the association between two airways, in this case are the drift and the drawpoint, are harder to model precisely.

Thus, it can be concluded that both results are verified, and the proposed friction factor correlation for porous media could be applied in Ventsim to estimate the flow rate and the pressure drop of flow through porous media.

3.3.2 Analysis of the air leakage and the pressure drop

Figure 3.3 and 3.4. present the Q_{leak} and ΔP based on the twenty scenarios simulations, respectively. While considering the effect of the porosity and diameter of the rocks, it can be seen that the quantity of the air that seeped through the drawpoint Q_{leak} is higher by increasing the porosity. It is evident that the wider void allows more room for the airflow

to penetrate. At the same time, the Q_{leak} is also increasing by having bigger broken rocks diameter as the porous zone. The blasted zone consists of a compilation of broken rocks that sits on top each other. Therefore, these broken rocks size affect how they contacted with each rocks which resulted in a bigger void when the broken rocks size increased. Similarly, increasing the ε and d_p are directly proportional with the ΔP values. With this information, mine engineers could better plan their MVN by knowing the nature of how the porous zone developed (i.e., tie in, drawbell blasting, longwall mining, etc), and input the necessary friction factor correlation to the MVN software.

3.3.3 Sensitivity analyses

The advantage of having a faster computational process is the ease of conducting a design optimization by doing parametric studies. In this study, we performed sensitivity analyses on different operating conditions to investigate the rate of effect of different variables to the system. As shown in Fig. 3.5, parameter Q_{leak} is used as a reference to compare the results obtained by varying the 4 different variables, which are: height of the drawpoint h_1 , the length of the gap between the duct and the drawpoint l_1 , the airflow rate Q_{in} , and the porosity of the blasted zone ε .

Out of four variables, varying the porosity gives the most significant effect to the change of the leaked airflow. Increasing the porosity by 25% resulted in an increase of the air leakage by approximately 40%. On the other hand, the duct placement did not significantly affect the air leakage through the broken zone. The airflow rate which seeped through the broken zone changed directly proportional with the change of the quantity of the airflow. A 25% increase in the Q_{in} leads to a 25% increase as well for the Q_{leak} . Lastly, a 30% increase in the drawpoint's height resulted in an 8% decrease in the air leakage. The chosen variables for the sensitivity analysis depend on the simulated airways' application and condition, which could further optimize the MVN planning.

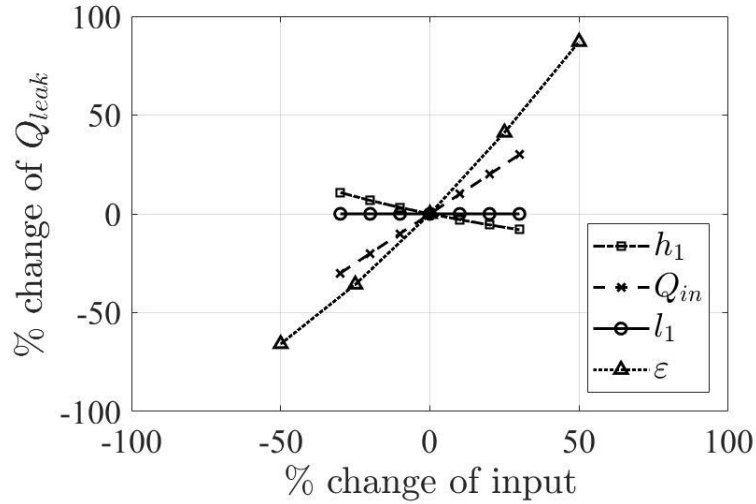


Figure 3.5: Sensitivity analyses based on different operating conditions: height of the drawpoint h_1 , airflow rate Q_{in} gap between the duct inlet and drawpoint l_1 , and the porosity ϵ .

3.3.4 Analysis of the computational time

The duration of the computational process by both models are calculated, aside from the model development duration. To simulate such models, Ansys Fluent needs four to six hours for its simulation to converged in each of the twenty scenarios simulation. On the other hand, Ventsim simulation is done almost instantly. It indicates that the computational time of Ventsim is incredibly faster than Ansys Fluent and provides similar accuracy as well. Therefore, the utilization of Ventsim could replace Ansys Fluent in a day-to-day planning for mine ventilation engineers to model flow through porous zones.

3.4 Conclusion

We provided a novel analytical approach to simulate the flow through the porous zone on mine ventilation application effectively and accurately. This approach resulted from integrating the 3D CFD solver results into the 1D MVN software by verifying twenty scenarios simulated by both models. The main objective of integrating both models is to

use the versatile and fast to compute MVN software to model the flow through porous zones with the same accuracy provided by the CFD solver's simulation.

The main key findings of this study are:

1. The results of the comparison between airflow leakage Q_{leak} and the pressure drop ΔP indicate that good agreement was obtained by both models and was considered verified. Thus, we could use the MVN software to simulate flow through porous zone by compiling the proposed friction factor correlation as the user input in the software.
2. With similar accuracy, simulating the flow through porous zone using MVN software is several degrees faster than using the CFD solver.

In summary, mine ventilation engineers could use the f_{por} to be compiled in their mine ventilation design using MVN software. Due to the fast-changing nature of underground mine development, this method could effectively create an MVN plan efficiently. This study could be extended by validating the numerical simulation results with the field-scale experimental study in an underground mine as a proof of concept. Several other additional parameters could also be studied such as adding push/pull airflow from the undercut level, or analyze the temperature-humidity control of the system.

References

- [1] Leyla Amiri, Seyed Ali Ghoreishi-Madiseh, Ferri P Hassani, and Agus P Sasmito. Friction factor correlation for airflow through broken rocks and its applications in mine ventilation. *International Journal of Mining Science and Technology*, 30(4):455–462, 2020.
- [2] Malcolm J McPherson. *Subsurface ventilation and environmental engineering*. Springer Science & Business Media, 2012.
- [3] LL Sloss. Assessing and managing spontaneous combustion of coal. *IEA Clean Coal Centre*, 2015.
- [4] C Özgen Karacan. Modeling and prediction of ventilation methane emissions of us longwall mines using supervised artificial neural networks. *International Journal of Coal Geology*, 73(3-4):371–387, 2008.
- [5] Leyla Amiri, Seyed Ali Ghoreishi-Madiseh, Ferri P Hassani, and Agus P Sasmito. Estimating pressure drop and ergun/forchheimer parameters of flow through packed bed of spheres with large particle diameters. *Powder Technology*, 356:310–324, 2019.
- [6] Jarosław Brodny and Magdalena Tutak. Applying computational fluid dynamics in research on ventilation safety during underground hard coal mining: A systematic literature review. *Process Safety and Environmental Protection*, 2021.

- [7] Ting Xiang Ren and JS Edwards. Three-dimensional computational fluid dynamics modelling of methane flow through permeable strata around a longwall face. *Mining technology*, 109(1):41–48, 2000.
- [8] Liming Yuan and Alex C Smith. Numerical study on effects of coal properties on spontaneous heating in longwall gob areas. *Fuel*, 87(15-16):3409–3419, 2008.
- [9] Jian-rang Zhang, Chun-qiao Wang, and Ding-wen Dong. Numerical simulation study of gob air leakage field and gas migration regularity in downlink ventilation. *Journal of Coal Science and Engineering (China)*, 17(3):316–320, 2011.
- [10] Yunzhuo Li, Hetao Su, Huaijun Ji, and Wuyi Cheng. Numerical simulation to determine the gas explosion risk in longwall goaf areas: A case study of xutuan colliery. *International Journal of Mining Science and Technology*, 30(6):875–882, 2020.
- [11] Jian Zhang, Jingyu An, Zhihui Wen, Kaixuan Zhang, Rongkun Pan, and Nahid Akter Al Mamun. Numerical investigation of coal self-heating in longwall goaf considering airflow leakage from mining induced crack. *Process Safety and Environmental Protection*, 134:353–370, 2020.
- [12] Saqib Ahmad Saki, Jürgen F Brune, and Muhammad Usman Khan. Optimization of gob ventilation boreholes design in longwall mining. *International Journal of Mining Science and Technology*, 30(6):811–817, 2020.
- [13] Gabriel S Esterhuizen and C Ozgen Karacan. A methodology for determining gob permeability distributions and its application to reservoir modeling of coal mine longwalls. 2007.
- [14] Jian Zhang, Hongtu Zhang, Ting Ren, Jianping Wei, and Yuntao Liang. Proactive inertisation in longwall goaf for coal spontaneous combustion control—a CFD approach. *Safety science*, 113:445–460, 2019.

- [15] Rao Balusu, Patrick Humpries, Paul Harrington, Michael Wendt, and Sheng Xue. Optimum inertisation strategies. *The QCO/DME Coal Industry Safety Conference*, page 7, 2002.
- [16] Ting Xiang Ren, Rao Balusu, and Patrick Humphries. Development of innovative goaf inertisation practices to improve coal mine safety. 2005.
- [17] Ting Xiang Ren and Rao Balusu. Proactive goaf inertisation for controlling longwall goaf heatings. *Procedia Earth and Planetary Science*, 1(1):309–315, 2009.
- [18] Ting Ren and Rao Balusu. The use of CFD modelling as a tool for solving mining health and safety problems. 2010.
- [19] Yingke Liu, Sihua Shao, Xinxin Wang, Lipeng Chang, Guanglei Cui, and Fubao Zhou. Gas flow analysis for the impact of gob gas ventholes on coalbed methane drainage from a longwall gob. *Journal of Natural Gas Science and Engineering*, 36:1312–1325, 2016.
- [20] Xiaowei Li, Chaojie Wang, Yujia Chen, Jun Tang, and Yawei Li. Design of gas drainage modes based on gas emission rate in a gob: a simulation study. *Arabian Journal of Geosciences*, 11(16):1–12, 2018.
- [21] Ting Xiang Ren. CFD modelling of longwall goaf gas flow to improve gas capture and prevent goaf self-heating. *Journal of Coal Science and Engineering (China)*, 15(3):225–228, 2009.
- [22] Michel J-G Sylvestre. Heating and ventilation study of inco’s creighton mine. 1999.
- [23] Seyed Ali Ghoreishi-Madiseh, Agus P Sasmito, Ferri P Hassani, and Leyla Amiri. Performance evaluation of large scale rock-pit seasonal thermal energy storage for application in underground mine ventilation. *Applied Energy*, 185:1940–1947, 2017.

- [24] Kayode M Ajayi, Khosro Shahbazi, Purushotham Tukkaraja, and Kurt Katzenstein. Prediction of airway resistance in panel cave mines using a discrete and continuum model. *International Journal of Mining Science and Technology*, 29(5):781–784, 2019.
- [25] Zhongwei Wang, Ting Ren, Liqiang Ma, and Jian Zhang. Investigations of ventilation airflow characteristics on a longwall face—a computational approach. *Energies*, 11(6):1564, 2018.
- [26] Y Pan, R Bhargava, A Jha, P Tukkaraja, K Shahbazi, K Katzenstein, and D Loring. An investigation of the effects of particle size, porosity, and cave size on the airflow resistance of a block/panel cave. In *Proceedings of the 11th International Mine Ventilation Congress*, pages 82–91. Springer, 2019.
- [27] Ang Liu, Shimin Liu, Gang Wang, and Derek Elsworth. Predicting fugitive gas emissions from gob-to-face in longwall coal mines: Coupled analytical and numerical modeling. *International Journal of Heat and Mass Transfer*, 150:119392, 2020.
- [28] Donald A Nield, Adrian Bejan, et al. *Convection in porous media*, volume 3. Springer, 2006.
- [29] PH Agson-Gani, L Amiri, SA Ghoreishi Madiseh, S Poncet, FP Hassani, and AP Sasmito. Integration of conjugate porous media model into mine ventilation network software. In *Mine Ventilation*, pages 47–55. CRC Press, 2021.

Chapter 4

Thermal and Hydraulic Analysis of a Novel Double-Pipe Geothermal Heat Exchanger with a Controlled Fractured Zone at the Bottom of the Well

Contents

| | | |
|-----|----------------------------------|----|
| 4.1 | Introduction | 43 |
| 4.2 | Model Description | 47 |
| 4.3 | Results and Discussion | 58 |
| 4.4 | Conclusion | 64 |

Preface (Linking Paragraphs)

Similar to the previous chapter, this chapter also talks about the effect of conjugate porous media. Compared to the previous chapter in which the model was in an underground mine drift, the porous media has now been implemented in a geothermal heat exchanger to improve the heat performance of the system. Thus, additional conservation of energy is considered. The porous zone is also different than Chapter 3, which is based on the derivation of the packed rock bed. In this chapter, the porous zone formation emulates a tree-like network caused by the hydraulic fracturing process. Hence, the fractal theory was implemented. The short version of this article was presented at the International Conference on Applied Energy 2021:

Agson-Gani, P. H., Zueter, A. F., Ghoreishi-Madiseh S. A., Kurnia, J. C., Sasmito, A. P. (2020). Development of a Novel Double-Pipe Heat Exchanger with a Controlled Fractured Zone at the Bottom of the Well: Thermal and Hydraulic Analysis, 12th International Conference on Applied Energy (ICAE2020), Virtual, 2020.

Later, the substantial extended version was submitted to the special issue of Applied Energy Journal:

Agson-Gani, P. H., Zueter, A. F., Xu, M., Ghoreishi-Madiseh S. A., Kurnia, J. C., Sasmito, A. P. (2021). Thermal and hydraulic analysis of a novel double-pipe geothermal heat exchanger with a controlled fractured zone at the well bottom, submitted to the special issue of Applied Energy Journal, 2021, under review.

Abstract

This study introduces a novel concept of semi closed-loop double-pipe heat exchangers with a controlled fractured zone at the well bottom to improve the geothermal heat extraction. The proposed model is benefitted from the reliable design of a double-pipe and the higher heat extraction rate of open geothermal systems. A conjugate mathematical model is developed and validated to simulate geothermal heat extraction, while the fractured zone is calculated by implementing the fractal theory. The results suggest that the

proposed model can significantly improve the heat extraction rate and thermal power by up to more than 90%, with an additional 28% of pumping power. Several operating parameters of the fractured zone are also evaluated, indicating that the increase of the heat extraction rate compared to the closed-loop model was within the range of 48-144% based on its design. Overall, this novel design shows the potential to improve the thermal and hydraulic performances of the conventional closed-loop geothermal system.

4.1 Introduction

Geothermal heat is one of the preferred sources of renewable energy to meet the world's energy demand because of its economic, environmental and social benefits [1]. Low and medium enthalpy geothermal heat can be extracted using a geothermal heat exchanger (GHE), which collects the earth's thermal energy and brings it to the ground surface using a closed-loop system of single-phase heat transfer fluid (HTF) using a double-pipe design. The double-pipe geothermal heat exchanger (DPGHE) works by drilling a borehole and sinking two coaxial cylindrical tubes that consist of an inner tube and an outer tube inside the borehole. The system works by pumping the water through the inlet, and the water is then heated by the geothermal heat, where the heated water is later extracted from the outlet. The extracted energy could be further utilized for direct use applications, space heating/cooling or power generation [2]. Geothermal energy is sustainable and could be collected in any weather condition. Due to its renewable nature, extraction of the geothermal heat, as well as the improvement of the GHE, are of paramount importance.

Several heat exchanger methods have been studied by many researchers, such as U-tube and double-pipe heat exchanger (DPHE). In 1992, Morita et al. [3, 4] conducted the earliest experimental study of DPHE utilization on geothermal energy extraction in Hawaii. In 2004, Kujawa et al. [5] analytically studied the feasibility of refurbishing abandoned oil wells into a GHE. In addition, Templeton et al. [6] developed a numerical heat transfer model based on the previous study to determine the reliability and accuracy

of the proposed model. Constant inlet temperature and constant power output concepts are applied to find the effect of a multitude of parameters on the proposed model. Bu et al. [7] investigated the feasibility of extracting the geothermal energy from the gas wells. In addition, Cheng et al. [8] is the earliest to optimize the performance of the wellbore from retrofitted oil wells by modifying the geometry of the well. They introduced a well bottom curvature design to further improve the heat transfer performance of the DPGHE. Pokhrel et al. [9] conducted both experimental investigation and numerical simulation to elevated the heat performance potential of a 500 m deep double-pipe heat exchanger in Japan. They analyzed the temperature of the ground after the simulation which indicating that it took 456 h for the temperature-depleted surrounding ground to recover 86% of its original temperature. Pokhrel et al. [10] also developed a semi-conjugate reduced order numerical model of borehole heat exchanger coupled with a solar thermal system. This model allows a computationally efficient simulation of such system. Ghoreishi-Madiseh et al. [11] solved a 1D transient heat equation with a constant temperature boundary. Later, they extended the single borehole solution to double and N-by-N boreholes with the use of symmetry, namely thermal superposition principle. Hefni et al. [12] extended Ghoreishi-Madiseh's paper by working on a transient heat conduction problem with a time-dependent boundary to analyze the effect of the seasonal changes in thermal energy storage systems.

At the same time, numerous techniques have been introduced to enhance heat transfer performance in engineering practices. Primarily, the techniques based on increasing the heat transfer area or convection coefficient, leading to the enhancement of the turbulence, secondary flow creation, and swirls flow inducement. Some of the methods are driven by introducing additional structures to the system based on the applications.

For instance, Alkam and Al-Nimr [13] considerably improved the heat performance of DPHE by inserting porous substrates at both sides of the innertube wall; while also increasing the pressure drop within the heat exchanger. Similar results were also analyzed by Lu et al. [14], where they improved the heat transfer rate as well as the pressure drop

by adding additional metal foam into a heat exchanger. The effect of baffle arrangement on the heat transfer rate in a 3D enclosure using multiphase nanofluid was investigated by Peiravi et al. [15]. The results indicated that the Nusselt number can be changed by 57% based on the baffles configuration. Ghoreishi-Madiseh et al. [16] analyzed the heat performance of an open-pit filled with a massive amount of waste rocks. The open-pit turned into seasonal thermal energy storage, which helps ventilate the underground mine below the pit. The utilization of fin arrangements are also widely used. Asgari et al. [17] accelerated the solidification process of phase change material by inserting branch-shaped fins to the heat exchanger. Alizadeh et al. [18] also utilized curved fins to optimized the solidification process within the latent heat thermal energy storage system. Thus, it was evident that increasing the heat transfer area or convection coefficient through additional structures could improve the heat transfer rate.

On geothermal heat exchanger application, geothermal heat extraction processes are closely related to the formation of a porous medium in the form of fractured networks. Especially, in the enhanced geothermal system (EGS), where a hydraulic stimulation process is used to create fractures in the subsurface rock [19, 20, 21]. These fractured networks act as additional flow channels for the HTF and simultaneously improve the effectiveness of the heat transfer mechanism in the system [22]. EGS is created to seek alternative solutions for extracting natural geothermal reservoir, which is limited. Instead of extracting fluid from the natural reservoir, EGS pumps water into the reservoir to make the system more sustainable. EGS works by inserting an injection well with a depth of 3-10 km below the surface. High-pressure fluids at a high flow rate is then injected to the subsurface rock formation. The fluid fractures the underlying rock and creates permeable channels where the water circulates and exchanges heat extraction from the rock [23]. Lastly, a production well is drilled to extract the heated water. This method makes full use of the improvement of the heat transfer of the porous medium and an increasing area of contact between the fluid and the ground, enhancing the system's performance. In 2014, Chen and Jiang [19] numerically simulated conventional EGS in various layouts and studied

its effect on heat performance. In 2018, Song et al. [24] proposed a novel EGS system by modifying the conventional EGS with added multilateral wells to extract more heat from the hot dry rock. The multilateral wells widened the contact area between the HTF and the solid domain, which resulted in an enhancement of heat extraction. Increasing the contact area is also considered a passive heat transfer enhancement method because the heat transfer rate is directly proportional to the size of the surface area in which the heat is being conducted. In 2021, Wang et al. [25] proposed a modified EGS by introducing a multilateral-well DPGHE which constructs lateral wellbores at the well bottom. This design allows water to spend most of the thermal process in the lateral wellbores, which is placed at the hottest part of the system. Shi et al. [26] extended the previous study by numerically investigating a multilateral well EGS and emphasizing the complex hydraulic and natural fractures of the ground between the injection well and production well. They studied 11 cases of different complex fracture networks and analyzed the contribution to the heat extraction in the system.

Fluid flow and heat transfer in the porous medium has been studied extensively [27, 28] and abundant theoretical studies have been conducted to advance mathematical modeling of transport phenomena in fractured medium or reservoirs. Since the development of the fractured zone in the geothermal system is done by hydraulic fracturing of the ground, the fracture formation resembles tree-like fractal networks based on the fractal theory. Thus, one of the most effective modeling approaches is to apply the fractal theory; the success of this theory was attributed to self-similar geometry, which occurs naturally and synthetically in fractured medium [29, 30]. While some fractal resistance models were developed based on the fractal characteristics of porous media and the pore-throat framework for capillaries [31, 32, 33], the tree-like fractal networks have also received considerable attention for decades because of their high transport efficiency and plentiful natural and man-made structures [34, 35, 36]. Owing to the tree-like fractal theory, numerous studies derived the permeability in various types of media, and fractal branches

[37, 38, 39, 40], which in turn would determine the value of viscous resistance. The determination of inertial resistance, however, has not been explored thoroughly.

In EGS, the fracture zone between the injection well and the production well has to be connected through fractured networks, providing a flow channels for the HTF. However, developing this network by hydraulic fracture process is considered to be challenging and expensive [41]. Therefore, the present study introduced a novel semi closed-loop DPGHE with a controlled fractured zone at the well bottom. Unlike the conventional EGS, the fractured zone in the proposed model is more localized and placed beneath the well. The system utilizes the fractured zone as the flow channels for the HTF and improves the heat transfer rate while keeping the process with only one coaxial well. This concept is numerically modeled based on the conservation of mass, momentum and energy. The based closed-loop DPGHE is validated against the experimental data before modifying the model with a fractured zone. In this paper, we also apply a fractal tree-like network model over the areas with fractured rocks, in which both viscous and inertial resistance coefficients are derived from the fractal geometry theory. Additionally, comparisons between the semi closed-loop model and the conventional closed-loop system are shown. Finally, the influence of key operating parameters in the GHE system, such as geometrical and physical properties of the fractured zone, are studied.

4.2 Model Description

This paper aims to present the novel semi-closed loop geothermal heat exchanger based on a double-pipe design. The novel semi-closed loop DPGHE system was made by drilling a vertical well and hydraulically fracturing the bottom part of the well. Once the fractured zone is created, a double-pipe is installed consisting of a conductor case and an insulated inner pipe. This double-pipe will separate the downward injected flow from the inlet and the upward extracted water to the outlet. Then, the surrounding part of the well is grouted to prevent liquid from seeping out of the well. Since there is no

previous study and experiment that emulate the proposed model, a proper validation for the based closed-loop DPGHE of a similar study is needed. Thus, a numerical simulation of the semi closed-loop DPGHE will be compared against the experimental data of closed-loop DPGHE in Hawaii [3, 4]. The illustrations of both models are shown in Fig. 4.1. Once the semi-closed loop model is validated, a computational fluid dynamics (CFD) simulation of closed-loop DPGHE is converted into semi closed-loop DPGHE by changing the bottom part of the well into a controlled fractured zone. Due to this additional feature, the water seeps into the fractured zone before flowing upward to the outlet.

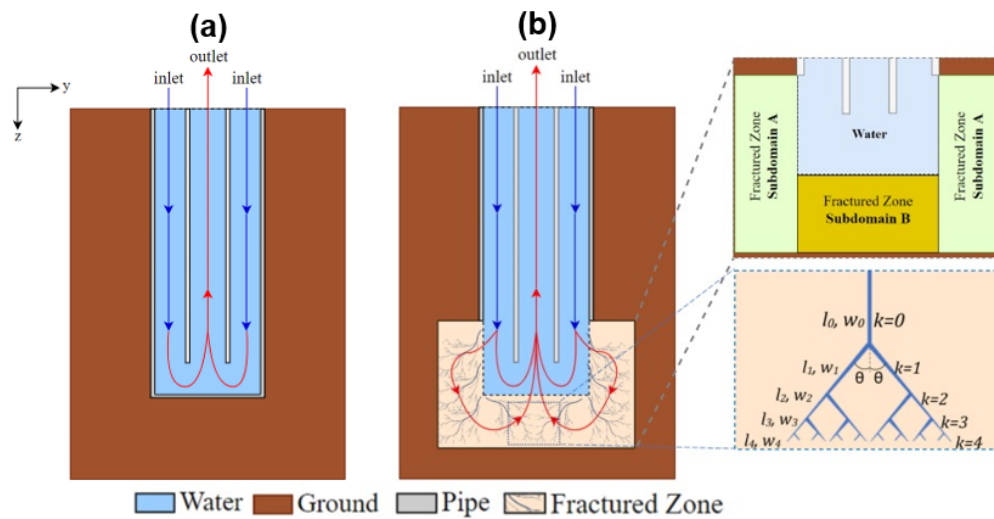


Figure 4.1: Not-to-scale side view illustrations of: (a) closed-loop DPGHE; (b) semi closed-loop model DPGHE.

Figure 4.2 provides comprehensive information and illustration of the semi closed-loop DPGHE geometry, and Table 4.1 shows the thermophysical properties of the system. The computational domain was developed as a 2-dimensional (2D) axisymmetric model with the size of 50×930 m (Width \times Height). The pipes, cement and the ground are assumed to be homogeneous and isotropic and the temperature-dependent properties of the water are shown in Fig. 4.3. According to the difference in fractal directions, the controlled fractured zone is divided into two parts, namely subdomain A and B, as shown

in Fig. 4.1(b). This division was made to enable the utilization of fractal tree-like network model.

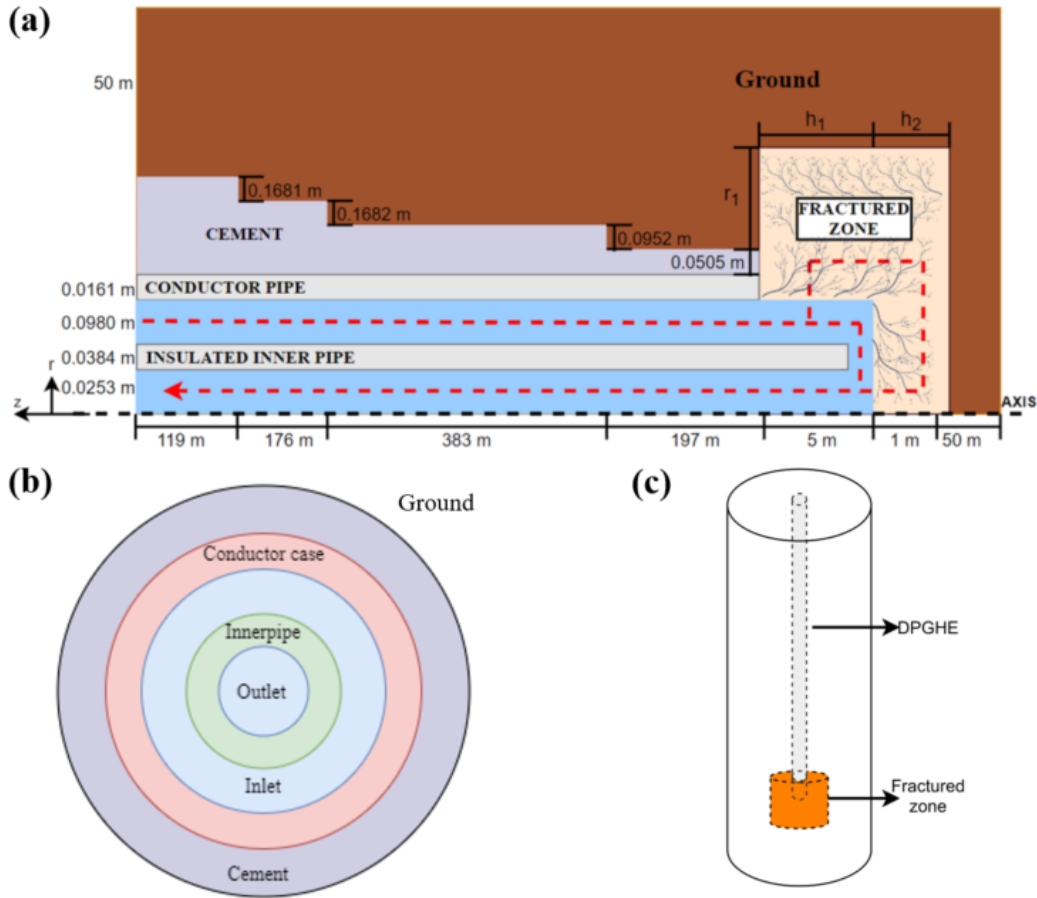


Figure 4.2: Not-to-scale semi closed loop DPGHE: (a) computational domain (rotated 90°); (b) A-A cross-cut; (c) isometric view.

Table 4.1: Thermophysical properties of the materials used in DPGHE.

| Material | ρ [kg/m^3] | c_p [$J/(kgK)$] | k [$W/(mK)$] |
|----------------|-----------------------|-----------------------|------------------|
| Water | Temperature dependent | Temperature dependent | |
| in Fig. 4.3(a) | 4182 | | |
| in Fig. 4.3(b) | | | |
| Inner pipe | 5240 | 310 | 0.06 |
| Conductor pipe | 7850 | 470 | 46.1 |
| Cement | 1830 | 1900 | 0.99 |
| Rock | 3050 | 870 | 1.6 |

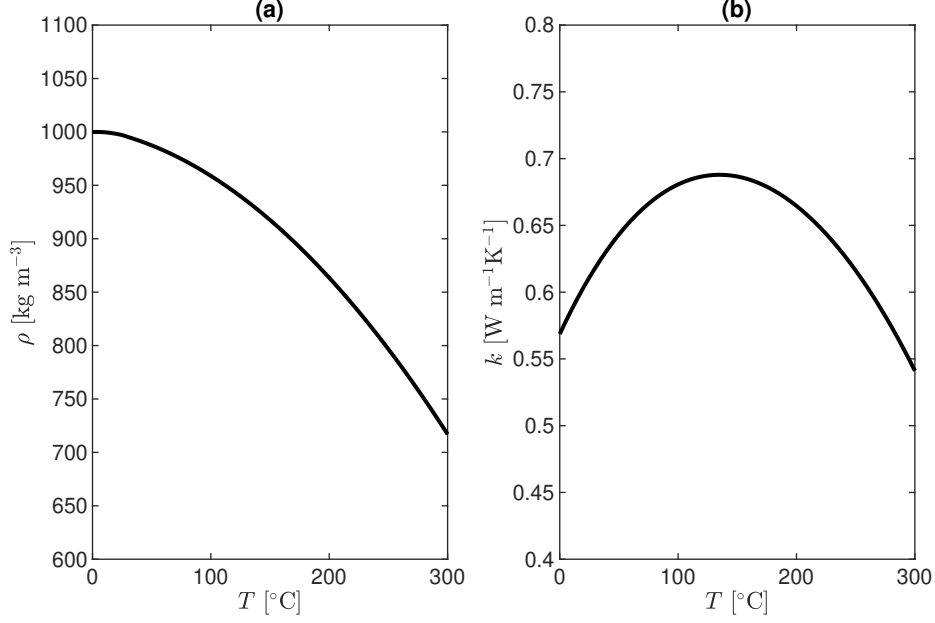


Figure 4.3: Temperature dependent thermophysical properties of the water: (a) density; (b) thermal conductivity (data from [42]).

4.2.1 Governing equations

The DPGHE system consists of three main domains, which are: (a) the solid domains, which comprised of the ground, cement, and cases; (b) the flow of the water in the pipe; and (c) the seepage of the water flowing from the DPGHE to the controlled fractured zone.

Solid domain

In the solid domains, the conduction heat transfer mechanism is applied as follows [43]:

$$\frac{\partial}{\partial t}(\rho c_p T) = \frac{1}{r} \frac{\partial}{\partial r} \left(r k \frac{\partial T}{\partial r} \right) + \frac{\partial}{\partial z} \left(k \frac{\partial T}{\partial z} \right) \quad (4.1)$$

where ρ is the density, c_p is the specific heat, T is the temperature, k is the thermal conductivity, and r and z are the radial and axial directions in cylindrical coordinates.

The fluid zones are divided into the flow in the DPHE and in the controlled fractured zone:

Double-pipe heat exchanger

The DPHE consist of two coaxial pipes which pump the water from the annulus and extract the water by the outlet in the innerpipe. The flow of the water is assumed to be single-phase flow and turbulent flow due to the high Reynolds number. Furthermore, the properties of the water change based on the temperature as shown in Fig. 4.3. Therefore, the governing equations of an unsteady and axisymmetric flow can be written in the cylindrical coordinates. The continuity equation is given as [43]:

$$\frac{\partial}{\partial t}(\rho_f) + \frac{\partial}{\partial z}(\rho_f \mathbf{U}_z) + \frac{\partial}{\partial r}(\rho_f \mathbf{U}_r) + \frac{\rho_f \mathbf{U}_r}{r} = 0 \quad (4.2)$$

The momentum equation in the axial and radial directions are as follow:

$$\begin{aligned} \frac{\partial}{\partial t}(\rho_f \mathbf{U}_z) + \frac{1}{r} \frac{\partial}{\partial z}(r \rho_f \mathbf{U}_z \mathbf{U}_z) + \frac{1}{r} \frac{\partial}{\partial r}(r \rho_f \mathbf{U}_r \mathbf{U}_z) = -\frac{\partial p}{\partial z} + \\ \frac{1}{r} \frac{\partial}{\partial z} \left[r \mu_f \left(2 \frac{\partial \mathbf{U}_z}{\partial z} - \frac{2}{3} \left(\frac{\partial \mathbf{U}_z}{\partial z} + \frac{\partial \mathbf{U}_r}{\partial r} + \frac{\mathbf{U}_r}{r} \right) \right) \right] + \\ \frac{1}{r} \frac{\partial}{\partial r} \left[r \mu_f \left(\frac{\partial \mathbf{U}_z}{\partial r} + \frac{\partial \mathbf{U}_r}{\partial z} \right) \right] + \rho_f \mathbf{g} \end{aligned} \quad (4.3)$$

$$\begin{aligned} \frac{\partial}{\partial t}(\rho_f \mathbf{U}_r) + \frac{1}{r} \frac{\partial}{\partial z}(r \rho_f \mathbf{U}_z \mathbf{U}_r) + \frac{1}{r} \frac{\partial}{\partial r}(r \rho_f \mathbf{U}_r \mathbf{U}_r) = -\frac{\partial p}{\partial r} \\ + \frac{1}{r} \frac{\partial}{\partial z} \left[r \mu_f \left(\frac{\partial \mathbf{U}_r}{\partial z} + \frac{\partial \mathbf{U}_z}{\partial r} \right) \right] \\ + \frac{1}{r} \frac{\partial}{\partial r} \left[r \mu_f \left(2 \frac{\partial \mathbf{U}_r}{\partial r} - \frac{2}{3} \left(\frac{\partial \mathbf{U}_z}{\partial z} + \frac{\partial \mathbf{U}_r}{\partial r} + \frac{\mathbf{U}_r}{r} \right) \right) \right] \\ - 2 \mu_f \frac{\mathbf{U}_r}{r^2} + \frac{2}{3} \frac{\mu_f}{r} \left(\frac{\partial \mathbf{U}_z}{\partial z} + \frac{\partial \mathbf{U}_r}{\partial r} + \frac{\mathbf{U}_r}{r} \right) + \rho_f \frac{\mathbf{U}_z^2}{r} \end{aligned} \quad (4.4)$$

Lastly, the energy equation are written as:

$$\frac{\partial}{\partial t}(\rho_f c_{p,f} T) + \rho_f c_{p,f} \left(\mathbf{U}_r \frac{\partial T}{\partial r} + \mathbf{U}_z \frac{\partial T}{\partial z} \right) = \frac{1}{r} \frac{\partial}{\partial r} \left(r k \frac{\partial T}{\partial r} \right) + \frac{\partial}{\partial z} \left(k \frac{\partial T}{\partial z} \right) \quad (4.5)$$

where \mathbf{U} is the fluid velocity, p is the pressure, μ is the dynamic viscosity, \mathbf{g} is the gravity. The subscripts f and t are fluid and turbulent, respectively.

The current study employs the standard k-epsilon turbulence model with scalable wall treatment. The model incorporates two equations that solves for turbulent kinetic energy κ , and its rate of dissipation ϵ , which given by [44]:

$$\frac{\partial}{\partial t}(\rho \kappa) + \nabla \cdot (\rho \kappa \mathbf{U}) = \nabla \cdot \left[\left(\mu + \frac{\mu_t}{\sigma_\kappa} \right) \nabla \kappa \right] + G_\kappa - \rho \epsilon \quad (4.6)$$

$$\frac{\partial}{\partial t}(\rho \epsilon) + \nabla \cdot (\rho \epsilon \mathbf{U}) = \nabla \cdot \left[\left(\mu + \frac{\mu_t}{\sigma_\epsilon} \right) \nabla \epsilon \right] + C_{1\epsilon} G_\kappa - C_{2\epsilon} \rho \frac{\epsilon^2}{\kappa} \quad (4.7)$$

where σ_κ and σ_ϵ are the Prandtl numbers for κ and ϵ , respectively. G_κ is the turbulent kinetic energy due to the mean velocity gradients. The turbulent viscosity μ_t is formulated by combining κ and ϵ as follows [45]:

$$\mu_t = \rho C_\mu \frac{\kappa^2}{\epsilon} \quad (4.8)$$

where $C_{1\epsilon}$, $C_{2\epsilon}$, and C_μ are constants.

Controlled fractured zone

At the well bottom, a controlled fracture zone is made with hydraulic fracture process. This process creates a dendritic fractured zone which consists of broken rocks formation and water as the heat transfer fluid, as shown in Fig. 4.1(b). The flow that circulates in the porous zone is assumed to be laminar and unsteady. The local thermal equilibrium (LTE) is implemented to solve the energy equation of the porous medium. The concept of LTE is assuming that the temperature within each elementary volume between the

water and broken rock as equal [46]. Based on the LTE assumption, the followings are the governing equations for flow through the controlled fractured zone. The continuity equation are given as follows [43]:

$$\frac{\partial}{\partial t}(\varepsilon\rho_f) + \frac{\partial}{\partial z}(\rho_f\mathbf{u}_z) + \frac{\partial}{\partial r}(\rho_f\mathbf{u}_r) + \frac{\rho_f\mathbf{u}_r}{r} = 0 \quad (4.9)$$

The conservation of momentum in the axial and radial directions, respectively, are written as:

$$\begin{aligned} \frac{\partial}{\partial t}(\rho_f\mathbf{u}_z) + \frac{1}{r}\frac{\partial}{\partial z}(r\rho_f\mathbf{u}_z\mathbf{u}_z) + \frac{1}{r}\frac{\partial}{\partial r}(r\rho_f\mathbf{u}_r\mathbf{u}_z) = -\frac{\partial p}{\partial z} + \\ \frac{1}{r}\frac{\partial}{\partial z}\left[r\mu_f\left(2\frac{\partial\mathbf{u}_z}{\partial z} - \frac{2}{3}\left(\frac{\partial\mathbf{u}_z}{\partial z} + \frac{\partial\mathbf{u}_r}{\partial r} + \frac{\mathbf{u}_r}{r}\right)\right)\right] + \\ \frac{1}{r}\frac{\partial}{\partial r}\left[r\mu_f\left(\frac{\partial\mathbf{u}_z}{\partial r} + \frac{\partial\mathbf{u}_r}{\partial z}\right)\right] + S_D + S_F + \rho_f\mathbf{g} \end{aligned} \quad (4.10)$$

$$\begin{aligned} \frac{\partial}{\partial t}(\rho_f\mathbf{u}_r) + \frac{1}{r}\frac{\partial}{\partial z}(r\rho_f\mathbf{u}_z\mathbf{u}_r) + \frac{1}{r}\frac{\partial}{\partial r}(r\rho_f\mathbf{u}_r\mathbf{u}_r) = -\frac{\partial p}{\partial r} \\ + \frac{1}{r}\frac{\partial}{\partial z}\left[r\mu_f\left(\frac{\partial\mathbf{u}_r}{\partial z} + \frac{\partial\mathbf{u}_z}{\partial r}\right)\right] \\ + \frac{1}{r}\frac{\partial}{\partial r}\left[r\mu_f\left(2\frac{\partial\mathbf{u}_r}{\partial r} - \frac{2}{3}\left(\frac{\partial\mathbf{u}_z}{\partial z} + \frac{\partial\mathbf{u}_r}{\partial r} + \frac{\mathbf{u}_r}{r}\right)\right)\right] \\ - 2\mu_f\frac{\mathbf{u}_r}{r^2} + \frac{2}{3}\frac{\mu_f}{r}\left(\frac{\partial\mathbf{u}_z}{\partial z} + \frac{\partial\mathbf{u}_r}{\partial r} + \frac{\mathbf{u}_r}{r}\right) + \rho_f\frac{\mathbf{u}_z^2}{r} \end{aligned} \quad (4.11)$$

Finally, the energy equation are written as:

$$\frac{\partial}{\partial t}(\rho_{eff}c_{p,eff}T) + \rho_{eff}c_{p,eff}\left(\mathbf{u}_r\frac{\partial T}{\partial r} + \mathbf{u}_z\frac{\partial T}{\partial z}\right) = \frac{1}{r}\frac{\partial}{\partial r}\left(rk_{eff}\frac{\partial T}{\partial r}\right) + \frac{\partial}{\partial z}\left(k_{eff}\frac{\partial T}{\partial z}\right) \quad (4.12)$$

where \mathbf{u} the superficial velocity, ε is the porosity, and subscript *eff* is the effective properties of water and rock. The S_D and S_F are the Darcy and Forchheimer terms which are given as [27]:

$$S_D = -\frac{\mu}{K}\mathbf{u} \quad (4.13)$$

$$S_F = -\beta\rho\mathbf{u}^2 \quad (4.14)$$

A fractal tree-like network model is implemented in the fractured zone which assumed to be isotropic. This fractal analysis was firstly proposed by Xu et al. [39], where a tree-shaped topology was considered in a two-dimensional space. An arithmetic mean of fracture permeability and porous matrix permeability was also calculated as the so-called effective permeability. In this study, we employ a similar model of a fractal tree-like network yet only examining the fracture permeability due to its fractured nature.

As schematically shown in Fig. 4.1(b), the fractal tree-like network initiates around the bottom of the DPGHE, where the first (parent) branch at level 0 splits into two (child) branches at level 1. The branch length and width at level i is denoted as l_i and w_i respectively. Here we assume that each parent branch will always generate two child branches of equal length and width at the next level with an angle 2θ apart. Owing to the fractal tree-like theory, the permeability K can be expressed as [39]:

$$K = \frac{w_0^3}{12W} \frac{L^2}{l_0^2} \frac{1 - n^{-\frac{1}{D_l}}}{1 - n^{-\frac{m+1}{D_l}}} \frac{1 - n^{\frac{3}{D_w} - \frac{1}{D_l} - 1}}{1 - n^{\left(\frac{3}{D_w} - \frac{1}{D_l} - 1\right)(m+1)}} \quad (4.15)$$

where $W, L, w_0, l_0, m, n, D_w, D_l$ are the domain width, domain length, width of the initial branch, length of the initial branch, number of branches, number of child branches, fractal dimension of the width, and fractal dimension of the length, respectively. However, to incorporate the mechanical damage during the hydraulic fracturing, a damage factor D is introduced. The viscous resistance coefficient α is therefore given by:

$$\alpha = \frac{1}{K \times \exp(D)} \quad (4.16)$$

where D is within the range from 0 to 1 based on the damage intensity. It is noted that this expression is the same as the inverse of the permeability presented in [40] but without the porous matrix.

In addition to the viscous resistance, the inertial resistance coefficient β , also known as non-Darcy or Forchheimer coefficient is also needed. We begin with the pressure drop ($\Delta P/L$) for kinetic energy loss associated with the inertial resistance, in which the friction factor in a rectangular duct is determined by [47]:

$$f = \frac{24}{Re_f} \left[1 - \frac{192}{S\pi^5} \sum_{j=1,3,5,\dots}^{\infty} \frac{\tanh(j\pi S/2)}{j^5} \right] \quad (4.17)$$

The ratio of the rectangular domain is denoted as S ; the Reynolds number can be written based on the fractal theory: $Re_f = \rho\tau\bar{d}v/(\varepsilon\mu)$, where the tortuosity τ for tortuous capillaries is defined in terms of the porosity ε :

$$\tau = \frac{1}{2} \left[1 + \frac{1}{2}\sqrt{1-\varepsilon} + \sqrt{1-\varepsilon} \frac{\sqrt{\left(\frac{1}{\sqrt{1-\varepsilon}} - 1\right)^2 + \frac{1}{4}}}{1 - \sqrt{1-\varepsilon}} \right], \quad (4.18)$$

and the averaged length \bar{d} is given by:

$$\bar{d} = \frac{d_0}{m+1} \frac{1 - n^{-\frac{1}{D_w}}(m+1)}{1 - n^{-\frac{1}{D_w}}} \quad (4.19)$$

As a result, the final expression of the inertial resistance coefficient β is calculated as:

$$\beta = \frac{12\mu\tau}{\rho\bar{d}^2v} \left[1 - \frac{192}{S\pi^5} \sum_{j=1,3,5,\dots}^{\infty} \frac{\tanh(j\pi S/2)}{j^5} \right] \quad (4.20)$$

4.2.2 Initial and boundary conditions

The initial and boundary conditions are based on the experimental data by Morita et al. [3]. Fig. 4.4(a) shows the temperature contour of the initial condition in the DPGHE system and the surrounding ground. The boundary conditions of the closed-loop DPGHE and semi closed-loop DPGHE systems are:

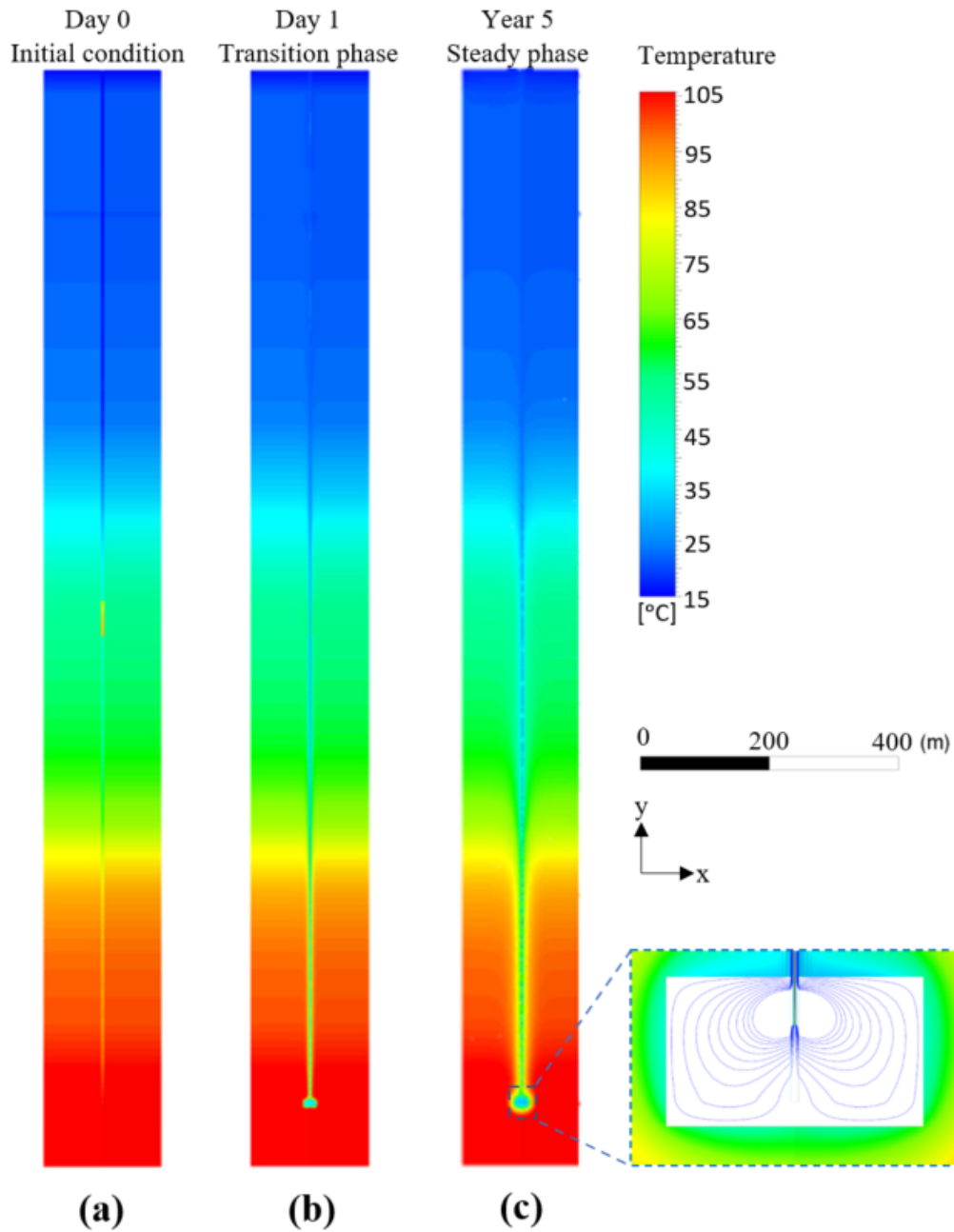


Figure 4.4: Temperature contour of semi closed-loop DPGHE at: (a) initial condition (Day 0); (b) transition phase (Day 1); (c) steady phase (Year 5).

- Axisymmetric: velocity and temperature along the axis of the symmetry (Fig. 4.2(a)) are given by

$$\frac{\partial \mathbf{U}_{axis}}{\partial r} = 0 \quad (4.21)$$

$$\frac{\partial T_{axis}}{\partial r} = 0 \quad (4.22)$$

- At the inlet: injection flow rate and temperature are set as constant. The injection temperature (T_{in}) is 303.15 K and the water flow rate (Q_{in}) is 0.00133 m³/s

$$T = T_{in} \quad (4.23)$$

$$\mathbf{U} = \mathbf{U}_{in} \quad (4.24)$$

- At the wall layer interface: no-slip condition and coupled heat transfer is applied.

$$\mathbf{U} = 0 \quad (4.25)$$

$$k_1 \frac{\partial T_1}{\partial n} = k_2 \frac{\partial T_2}{\partial n}; T_1 = T_2 \quad (4.26)$$

- At the surface: no-slip condition and atmospheric heat convection is applied.

$$\mathbf{U} = 0 \quad (4.27)$$

$$-k \frac{\partial T_{surface}}{\partial p} = h(T_{surface} - T_{atm}) \quad (4.28)$$

- At the outer domain wall: no-slip condition and the geothermal gradient is applied.

$$\mathbf{U} = 0 \quad (4.29)$$

$$T = T_{init} \quad (4.30)$$

- At the outlet: the pressure is set as 0, and zero heat flux is applied.

$$P = P_{out} = 0 \quad (4.31)$$

$$\mathbf{n} \cdot \nabla T = 0 \quad (4.32)$$

4.2.3 Numerical simulations

ANSYS 2019 R3 was used to create and mesh the computational domain. A two-dimensional axisymmetric model is used for the simulation (Fig. 4.2(a)), and it gives an accurate result with less computational power. The mesh-independent solution was ensured by conducting several tests, with a final mesh size of 3×10^5 elements. The governing equations with the initial and boundary conditions were computed using the finite volume method by ANSYS Fluent. User-defined functions (UDFs) were used to define the initial temperature conditions and temperature gradient applied at the outer domain of the wall. The model was solved with the Semi-Implicit Pressure-Linked Equation (SIMPLE) algorithm and the second-order upwind discretization schemes for all conservation equations. The residual of 1×10^{-6} was set as the convergence criteria for all equations.

4.3 Results and Discussion

4.3.1 Model validation

The CFD model was validated against the field data results of GHE in Hawaii [3, 4]. The entire experiment duration was 7 days, and all the control systems were considered to work properly throughout the test. At the early stage of the test, the residue in the GHE system, such as scale and cement, flowed out of the system by flushing two filters installed in the production line. This process was repeated until the amount of the particles decreased and became negligible to be flushed. After 1.8 days of simulation, an unexpected power failure occurred, leading to the closure of inlet and outlet valves to halt the circulation. This issue resulted in the fluctuating data presented and pointed in Fig. 4.5. However, this problem did not affect the success of this experiment as the temperature and pressure parameters were showing similar outcomes with the predicted results.

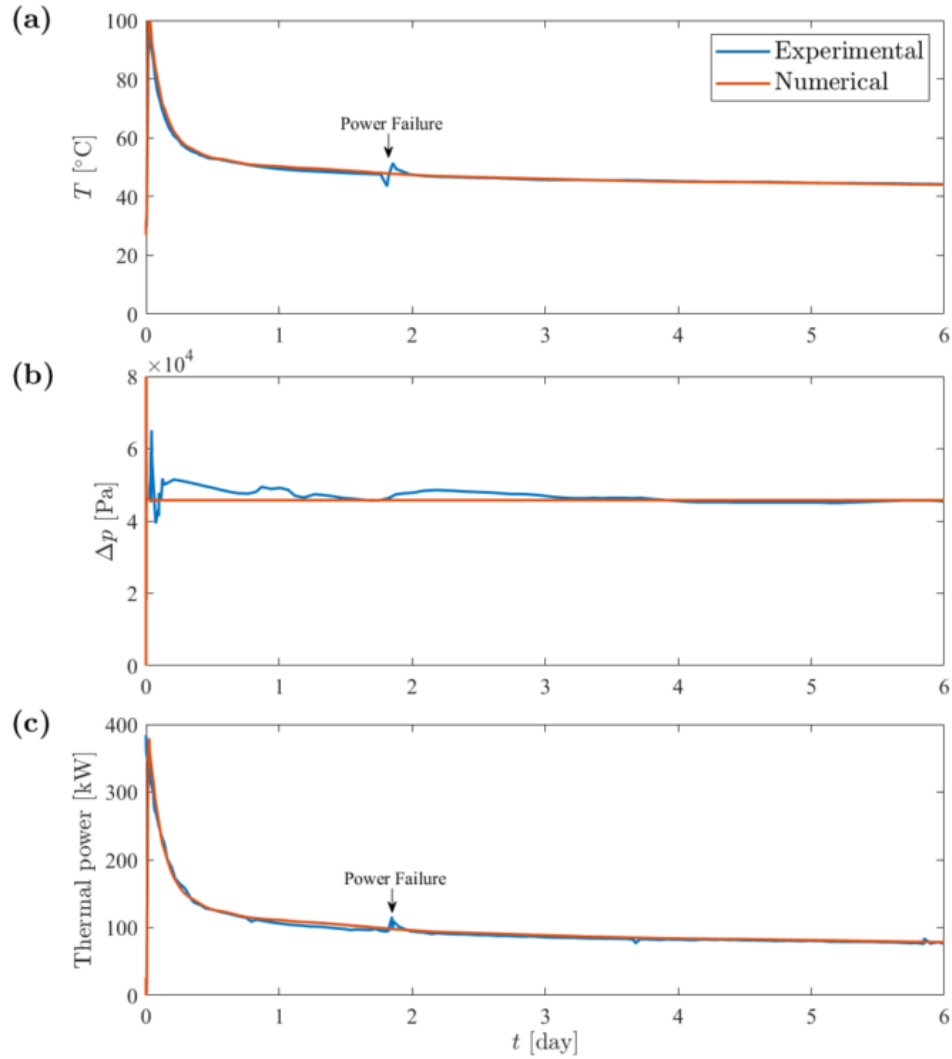


Figure 4.5: Validation of the numerical model against the experimental measurement [3, 4]: (a) temperature difference between inlet and outlet; (b) pressure drop; (c) thermal power.

In regards of the numerical simulation, the UDFs were compiled into the model to simulate the initial ground temperature and geothermal gradient based on the actual field data. The numerical model used output temperature, pressure drop and thermal power as the parameters to prove the validity of the simulation. The goal of this validation is to ensure the validity of the closed-loop CFD model, which will be modified into

semi closed-loop model. Good agreements are shown between the numerical model and experimental results, which are shown in Fig. 4.5.

4.3.2 Comparison of the closed-loop heat exchanger and the semi closed-loop heat exchanger

It is important to disclose the increase of the thermal power generated and the needed pumping power between the conventional closed-loop model and the proposed semi closed-loop model. These indicators were chosen to assess the practicality of the proposed model. The time-dependent output temperature in Fig. 4.6(a) shows the comparison between both models.

Initially, the DPGHE was draining the initial water in the system; it is observed that the temperature reaches a plateau and drops rapidly in the first few hours due to the high temperature difference between the water and the ground. This temperature contour of this transition process is shown in Fig. 4.4(b), where the flow starts getting steady. Afterward, the water cools down, the transient rate of change of the output temperature decrease as well, and the output temperature maintains a steady trend, as shown in Fig. 4.4(c). It shows that the temperature trend of the semi closed-loop GHE system is always higher than the closed loop's trend. By implementing the semi closed-loop model, the output temperature increases by 4.3 °C which is a 92.8% increase of temperature difference between injection and extracted temperature. However, due to the water that is flowing through a fractured zone that has higher resistances compare to the pipe; thus, an increase of pressure drop by 11.7% is caused by the proposed model, as shown in Fig. 4.6(b).

The flow of the water in the fractured zone could be seen in Fig. 4.4(c). Subsequently, the thermal power generated and the pumping power of both models are compared. The thermal power generated is a function of the water mass flow rate and the difference between the injection temperature and the output temperature, while the pumping power

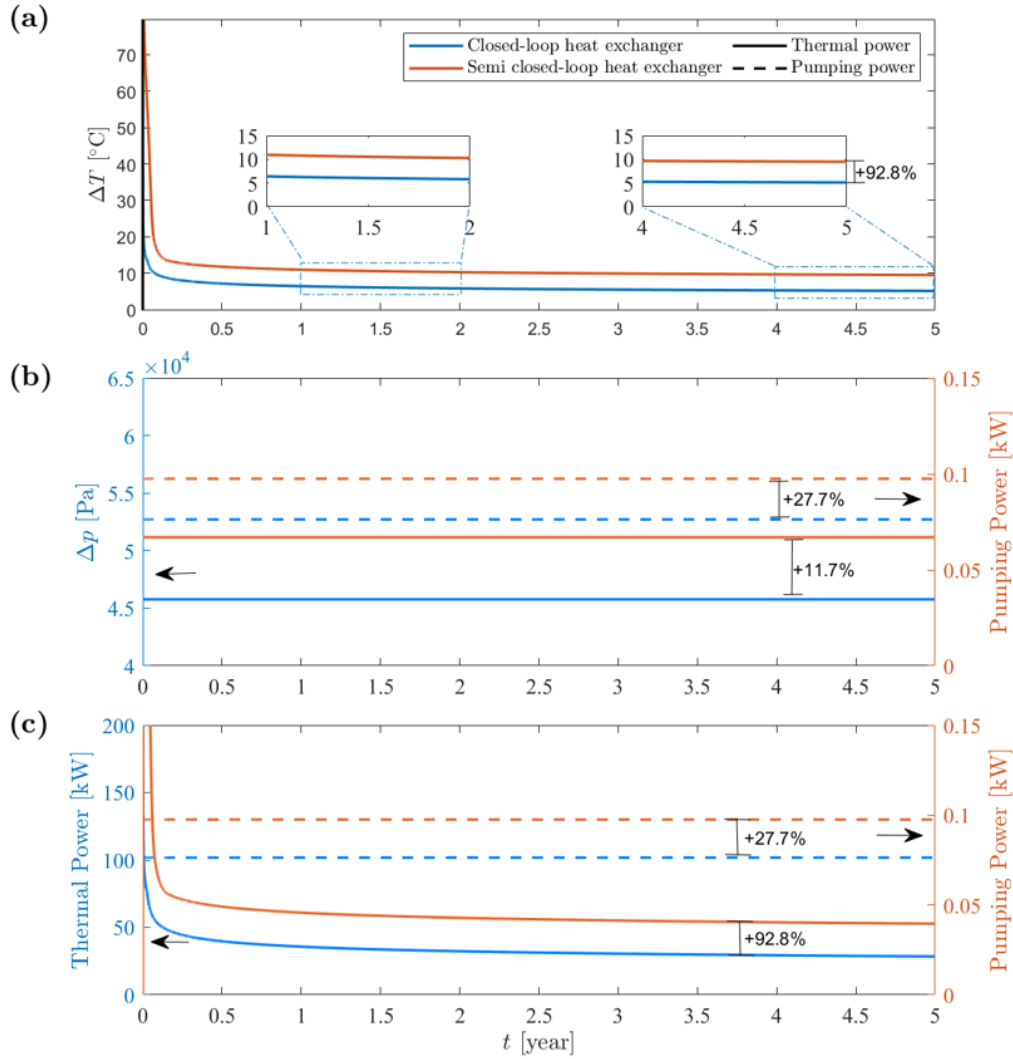


Figure 4.6: Comparison of the closed-loop heat exchanger and the proposed semi closed-loop heat exchanger, in terms of: (a) temperature difference between inlet and outlet; (b) pressure drop; (c) thermal power and pumping power.

takes pressure drop and water flow rate into account. According to Fig. 4.6(c), when the system is already stabilized, the proposed model generates 49.8 [kW] thermal power with the requirement of 0.1 [kW] for its pumping power. These results indicate that the proposed model generates 92.8% more thermal power due to the increase of the temperature in the water. However, the pumping power needed is also increased by 27.7% as a result of an increase in the pressure drop. Based on the comparison of the needed and generated

power, the proposed model is considered to enhance the performance of the heat transfer in the system.

4.3.3 Influence of the physical and geometrical properties of the controlled fractured zone

The geometrical and physical properties of the modified well bottom are important indicators that influence the thermal process in the system. Fig.4.1(b) shows a not-to-scale illustration of the fractured zone at the well bottom, where h_1 is the height of the porous zone from the bottom pipe to the top boundary of the fractured zone, h_2 is the height of the porous zone from the bottom pipe to the bottom boundary of the fractured zone, and r_1 indicates the radius of the fractured zone. These three geometrical parameters are affecting the size of the contact area between the fractured zone and the ground $A_{contact}$. The effect of these geometrical parameters and the damage factor of the fractured zone was studied. The details of the parametric analysis are displayed in Table 4.2. The analysis is started by determining a based-model (C0) as an initial reference for the comparison analysis. Then, the value of geometrical and physical properties of the fractured zone are varied and compared with the based-model. The difference between these parameters affected the value of viscous and inertia resistances as well as the contact area of the fractured zone, which tabulated in Table 4.3.

The parametric analysis was plotted based on the different parameters, which were varied, as shown in Table. 4.2. The chosen comparison parameters are thermal power P_{ther} and pumping power P_{pump} . The thermal power was a function of the mass flow rate of the water, specific heat capacity of the water, and the temperature as well: $P_{ther} = \dot{m}c_p\Delta T$. In comparison, the pumping power takes pressure drop and water flow rate calculations into account: $P_{pump} = \frac{\Delta p Q}{\eta}$.

The effect of the $A_{contact}$ can be seen in Fig. 4.8(a-b). The increase of contact area in the fractured region is directly proportional to thermal power and pumping power. By

Table 4.2: Geometrical and physical properties for parametric analysis.

| Description | ID | h_1 [m] | h_2 [m] | r_1 [m] | D [-] |
|------------------|-----------|------------|------------|------------|------------|
| Base Case | C0 | 5 | 1 | 5 | 0.5 |
| Vary h_1 | C1 | 1.5 | 1 | 5 | 0.5 |
| | C2 | 10 | 1 | 5 | 0.5 |
| Vary h_2 | C3 | 5 | 0.5 | 5 | 0.5 |
| | C4 | 5 | 5 | 5 | 0.5 |
| Vary r_1 | C5 | 5 | 1 | 2.5 | 0.5 |
| | C6 | 5 | 1 | 10 | 0.5 |
| Vary D | C7 | 5 | 1 | 5 | 0.1 |
| | C8 | 5 | 1 | 5 | 1.0 |

Table 4.3: Tabulation of viscous α and inertia β resistances caused by the geometrical and physical properties of the controlled fractured zone. In addition, the thermal and pumping powers at the 10th year are listed.

| ID | Subdomain A | | Subdomain B | | At the 10 th year | |
|--------------------|--------------------|--------------------|--------------------|------------|------------------------------|-----------------------------|
| | α | β | α | β | P_{ther} [kW] | P_{pump} [kW] |
| Closed-loop | N/A | N/A | N/A | N/A | 25.83 | 763 $\times 10^{-4}$ |
| C0 | 1.12 $\times 10^5$ | 249.9 | 0.37 $\times 10^5$ | 443.4 | 49.82 | 974 $\times 10^{-4}$ |
| C1 | 7.27 $\times 10^5$ | 2685.9 | 0.37 $\times 10^5$ | 443.4 | 40.35 | 954 $\times 10^{-4}$ |
| C2 | 0.22 $\times 10^5$ | 13.4 | 0.37 $\times 10^5$ | 443.4 | 55.91 | 986 $\times 10^{-4}$ |
| C3 | 1.12 $\times 10^5$ | 249.9 | 0.35 $\times 10^5$ | 206.6 | 49.01 | 962 $\times 10^{-4}$ |
| C4 | 1.12 $\times 10^5$ | 249.9 | 0.37 $\times 10^5$ | 5635.7 | 54.74 | 985 $\times 10^{-4}$ |
| C5 | 1.16 $\times 10^5$ | 278.7 | 1.48 $\times 10^5$ | 7804.2 | 37.24 | 952 $\times 10^{-4}$ |
| C6 | 1.16 $\times 10^5$ | 1.77 $\times 10^4$ | 0.92 $\times 10^5$ | 8235.1 | 60.25 | 989 $\times 10^{-4}$ |
| C7 | 1.68 $\times 10^5$ | 249.9 | 0.55 $\times 10^5$ | 443.4 | 61.65 | 1025 $\times 10^{-4}$ |
| C8 | 0.68 $\times 10^5$ | 249.9 | 0.22 $\times 10^5$ | 443.4 | 48.40 | 967 $\times 10^{-4}$ |

increasing the height or the radius of the fractured zone, the heat generation rate is optimized as well. The pumping power increases due to the expansion of the fractured zone, which gives rise to the flow resistances. Those three parameters are compared with linear regression by calculating the increase of the thermal power if 5 m of length is added to each parameter. Fig. 4.7a shows that increasing the opening length of DPGHE to the fracture zone h_1 from 5 m to 10 m improves heat extraction rate by about 10% with additional pumping power increase of 3%. Similarly, increasing the depth of the fracture from

bottom of the DPGHE well, h_2 by 5 m increases the heat extraction rate for about 10%(Fig. 4.7b). Looking into the effect of fracture radius, r_1 , it is interesting that increasing fracture radius from 5 to 10 m, increases the heat extraction rate by 25%(Fig. 4.7c), while keeping the additional pumping power at minimum (3%). A more detailed plot displaying the effect of contact area on the temperature generated and thermal power is shown in Fig. 4.8(a). Even though the varying parameter is different (h_1 , h_2 and r_1), the plot indicates that the contact area is directly proportional to ΔT and the thermal power. As the size of the contact area is larger, the volume of the fractured zone increases as well. Thus, more water is flowing through the fractured which leads to an increase in the pressure drop and the pumping power, as shown in Fig. 4.8(b).

Fig. 4.7(d) shows the effect of the damage factor to the DPGHE system. If the ground is more damaged due to more impact on the hydraulic fracturing process, then the heat will transfer at a lower rate. The damage factor is also directly proportional to the porosity of the fractured zone. Thus, if the void in the fractured zone becomes bigger, then the heat transfer rate will be less efficient.

To conclude, the needed and generated powers provided by the closed-loop heat exchanger were compared against the parametric results of the semi-closed loop heat exchanger, as shown in Table 4.3. The increase of the heat generation rate was within 48-144%, while the pumping power had a 25-35% increase.

4.4 Conclusion

In this study, a mathematical model of a novel semi closed-loop double pipe geothermal heat exchanger with a controlled fractured zone at the well bottom is developed. A fractal tree-like network model is utilized to characterize the fracture zone. The base-case model was validated against experimental data by Morita et al. [3]. The operational parameters, such as the physical model, material properties, and the initial and boundary conditions, were discussed comprehensively. The key findings for this study are:

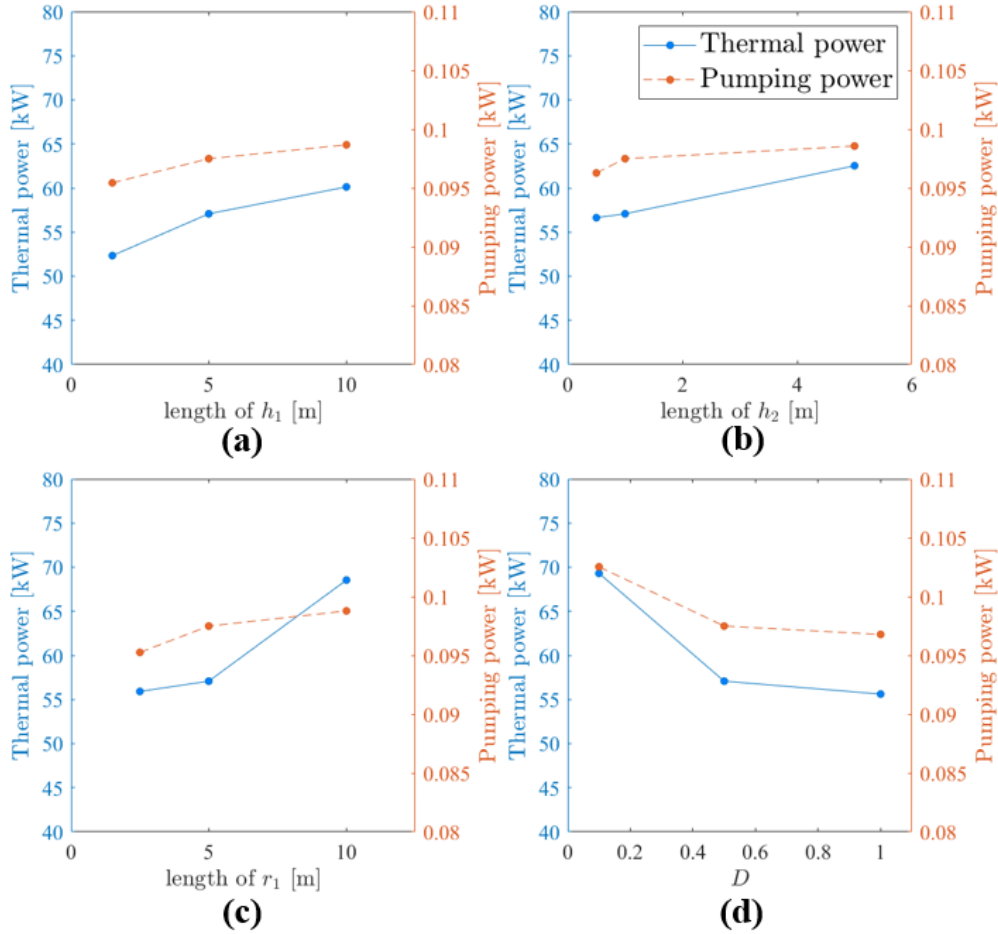


Figure 4.7: Comparison of thermal power and pumping power based on the parametric analysis of semi-closed loop heat exchanger varying the geometrical and physical properties of the fractured zone based on the: (a) length of h_1 ; (b) length of h_2 ; (c) length of r_1 ; (d) damage.

- The proposed semi-closed loop DPGHE was compared with the closed-loop model to assess the improvement on the heat transfer rate. The comparisons suggest that the proposed model could significantly improve heat extraction rate and thermal power by 93%, with additional approximately 28% of pumping power.
- Parametric studies were conducted to assess the effect of the geometrical and physical configuration of the fractured zone on the thermal power and pumping power. The results could be used as a reference to further optimize the proposed model. It

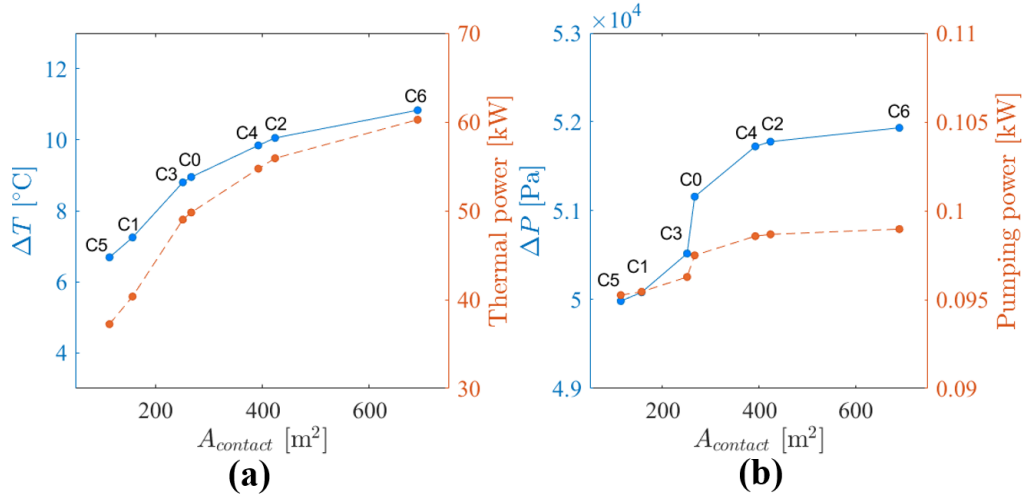


Figure 4.8: The effect of contact area between the fractured zone and the ground ($A_{contact}$) to: (a) ΔT and the thermal power; and (b) ΔP and the pumping power.

is found that the fracture radius plays significant role in enhancing heat extraction rate, while minimizing pumping power. In regards to the heat exchanger performance, the heat extraction rate increased by 48 to 144% and the pumping power elevated by 25 to 35% compared with the closed-loop heat exchanger. The semi closed-loop heat exchangers' heat transfer performances were based on the geometrical configuration of the porous zone as well as the mechanical damage caused by the hydraulic fracturing process.

- In general, the novel semi closed-loop DPGHE shows great potential to significantly improve the performance of the geothermal heat exchanger system.

Future works can focus on laboratory or field scale experiment to evaluate the feasibility and techno-economics of such system in practice.

References

- [1] Monique De Moel, Peter M Bach, Abdelmalek Bouazza, Rao M Singh, and JingLiang O Sun. Technological advances and applications of geothermal energy pile foundations and their feasibility in australia. *Renewable and Sustainable Energy Reviews*, 14(9):2683–2696, 2010.
- [2] Baldur Lindal. Industrial and other applications of geothermal energy. *Geothermal Energy*, pages 135–148, 1973.
- [3] Koji Morita, Warren S Bollmeier, and Husanobu Mizogami. An experiment to prove the concept of the downhole coaxial heat exchanger (DCHE) in hawaii. *Transactions - Geothermal Resources Council*, 16:9–16, 1992.
- [4] Koji Morita, Warren S Bollmeier, and Husanobu Mizogami. Analysis of the results from the downhole coaxial heat exchanger (DCHE) experiment in hawaii. *Transactions - Geothermal Resources Council*, 1992.
- [5] Tomasz Kujawa, Wladyslaw Nowak, and Aleksander A Stachel. Utilization of existing deep geological wells for acquisitions of geothermal energy. In *Thermal Sciences 2004. Proceedings of the ASME-ZSIS International Thermal Science Seminar II*. Begel House Inc., 2004.
- [6] JD Templeton, SA Ghoreishi-Madiseh, F Hassani, and MJ Al-Khawaja. Abandoned petroleum wells as sustainable sources of geothermal energy. *Energy*, 70:366–373, 2014.

- [7] Xianbiao Bu, Weibin Ma, and Huashan Li. Geothermal energy production utilizing abandoned oil and gas wells. *Renewable Energy*, 41:80–85, 2012.
- [8] Sharon WY Cheng, Jundika C Kurnia, Seyed Ali Ghoreishi-Madiseh, and Agus P Sasmito. Optimization of geothermal energy extraction from abandoned oil well with a novel well bottom curvature design utilizing taguchi method. *Energy*, 188:116098, 2019.
- [9] Sajjan Pokhrel, Agus P. Sasmito, Atsushi Sainoki, Toshiyuki Tosha, Tatsuya Tanaka, Chiaki Nagai, and Seyed Ali Ghoreishi-Madiseh. Field-scale experimental and numerical analysis of a downhole coaxial heat exchanger for geothermal energy production. *Renewable Energy*, 182:521–535, 2022.
- [10] Sajjan Pokhrel, Leyla Amiri, Ahmad Zueter, Sébastien Poncet, Ferri P Hassani, Agus P Sasmito, and Seyed Ali Ghoreishi-Madiseh. Thermal performance evaluation of integrated solar-geothermal system; a semi-conjugate reduced order numerical model. *Applied Energy*, 303:117676, 2021.
- [11] Seyed Ali Ghoreishi-Madiseh, Ali Fahrettin Kuyuk, and Marco Antonio Rodrigues de Brito. An analytical model for transient heat transfer in ground-coupled heat exchangers of closed-loop geothermal systems. *Applied Thermal Engineering*, 150:696–705, 2019.
- [12] Mohammed A Hefni, Minghan Xu, Ferri Hassani, Seyed Ali Ghoreishi-Madiseh, Haitham M Ahmed, Hussein A Saleem, Hussin AM Ahmed, Gamal SA Hassan, Khaled I Ahmed, and Agus P Sasmito. An analytical model for transient heat transfer with a time-dependent boundary in solar-and waste-heat-assisted geothermal borehole systems: From single to multiple boreholes. *Applied Sciences*, 11(21):10338, 2021.

- [13] MK Alkam and MA Al-Nimr. Improving the performance of double-pipe heat exchangers by using porous substrates. *International Journal of Heat and Mass Transfer*, 42(19):3609–3618, 1999.
- [14] Wei Lu, CY Zhao, and SA Tassou. Thermal analysis on metal-foam filled heat exchangers. part i: Metal-foam filled pipes. *International Journal of Heat and Mass Transfer*, 49(15-16):2751–2761, 2006.
- [15] Mohammad Mohsen Peiravi, Javad Alinejad, D Domairry Ganji, and Soroush Madad. 3d optimization of baffle arrangement in a multi-phase nanofluid natural convection based on numerical simulation. *International Journal of Numerical Methods for Heat & Fluid Flow*, 2019.
- [16] Seyed Ali Ghoreishi-Madiseh, Agus P Sasmito, Ferri P Hassani, and Leyla Amiri. Performance evaluation of large scale rock-pit seasonal thermal energy storage for application in underground mine ventilation. *Applied Energy*, 185:1940–1947, 2017.
- [17] M Asgari, M Javidan, M Nozari, A Asgari, and DD Ganji. Simulation of solidification process of phase change materials in a heat exchanger using branch-shaped fins. *Case Studies in Thermal Engineering*, 25:100835, 2021.
- [18] M Alizadeh, A Nabizadeh, A Fazlollahtabar, and DD Ganji. An optimization study of solidification procedure in a wavy-wall storage unit considering the impacts of nepcm and curved fin. *International Communications in Heat and Mass Transfer*, 124:105249, 2021.
- [19] Jiliang Chen and Fangming Jiang. Designing multi-well layout for enhanced geothermal system to better exploit hot dry rock geothermal energy. *Renewable Energy*, 74:37–48, 2015.
- [20] P Olasolo, MC Juárez, MP Morales, IA Liarte, et al. Enhanced geothermal systems (EGS): A review. *Renewable and Sustainable Energy Reviews*, 56:133–144, 2016.

- [21] Shyi-Min Lu. A global review of enhanced geothermal system (egs). *Renewable and Sustainable Energy Reviews*, 81:2902–2921, 2018.
- [22] Mohamad Omid, Mousa Farhadi, and Mohamad Jafari. A comprehensive review on double pipe heat exchangers. *Applied Thermal Engineering*, 110:1075–1090, 2017.
- [23] Hannes Hofmann, Guido Blöcher, Nele Börsing, Nico Maronde, Nicole Pastrik, and Günter Zimmermann. Potential for enhanced geothermal systems in low permeability limestones—stimulation strategies for the western malm karst (bavaria). *Geothermics*, 51:351–367, 2014.
- [24] Xianzhi Song, Yu Shi, Gensheng Li, Ruiyue Yang, Gaosheng Wang, Rui Zheng, Jiacheng Li, and Zehao Lyu. Numerical simulation of heat extraction performance in enhanced geothermal system with multilateral wells. *Applied Energy*, 218:325–337, 2018.
- [25] Gaosheng Wang, Xianzhi Song, Yu Shi, Ruiyue Yang, Feixue Yulong, Rui Zheng, and Jiacheng Li. Heat extraction analysis of a novel multilateral-well coaxial closed-loop geothermal system. *Renewable Energy*, 163:974–986, 2021.
- [26] Yu Shi, Xianzhi Song, Gaosheng Wang, Jiacheng Li, Lidong Geng, and Xiaojiang Li. Numerical study on heat extraction performance of a multilateral-well enhanced geothermal system considering complex hydraulic and natural fractures. *Renewable Energy*, 141:950–963, 2019.
- [27] Donald A Nield, Adrian Bejan, et al. *Convection in porous media*, volume 3. Springer, 2006.
- [28] Maasoud Kaviany. *Principles of heat transfer in porous media*. Springer Science & Business Media, 2012.
- [29] Boming Yu. Analysis of flow in fractal porous media. *Applied Mechanics Reviews*, 61(5), 2008.

- [30] Jianchao Cai, Liehui Zhang, and Wei Wei. *Modelling of flow and transport in fractal porous media*. Elsevier, 2021.
- [31] Boming Yu and Jianhua Li. Some fractal characters of porous media. *Fractals*, 9(03):365–372, 2001.
- [32] Jinsui Wu and Boming Yu. A fractal resistance model for flow through porous media. *International Journal of Heat and Mass Transfer*, 50(19-20):3925–3932, 2007.
- [33] Jinsui Wu, Boming Yu, and Meijuan Yun. A resistance model for flow through porous media. *Transport in Porous Media*, 71(3):331–343, 2008.
- [34] GA Ledezma, A Bejan, and MR Errera. Constructal tree networks for heat transfer. *Journal of Applied Physics*, 82(1):89–100, 1997.
- [35] Adrian Bejan. *Shape and structure, from engineering to nature*. Cambridge university press, 2000.
- [36] Peng Xu, Agus Pulung Sasmito, Boming Yu, and Arun Sadashiv Mujumdar. Transport phenomena and properties in treelike networks. *Applied Mechanics Reviews*, 68(4), 2016.
- [37] Peng Xu, Boming Yu, Shuxia Qiu, and Jianchao Cai. An analysis of the radial flow in the heterogeneous porous media based on fractal and constructal tree networks. *Physica A: Statistical Mechanics and its Applications*, 387(26):6471–6483, 2008.
- [38] Tongjun Miao, Shanshan Yang, Zhangcai Long, and Boming Yu. Fractal analysis of permeability of dual-porosity media embedded with random fractures. *International Journal of Heat and Mass Transfer*, 88:814–821, 2015.
- [39] Peng Xu, Cuihong Li, Shuxia Qiu, and Agus Pulung Sasmito. A fractal network model for fractured porous media. *Fractals*, 24(02):1650018, 2016.

- [40] Jiyuan Zhao, Weitao Liu, Jianjun Shen, Minghan Xu, and Agus P Sasmito. Fractal treelike fracture network model for hydraulically and mechanically induced dynamic changes in the non-darcy coefficient during the process of mine water inrush from collapsed columns. *Fractals*, 29(7):2150218, 2021.
- [41] Maciej Z Lukawski, Rachel L Silverman, and Jefferson W Tester. Uncertainty analysis of geothermal well drilling and completion costs. *Geothermics*, 64:382–391, 2016.
- [42] Ekkehard O Holzbecher. *Modeling density-driven flow in porous media: principles, numerics, software*. Springer Science & Business Media, 1998.
- [43] R Byron Bird, Warren E Stewart, and Edwin N Lightfoot. *Transport phenomena*, volume 1. John Wiley & Sons, 2006.
- [44] Inc ANSYS. Ansys fluent theory guide, 2020.
- [45] Agus P Sasmito, Erik Birgersson, Hung C Ly, and Arun S Mujumdar. Some approaches to improve ventilation system in underground coal mines environment—a computational fluid dynamic study. *Tunnelling and Underground Space Technology*, 34:82–95, 2013.
- [46] Ahmad Zueter, Aurelien Nie-Rouquette, Mahmoud A Alzoubi, and Agus P Sasmito. Thermal and hydraulic analysis of selective artificial ground freezing using air insulation: Experiment and modeling. *Computers and Geotechnics*, 120:103416, 2020.
- [47] John A Wheeler and Eugene H Wissler. The friction factor–reynolds number relation for the steady flow of pseudoplastic fluids through rectangular ducts. part i. theory. *AIChE Journal*, 11(2):207–212, 1965.

Chapter 5

Development of a 1+1D Reduced-Order Model in Double-Pipe Geothermal Heat Exchanger Systems: From Single to Multiple Boreholes

Contents

| | | |
|-----|----------------------------------|----|
| 5.1 | Introduction | 75 |
| 5.2 | Model Description | 78 |
| 5.3 | Solution Algorithms | 82 |
| 5.4 | Results and Discussion | 87 |
| 5.5 | Conclusion | 90 |

Preface (Linking Paragraphs)

Following the realization of the expensive and time-consuming nature of the computational process of two-dimensional and three-dimensional numerical modeling based on the last two previous chapters, this chapter comprises a development of a one-plus-one-dimensional reduced-order model in a geothermal heat exchanger system. The developed model reduced the computational time with similar accuracy. Additionally, spatial symmetry and thermal superposition concepts were introduced to extend the single borehole into a multiple boreholes system. The below chapter will be presented at International Conference on Applied Energy 2021 and in preparation for submission:

Agson-Gani, P. H., Zueter, A. F., Xu, M., Sasmito, A. P. (2021). Development of a 1+1D Reduced-Order Model in Double-Pipe Geothermal Heat Exchanger Systems: From Single to Multiple Boreholes, 2021, in preparation.

Abstract

Geothermal heat is one of the preferred sources of renewable energy to meet the world's energy demand. Low and medium enthalpy geothermal heat can be extracted by using a geothermal heat exchanger (GHE), which collects the earth's thermal energy and brings it to the ground surface using a closed-loop system of single-phase heat transfer fluid (HTF). GHE systems are typically large (e.g., hundreds of meters deep) and long-running (e.g., decades). Therefore, numerical modelling of these systems can be computationally expensive and sometimes restrictive in practice, especially for large number of boreholes. The present study develops a novel computationally efficient one-plus-one-dimensional (1+1D) semi-conjugate heat transfer model of a double-pipe heat exchangers (DPHE), which solves a transient conservation equation of energy in the radial coordinate coupled with a space marching algorithm. Furthermore, the concept of spatial symmetry and thermal superpositions are implemented in order to expand the single borehole solution into a multiple geothermal boreholes system. The proposed model is validated against experimental data of GHE and verified with numerical solution from a full-scale three-

dimensional (3D) computational fluid dynamics (CFD) model. With regards to computational time, the proposed 1+1D model with spatial symmetry and thermal superposition is 99% faster to compute than the 3D fully-conjugate CFD model. This shows the potential of the proposed model to be used in practical applications for a wide range of parametric studies, thermal design and optimization.

5.1 Introduction

Based on the recently published Sixth Assessment Report (AR6) of the United Nations Intergovernmental Panel on Climate Change (IPCC) [1], the temperature of the surface of the earth is currently getting warmer by 1.1°C . If the carbon intensive development continues, the increase of the temperature is on the track to reach 1.5°C in the next two decades, and $3.3\text{-}5.7^{\circ}\text{C}$ at the end of the century. This condition provides an unprecedented degree of clarity about our planet future, and the need to implement climate legislation in all sectors. One of the most important societal transitions is from fossil-fuel based energy into renewable energy. As a renewable energy source, geothermal heat is an attractive choice to provide a significant environmental value while producing energy. This abundance of energy resides below the surface of the ground and its temperature is getting hotter as the depth is increased. To utilize such energy, a ground source heat pump (GSHP) system coupled with the geothermal heat exchanger (GHE) is usually installed. In particular, the use of double-pipe design for a GHE is commonly implemented [2, 3, 4]. The double-pipe geothermal heat exchanger (DPGHE) works by pumping water through the inlet downward; then the water goes upward coaxially, which is extracted from the outlet. Then, the extracted water could be further utilized for a heating/cooling source, direct use applications, or coupled the system for power generation.

Numerous studies have been done to investigate the operating performance and the sustainability of the DPGHE. One of the earliest is the experimental investigation conducted by Morita et al. [3, 5] in Hawaii. They performed one of the first proof of concept

of the DPGHE in a field-scale environment. In 2004, Kujawa et al. [2] analytically studied the feasibility of turning abandoned oil wells into a DPGHE system. This study then followed by Templeton et al. [6] who developed the numerical heat transfer model based on the previous study. They applied the constant inlet temperature and constant power output concepts to analyze the effect of a multitude of parameters on the DPGHE. In addition, Cheng et al. [4] numerically investigate the previous DPGHE model and further optimize it by applying a well bottom curvature to improve the heat performance of the system. It can be seen that the numerical simulation is widely used to investigate such models. The numerical models are usually built by using commercial software, such as Ansys Fluent [4, 7, 8], and COMSOL Multiphysics [9]. The numerical solutions are then validated against the experimental data to ensure the accuracy of the results. Despite the versatility of these fully-conjugate models, the requirement of large mesh counts which resulted in extremely long computational time caused this model to be impractical, especially during the design optimization process. The huge computational domain and long operating time are adding to the difficulty in developing this model.

In order to minimize the computational process of the numerical model, Fang et al. [10] developed a computationally efficient heat exchanger model through an incorporation of the Finite Difference Method (FDM). The developed model proved to be highly efficient due to the treatment of the flow and the convective heat transfer in the pipes is simplified as 1D. This treatment solves the issue of the great number of elements required to simulate such model. Yu et al. [11] created a novel 1D numerical model of the U-pipe GHE using Finite Element Method (FEM). A case-study data and TRNSYS model are used to validate the proposed model. Apart from the GHE problem, efforts to reduce the computational time in numerical modelling are also made in several other applications, such as in artificial ground freezing (AGF). Zueter et al. [12, 13] simulated lab-scale and field-scale coaxial AGFs systems by developing a reduced-order model which reduced 2D axisymmetric computational domain into several 1D gridlines. This method could reduce the computational time by more than 99%.

Moreover, to further enhance the performance of the GSHP system and meet the energy demand, multiple DPGHEs are usually sink instead of only one. Multiple vertical DPGHEs are usually called the borehole heat exchangers (BHEs). Nowadays, the implementation of multiple boreholes is widely used. The number of boreholes could reach tens to hundreds to accommodate for the energy demand [14]. The striking difference between a single borehole with the multiple boreholes solution is the thermal interaction between each borehole which affects the total heat performance of the DPGHEs system. Kurejiva et al. [15] analyzed the effect of borehole array geometry and the thermal interference of a geothermal heat pump system. Their results show that the effect of multiple boreholes on various geometric configurations influenced the heat performance of the system. Gultekin et al. [16] also studied the effects of different parameters in multiple borehole heat exchanger in terms of the heat transfer rate of the system. Their results provided the design optimization based on the performance loss of the system's center borehole.

The study of the GHE with multiple boreholes configuration is usually conducted by experimental investigation [14, 17] because performing a numerical study is highly challenging due to its complex structure (i.e., multiple boreholes), with the addition of its macroscopic features. An approach done by Gultekin et al. [16] was simulating the multiple boreholes numerically by reducing the 3D model into a 2D model. However, this method leads to the simulation not capturing the fully-conjugate model of the multiple boreholes DPGHE. Another approach to investigate the heat transfer mechanism in the multiple boreholes DPGHEs is by incorporating analytical treatments, e.g., a closed form analytical solution. Compared with numerical simulations, the analytical solutions are easy and fast to compute, but significant efforts are required in the development of these models. Ghoreishi-Madiseh et al. [18] solved a 1D transient heat equation subjected to a constant temperature boundary; they extended the closed-form exact solution from a single borehole to double and N-by-N boreholes with the use of symmetry, also referred as the superposition principle. Recently, Hefni et al. [19] applied this methodology in a

similar problem but subjected to a time-dependent boundary condition, which in turn facilitated the engineering utility in many geothermal applications, such as hybrid solar-geothermal systems.

Based on the presented literature thus far, we aim to resolve the computational issue in developing the DPGHE system with multiple boreholes configuration. The objective of this study is to develop a novel reduced-order 1+1D DPGHE system, coupled with a thermal superposition algorithm to extend the single borehole solution into double and multiple boreholes configurations. The proposed models will be validated against the experimental results and verified with fully-conjugate 3D models. Furthermore, the thermal analysis of the temperature profile of the ground in every model is thoroughly discussed. Finally, the computational performance of each model is studied, which reflects the efficiency of the proposed model.

5.2 Model Description

The objectives of this paper are to develop a reduced-order algorithm for double-pipe geothermal heat exchanger (DPGHE) systems with a single borehole configuration and extend the model into multiple boreholes configurations by implementing spatial symmetry and thermal superposition theories, as shown in Fig. 5.1. The thermophysical properties are shown in Table. 5.1.

Table 5.1: Thermophysical properties of the materials used in DPGHE

| Material | ρ [kg/m^3] | c_p [$J/(kgK)$] | k [$W/(mK)$] |
|----------------|---------------------|---------------------|------------------|
| Water | 997 | 4182 | 0.6 |
| Inner pipe | 5240 | 310 | 0.06 |
| Conductor pipe | 7850 | 470 | 46.1 |
| Cement | 1830 | 1900 | 0.99 |
| Rock | 3050 | 870 | 1.6 |

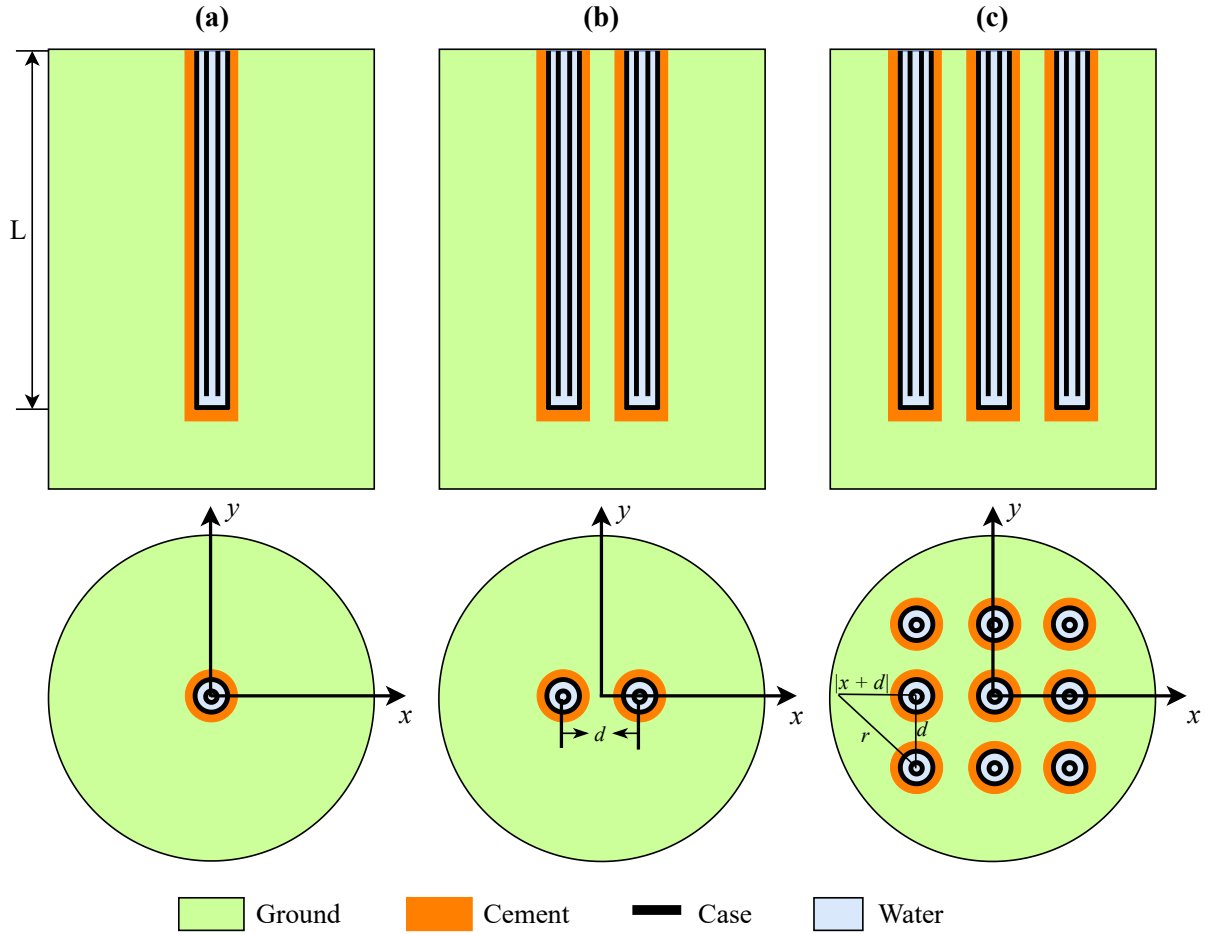


Figure 5.1: Side view and top view of (not-to-scale) GHE with the following configurations: (a) a single borehole; (B) double boreholes; (C) 3-by-3 boreholes.

In this section, the mathematical model formulation of this study is discussed. First, the governing equations which describe the computational domain of the 1+1D and 3D models are presented. It is important to note that there are different aspects between both models, which are:

- 1+1D model: axisymmetric, semi-conjugate, single-phase, turbulent flow, coded with MATLAB R2020
- 3D model: symmetry boundary condition, fully-conjugate, single-phase, turbulent flow, simulate with Ansys Fluent 2020R1

Then, the initial and boundary conditions are presented based on the values from the field data.

5.2.1 Governing equations

The numerical model solves heat transfer mechanisms in the solid domains of the GHE system (i.e., the ground), as shown in Fig. 5.1. In the solid domains, conduction is applied and calculated as follows:

$$\frac{\partial(\rho c_p T)}{\partial t} = \nabla \cdot (k \nabla T) \quad (5.1)$$

where ρ is the density, c_p is the specific heat capacity, T is the temperature, and k is the thermal conductivity of the solid part.

In order to make the computational performance in the fluid region (i.e., working fluid like water) more efficient, the proposed model only simulates a heat convection equation based on the 1st law of thermodynamics per area, as follows:

$$\dot{m} c_{p,f} \Delta T_f = h A (T_s - T_f) \quad (5.2)$$

where \dot{m} is the mass flow rate of the coolant, and h is the convection heat transfer coefficient. By only simulating this equation, the computational time reduced a lot compare with the 3D models. In the 3D model simulation, the meshes in the coolant region has to be specifically fine which each node is incorporating the conservation equation of mass, momentum and energy which are formulated as follows:

$$\frac{\partial}{\partial t}(\rho_f \mathbf{U}) + \nabla \cdot (\rho_f \mathbf{U}) = 0 \quad (5.3)$$

$$\frac{\partial}{\partial t}(\rho_f \mathbf{U}) + \nabla \cdot (\rho_f \mathbf{U} \mathbf{U}) = -\nabla p + \nabla \cdot [(\mu_f + \mu_{t,f})(\nabla \mathbf{U} + (\nabla \mathbf{U})^T)] + \rho_f \mathbf{g} \quad (5.4)$$

$$\frac{\partial}{\partial t}(\rho_f c_{p,f} T) + \nabla \cdot (\rho_f c_{p,f} \mathbf{U} T) = \nabla \cdot (k_f \nabla T) \quad (5.5)$$

where \mathbf{U} is the fluid velocity, p is the pressure, μ is the dynamic viscosity, \mathbf{g} is the gravity, and subscript f and t are fluid and turbulent, respectively.

5.2.2 Initial and boundary conditions

Based on the field data provided by Morita et al. [3, 5], the temperature profile initial condition is set. As for the boundary conditions, the 1+1D model implements the axisymmetric boundary in the axis. Therefore, the temperature along the axis are given by:

$$\frac{\partial T_{axis}}{\partial r} = 0. \quad (5.6)$$

On the other hand, the 3D model employs the symmetry boundary condition in order to simulate a quarter of the model, which reduces the computational time significantly. Therefore, a zero heat flux is assumed along the symmetry planes as follows:

$$\frac{\partial T_{symmetry}}{\partial r} = 0. \quad (5.7)$$

The outer part of the computational domain comprises of the side, and bottom boundaries. Geothermal gradient are applied at the side and bottom boundaries which given by:

$$T = T_{geo}, \quad (5.8)$$

Finally, at the outer part of the borehole wall, which is in contact with the grout, heat convection is applied:

$$-k \frac{\partial T_s}{\partial n} = h (T_s - T_f) \quad (5.9)$$

where k is the thermal conductivity and h is the convection heat transfer coefficient. Detailed explanation on the novel framework for the walls boundary condition can be found in [12].

Particularly, there are several additional boundary conditions which implemented to the 3D models due to its particular fluid domain. One of them is the inlet, the mass

flow rate and the temperature which are set as constant, which are 1.33 kg/s and 30°C, respectively:

$$\dot{m} = \dot{m}_{in}, \quad (5.10)$$

$$T = T_{in}. \quad (5.11)$$

Additionally in the outlet, the pressure is set as 0 and a zero heat flux is applied:

$$P = P_{out} = 0, \quad (5.12)$$

$$\mathbf{n} \cdot \nabla T = 0. \quad (5.13)$$

Finally, a no-slip condition is also applied at all walls.

5.3 Solution Algorithms

In this paper, the process of developing the 1+1D reduced-order model in multiple boreholes GHE systems is shown in Fig. 5.2. A two-step solution algorithm process is implemented, which are: (a) reduced-order 1+1D model, and (b) thermal superposition. Firstly, a single borehole GHE system is developed using a reduced-order 1+1D semi-conjugate model. This model allowed a more efficient computational process than 2D and 3D models. This model is validated against the field data to ensure the validity of the model. Then, the thermal superposition theorem is implemented to the model in order to expand a single borehole into multiple boreholes GHE systems. Further, the proposed models are verified against the 3D CFD models.

5.3.1 Single borehole solution: Development of 1+1D model using space marching algorithm

The numerical simulation of the GHE system is a challenging task due to its large computational domain and a high number of timesteps. In this study, a 1+1D model is developed

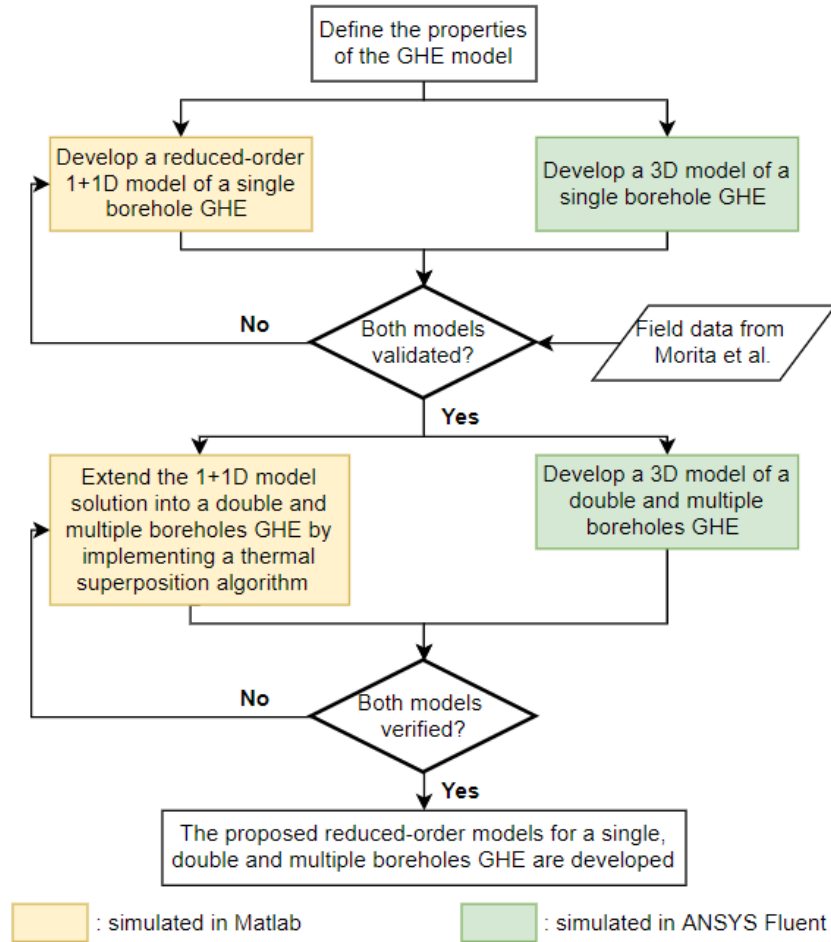


Figure 5.2: Flowchart of the development of the 1+1D semi-conjugate model, coupled with the thermal superpositions algorithm.

by applying a space marching algorithm that reduces a 2D axisymmetric problem dimensionally and significantly increases the computational process's efficiency. This algorithm works by discretizing the 2D domain into several 1D gridlines and visiting each grid in series, one after the other. In the GHE system, the 1D gridlines are created perpendicular from the fluid flow direction since this algorithm is solving a convective heat problem, as shown in Fig. 5.3. The followings are the detailed steps to develop the reduced-order 1+1D GHE model:

1. First, the temperature profile in the computational domain are set based on the initial condition.

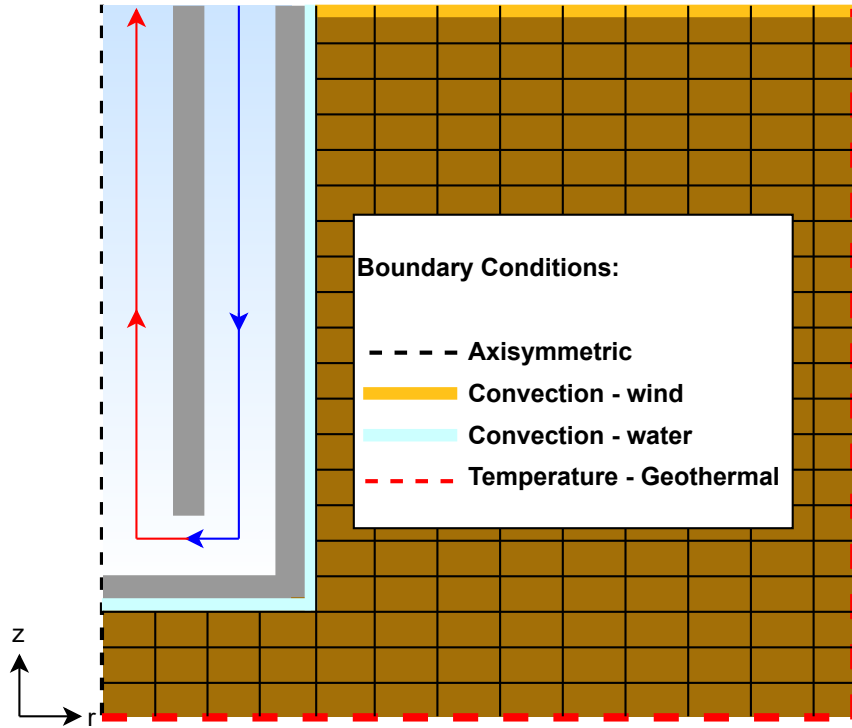


Figure 5.3: Computational domain of the 1+1D model of the DPGHE

2. Then, the conduction heat transfer between the borehole wall and the side boundary along the 1D gridlines are solved from the top gridline to the lowest of the computational domain. The 1D gridlines are solving Eq. 5.1, which marching between the borehole wall and the side boundary, modeled as Eqs. 5.9 and 5.8, respectively. Meanwhile, the water temperature is calculated with Eq. 5.3.
3. Each computational node stores a value for the temperature, which act as an initial condition for the next steps.
4. Steps 2-3 are repeated until the desired time steps are reached.

Once the simulation is convergent, the solution is stored and can be further extended into double and multiple boreholes configurations. More details on the space marching algorithm can be found in [12], which include the four variations differ due to the coupling with analytical solution and additional spatial correction.

5.3.2 Multiple boreholes solution: Incorporating the use of symmetry with thermal superpositions algorithm

In this paper, the concept of symmetry and thermal superpositions is implemented using the previously simulated single borehole 1+1-D model solutions as a system-based model. The used results comprise of the temperature profile data ranging from the depth of 0 m up to 800 m and the timeframe from 1 day to 10 years. The arrangements of the single, double, and multiple N-by-N boreholes are shown in Fig. 5.1. The thermal superpositions theory is computed in the radial direction based on the previous-mentioned configurations. The temperature profile calculation is done along the centreline at $y = 0$, equivalent to the line at $x = 0$, whereas the $T_{total}(x, y = 0, t)$ describes the temperature profile of all boreholes in the calculated domain. It is noted that this thermal superposition algorithm is consistent with Hefni et al.'s work [19].

In a single borehole configuration, the total temperature profile could be determined by mirroring the temperature values from space marching algorithm along the centreline at $x = 0$ as follows:

$$T_{total}(x, y = 0, t) = T_a(r = |x|, t) \quad (5.14)$$

where subscript a represents the only borehole in this configuration.

In double boreholes configuration, the boreholes are arranged at the center of the domain, separated by a fixed distance d . The total temperature profile is calculated as the summation of the 1+1-D model temperature solution in each borehole as follows:

$$T_{total}(x, y = 0, t) = T_a\left(r = \left|x + \frac{d}{2}\right|, t\right) + T_b\left(\left|x - \frac{d}{2}\right|, t\right) \quad (5.15)$$

where subscript a and b indicate the left and right boreholes in the domain, respectively.

For the case of multiple boreholes with N-by-N configurations, the total temperature profile is also affected by the boreholes placed above and below the centreline. In this

paper, 3-by-3 borehole GHE system is modeled and given as:

$$\begin{aligned}
T_{total}(x, y = 0, t) = & T_a \left(r = \sqrt{d^2 + (x + d)^2}, t \right) + T_b \left(r = \sqrt{d^2 + x^2}, t \right) \\
& + T_c \left(r = \sqrt{d^2 + (x - d)^2}, t \right) + T_d (r = |x + d|, t) + T_e (r = |x|, t) \\
& + T_f (r = |x - d|, t) + T_g \left(r = \sqrt{d^2 + (x + d)^2}, t \right) \\
& + T_h \left(r = \sqrt{d^2 + x^2}, t \right) + T_i \left(r = \sqrt{d^2 + (x - d)^2}, t \right)
\end{aligned} \tag{5.16}$$

where the subscripts $a - i$ show the boreholes label from top left corner to the bottom right corner, from the top row until bottom row. In this sense, this expression could be modified based on the desired number of boreholes in the system.

5.3.3 Three-dimensional numerical simulations

The 3D CFD models of GHE with single, double and multiple borehole configurations were made as a means of verification with the proposed 1+1D model which extended into multiple boreholes model with the thermal superposition theorem. Ansys 2020R1 was used to create and mesh the computational domain. Symmetry boundary condition is used conditions is to reduce the computational time by only simulating a quarter of the computational domain for a single and multiple borehole cases, and a half of the computational domain for the double boreholes case. The mesh size ranging from $1 \times 10^7 - 3 \times 10^7$ elements are used to model the GHE systems. In particular, the fluid domain makes up to the majority number of the mesh count, which make these models computationally expensive. The governing equations with the initial and boundary conditions were computed using the finite volume method by Ansys Fluent and were written in the user-defined functions (UDFs). The numerical model was solved by implementing the Semi-Implicit Pressure-Linked Equation (SIMPLE) algorithm and second-order up-

wind discretization schemes. The residual of 1×10^{-5} was set as the convergence criteria for all equations.

5.4 Results and Discussion

5.4.1 Development of Reduced-Order Model of GHE

This subsection discusses the steps to develop a robust and efficient reduced-order 1+1D numerical model for the GHE system. First, the 1+1D solution is validated against the experimental data to ensure the accuracy of the proposed model. Then, the mesh and boundary dependency solution is analyzed to ensure the reliability of the 1+1D model. Finally, a computational time analysis is done by comparing the computing time of the 1+1D models with the 3D models with similar operating conditions.

Model validation

Both 1+1D and 3D models of GHE with a single borehole are validated against the experiment conducted by Morita et al. in Hawaii. The initial temperature condition of the GHE system and the surrounding rock are set based on the ground temperature profile plot provided by the field data. The water injection rate and temperature are set as 1.33 kg/s and 30°C, respectively. Additionally, the geothermal gradient as the heat source is applied at the boundaries.

As shown in Fig. 5.4, the proposed 1+1D and 3D models can predict the outlet temperature of the system accurately. Considering this good agreement, we could couple the 1+1D model with the thermal superposition algorithm and develop the 3D CFD models as the verification and comparison model.

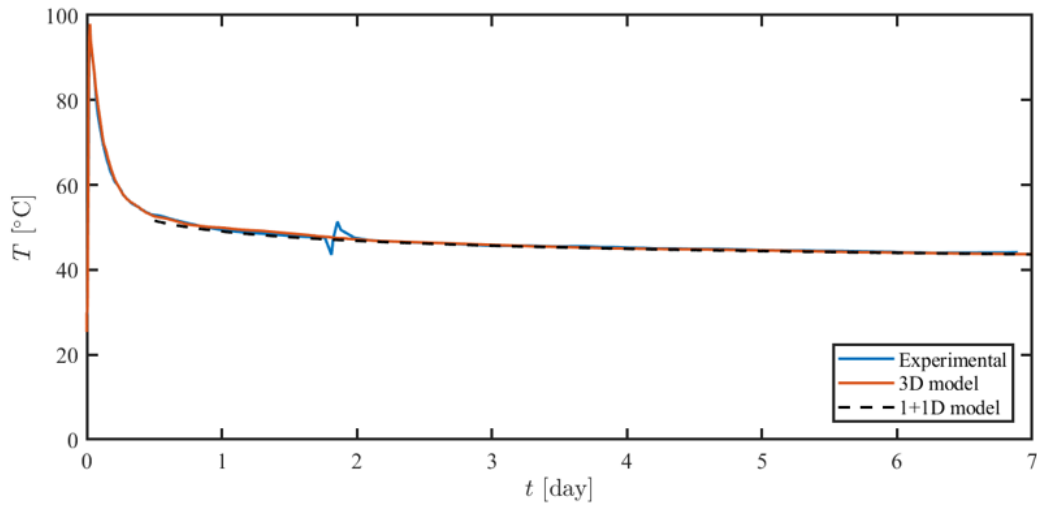


Figure 5.4: Validation of the outlet temperature value of the single borehole solution (MATLAB) with the field data [3], and the 3D model (ANSYS Fluent)

Mesh and boundary dependency analysis

The reliability of the numerical model of the GHE system depends on its mesh generation which represents the computational domain of the system. Fig. 5.5.(a) shows the correlation of the mesh count and the outlet temperature recorded in the first year. The change of the mesh count is based on the change of the mesh resolution in radial and y-directions. As the mesh gets finer, the change in the outlet temperature is lesser. The plots show that the change due to the resolution in the radial direction is more sensitive. These findings provide great insight to build an efficient meshing while maintaining the reliability of the model.

Based on the Templeton et al. [6] and comments on the double-pipe heat exchanger model built by Kujawa et al. [2], mistakes in defining the radius of the boundary could lead to the overestimation of the performance of the heat exchanger. Therefore, a boundary dependency analysis is conducted, as shown in Fig. 5.5.(b). The plots show that assigning a value of at least 20 m as the radius of the boundary leads to the model achieving its boundary dependence.

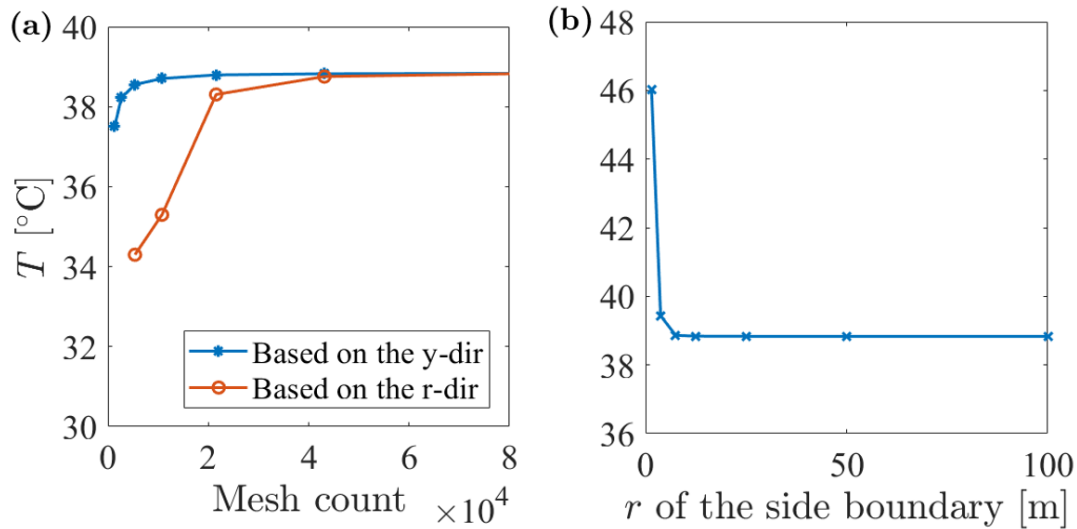


Figure 5.5: Comparison of the outlet temperature at Year 1 as a dependency analysis of: (a) mesh count; and (b) the side boundary length.

Computational time analysis

Computational performance is discussed to compare the computational time between each model. It is important to note that the 1+1D models are coded in MATLAB R2020, while the 3D models are simulated in Ansys Fluent 2020R1. To develop the 3D models, a considerable number of mesh counts is needed to achieve a convergent simulation, especially in the fluid domain.

As shown in Table. 5.2, the 1+1D models are drastically faster to compute than the 3D models. Additionally, the proposed models use the thermal superposition algorithm to extend the single borehole solution into double and multiple boreholes configurations which takes no additional time to compute. As a result, the computational time of the proposed models is 99% faster than the 3D models.

5.4.2 Thermal analysis on the 1+1D models

The developed 1+1D models, coupled with the thermal superposition algorithm, are compared with the fully-conjugate 3D numerical models. The comparison comprises the tem-

Table 5.2: Computational time of the numerical simulations

| Model | # borehole | Mesh count | Compt. time [hh:mm:ss] |
|-------------------|------------|------------|------------------------|
| 1+1D Axisymmetric | 1 | 75,000 | 00:18:53 |
| 2D Axisymmetric | 1 | 4,191,000 | 13:00:00 |
| 3D Symmetry | 1 (single) | 13,000,000 | 192:00:00 |
| 3D Symmetry | 2 (double) | 19,000,000 | 240:00:00 |
| 3D Symmetry | 3-by-3 | 33,000,000 | 432:00:00 |

perature profile in single, double, and multiple boreholes at different times: 1 day, 1 week, 1 month, 6 months, and 1 year. Additionally, the temperature profile of the ground is plotted in the radial direction at several depths; from 100 m to 800 m. Fig. 5.6 shows the temperature distribution of the single borehole problem. It can be seen from the graph, the temperature of the ground is depleted over time. It is one of the physical phenomena of the geothermal heat extraction.

The same condition is also applied in the double boreholes solution, as shown in Fig. 5.7. Particularly, the ground condition between the boreholes is decreasing more significantly than the surrounding area. It is due to the heat transfer rate being more significant in the boreholes area, which makes the ground temperature depleted faster.

The ground condition in the multiple boreholes solution is depleted even faster than in the single and double boreholes solutions, as shown in Fig. 5.8. This means that the heat extracted in each borehole will be lower than the previous models.

5.5 Conclusion

We proposed the novel semi-conjugate reduced-order models for the double-pipe geothermal heat exchanger (DPGHE) system with single, double, and multiple borehole configurations. The main objective of developing such a model is to reduce the computational time and cost of the heavy computational requirement for the DPGHE system, which has a complex structure, huge computational domain, and long operational time.

The main key findings of this paper are as follows:

- The reduced-order 1+1D algorithms are developed to simulate a DPGHE system. We could say that the 1+1D model is more efficient than the 3D models since the reduced-model computational time is 99% faster than the 3D models. It takes less than an hour to simulate a 10-year simulation with the proposed model, while it takes more than 7 days to simulate a similar model with the 3D numerical model. The solutions obtained by the proposed model is considered reliable in estimating the temperature profile of the GHE since it gives similar results with the 3D models and is also validated against the field data.
- Thermal superposition and spatial symmetry algorithms are implemented to analytically extend the 1+1D GHE model solution into double and multiple borehole configurations. Regarding the computational time, the proposed models are in several orders of magnitude faster to compute than the 3D CFD model while maintaining the same accuracy.

In summary, we could conclude that the proposed model shows the potential to simulate a complex GHE system with a long operation time efficiently. This study could be extended for a wide range of parametric studies, as well as design and optimization. The model could also be coupled with a solar-powered thermal model to simulate solar thermal borehole thermal energy storage.

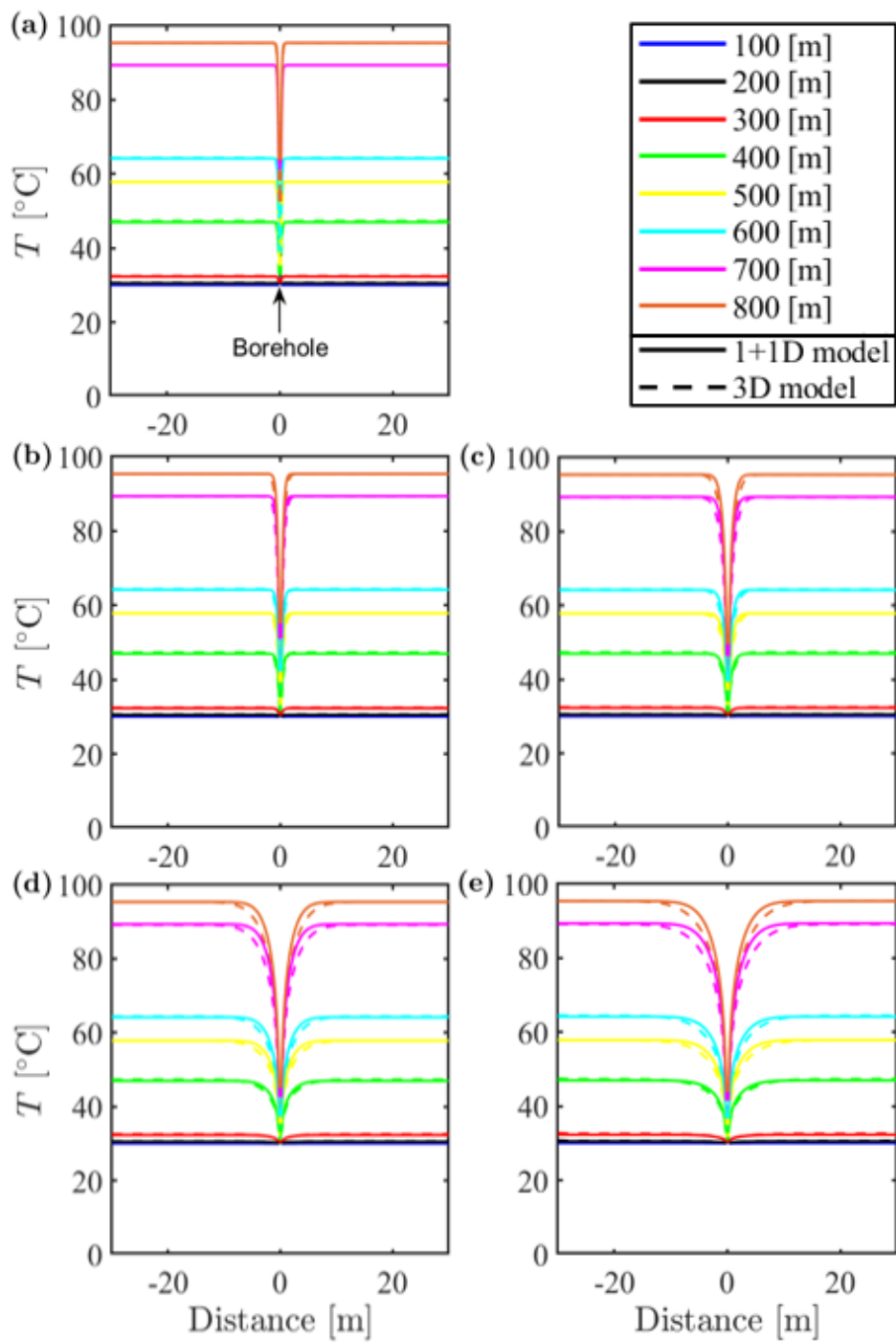


Figure 5.6: Temperature profile of the single borehole solutions at: (a) 1 day; (b) 1 week; (c) 1 month; (d) 6 months; and (e) 1 year.

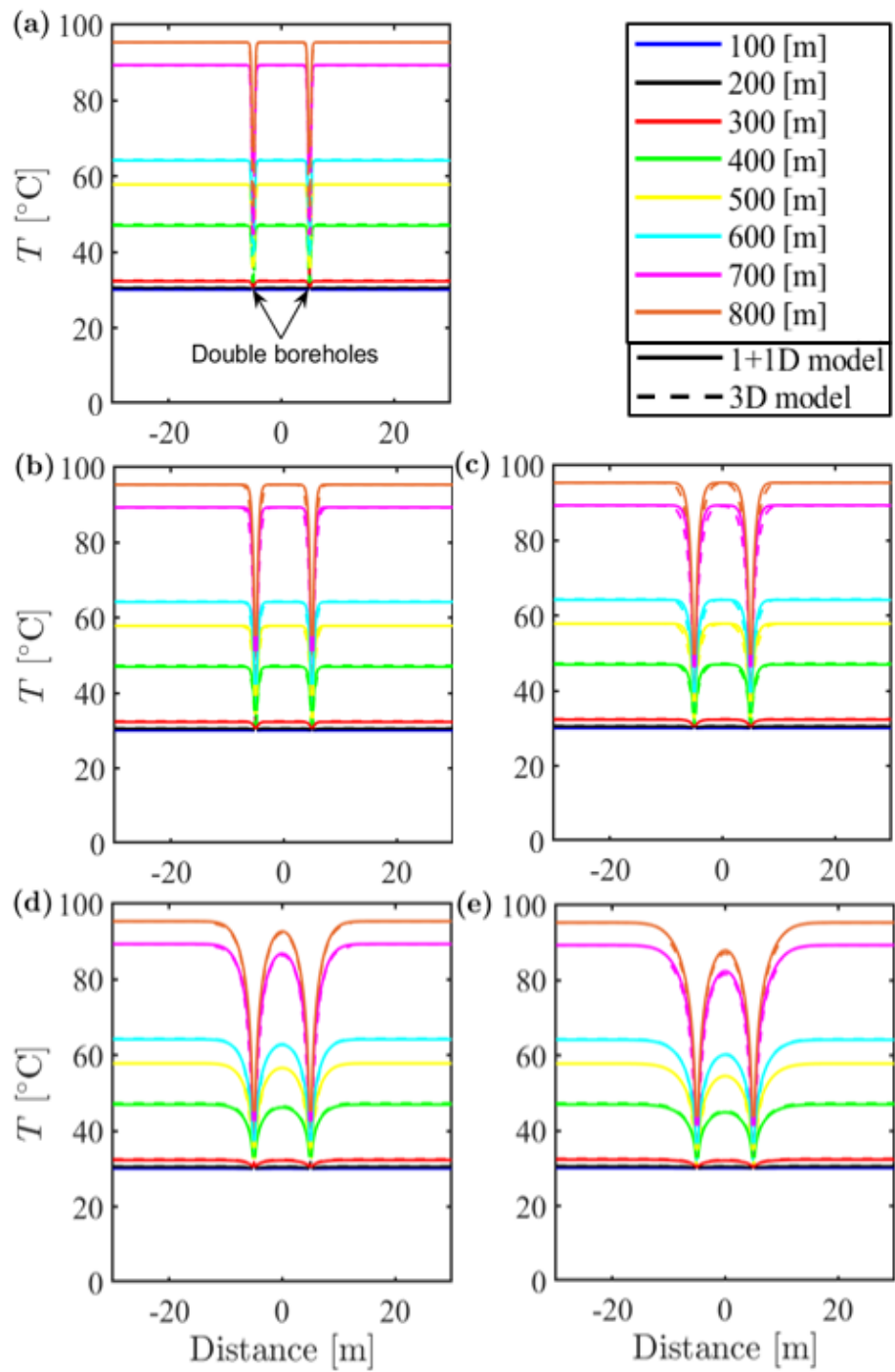


Figure 5.7: Temperature profile of the double boreholes solutions at: (a) 1 day; (b) 1 week; (c) 1 month; (d) 6 months; and (e) 1 year.

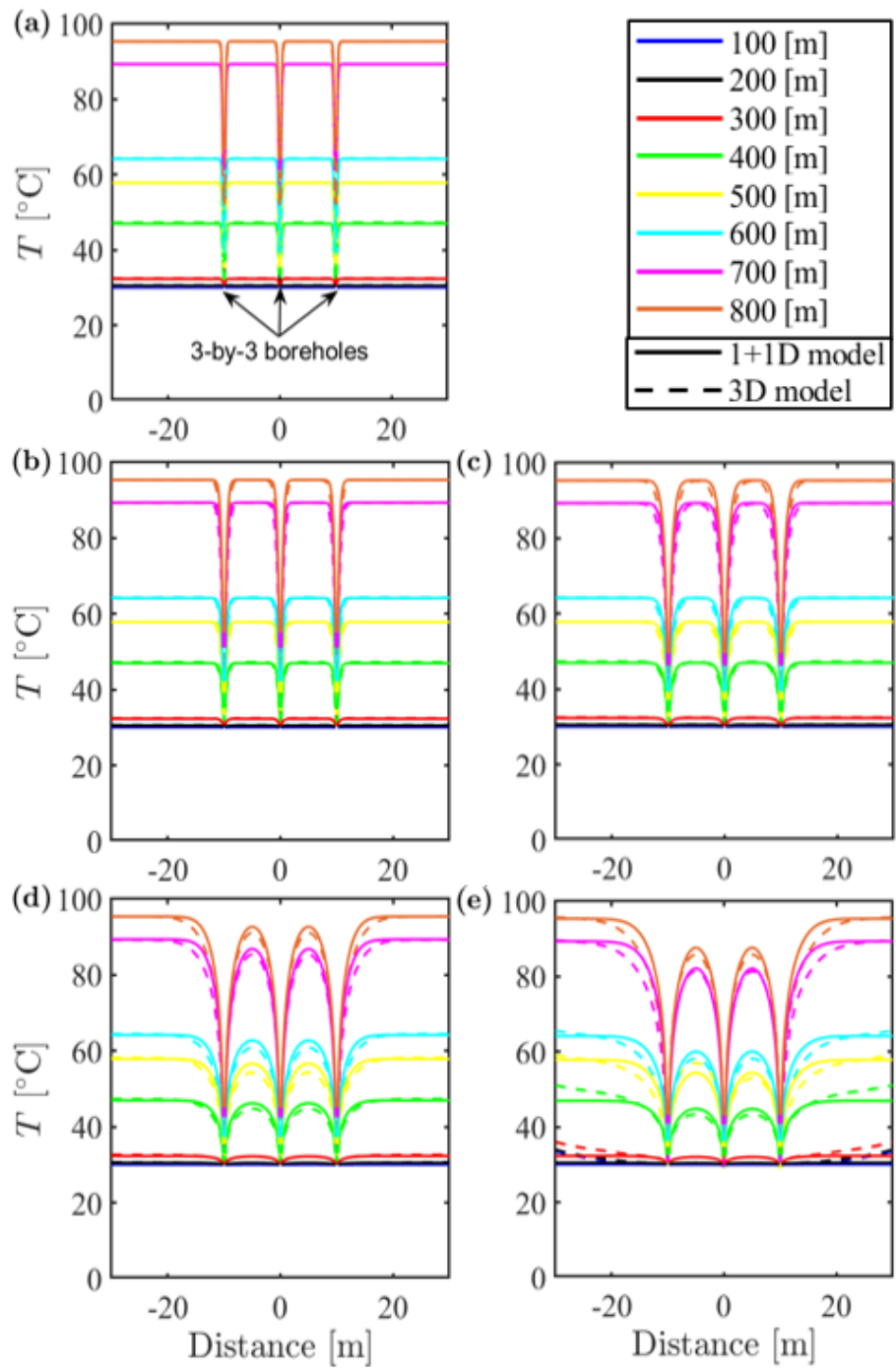


Figure 5.8: Temperature profile of the 3-by-3 boreholes solutions at: (a) 1 day; (b) 1 week; (c) 1 month; (d) 6 months; and (e) 1 year.

References

- [1] V. Masson-Delmotte, P. Zhai, A. Pirani, S. L. Connors, C. Péan, S. Berger, N. Caud, Y. Chen, L. Goldfarb, M. I. Gomis, M. Huang, K. Leitzell, E. Lonnoy, J. B. R. Matthews, T. K. Maycock, T. Waterfield, O. Yelekçi, R. Yu, and B. Zhou (eds.). Climate change 2021: The physical science basis. contribution of working group 1 to the sixth assessment report of the intergovernmental panel on climate change. 2021.
- [2] Tomasz Kujawa, Wladyslaw Nowak, and Aleksander A Stachel. Utilization of existing deep geological wells for acquisitions of geothermal energy. In *Thermal Sciences 2004. Proceedings of the ASME-ZSIS International Thermal Science Seminar II*. Begel House Inc., 2004.
- [3] Koji Morita, Warren S Bollmeier, and Husanobu Mizogami. Analysis of the results from the downhole coaxial heat exchanger (DCHE) experiment in Hawaii. *Transactions - Geothermal Resources Council*, 1992.
- [4] Sharon WY Cheng, Jundika C Kurnia, Seyed Ali Ghoreishi-Madiseh, and Agus P Sasmito. Optimization of geothermal energy extraction from abandoned oil well with a novel well bottom curvature design utilizing taguchi method. *Energy*, 188:116098, 2019.
- [5] Koji Morita, Warren S Bollmeier, and Husanobu Mizogami. An experiment to prove the concept of the downhole coaxial heat exchanger (DCHE) in Hawaii. *Transactions - Geothermal Resources Council*, 16:9–16, 1992.

- [6] JD Templeton, SA Ghoreishi-Madiseh, F Hassani, and MJ Al-Khawaja. Abandoned petroleum wells as sustainable sources of geothermal energy. *Energy*, 70:366–373, 2014.
- [7] Chao Li, Yanling Guan, Ruitao Yang, Xiong Lu, Wenxue Xiong, and Anjie Long. Effect of inner pipe type on the heat transfer performance of deep-buried coaxial double-pipe heat exchangers. *Renewable Energy*, 145:1049–1060, 2020.
- [8] Theo Renaud, Patrick Verdin, and Gioia Falcone. Numerical simulation of a deep borehole heat exchanger in the krafla geothermal system. *International Journal of Heat and Mass Transfer*, 143:118496, 2019.
- [9] Xincheng Hu, Jonathan Banks, Linping Wu, and Wei Victor Liu. Numerical modeling of a coaxial borehole heat exchanger to exploit geothermal energy from abandoned petroleum wells in hinton, alberta. *Renewable Energy*, 148:1110–1123, 2020.
- [10] Liang Fang, Nairen Diao, Zhukun Shao, Ke Zhu, and Zhaohong Fang. A computationally efficient numerical model for heat transfer simulation of deep borehole heat exchangers. *Energy and Buildings*, 167:79–88, 2018.
- [11] Xiaohui Yu, Hongwei Li, Sheng Yao, Vilhjalmur Nielsen, and Alfred Heller. Development of an efficient numerical model and analysis of heat transfer performance for borehole heat exchanger. *Renewable Energy*, 152:189–197, 2020.
- [12] Ahmad F Zueter, Minghan Xu, Mahmoud A Alzoubi, and Agus P Sasmito. Development of conjugate reduced-order models for selective artificial ground freezing: Thermal and computational analysis. *Applied Thermal Engineering*, 190:116782, 2021.
- [13] Ahmad Zueter, Ali Madiseh, Ferri Hassani, and Agus Pulung Sasmito. Effect of freeze pipe eccentricity in selective artificial ground freezing applications. *Journal of Thermal Science and Engineering Applications*, pages 1–33, 2021.

- [14] Jin Luo, Haifeng Zhao, Jia Jia, Wei Xiang, Joachim Rohn, and Philipp Blum. Study on operation management of borehole heat exchangers for a large-scale hybrid ground source heat pump system in china. *Energy*, 123:340–352, 2017.
- [15] Tomislav Kurevija, Domagoj Vulin, and Vedrana Krapec. Effect of borehole array geometry and thermal interferences on geothermal heat pump system. *Energy Conversion and Management*, 60:134–142, 2012.
- [16] Ahmet Gultekin, Murat Aydin, and Altug Sisman. Thermal performance analysis of multiple borehole heat exchangers. *Energy Conversion and Management*, 122:544–551, 2016.
- [17] Guang Jin, Zheng Li, Shaopeng Guo, Xuan Wu, Wenfei Wu, and Kai Zhang. Thermal performance analysis of multiple borehole heat exchangers in multilayer geotechnical media. *Energy*, 209:118236, 2020.
- [18] Seyed Ali Ghoreishi-Madiseh, Ali Fahrettin Kuyuk, and Marco Antonio Rodrigues de Brito. An analytical model for transient heat transfer in ground-coupled heat exchangers of closed-loop geothermal systems. *Applied Thermal Engineering*, 150:696–705, 2019.
- [19] Mohammed A Hefni, Minghan Xu, Ferri Hassani, Seyed Ali Ghoreishi-Madiseh, Haitham M Ahmed, Hussein A Saleem, Hussin AM Ahmed, Gamal SA Hassan, Khaled I Ahmed, and Agus P Sasmito. An analytical model for transient heat transfer with a time-dependent boundary in solar-and waste-heat-assisted geothermal borehole systems: From single to multiple boreholes. *Applied Sciences*, 11(21):10338, 2021.

Chapter 6

Concluding Remarks

Contents

| | | |
|-----|---|-----|
| 6.1 | Final conclusion | 99 |
| 6.2 | Recommendations for future work | 100 |

6.1 Final conclusion

This thesis discussed how conjugate porous media configuration could be utilized within engineering practice, such as for mine ventilation network (MVN) and geothermal heat exchanger (GHE) applications. Additionally, the development of the reduced-order computational fluid dynamics (CFD) model is also discussed due to the realization of the high computational cost while numerically investigating such models. This thesis's framework comprises the development of a two-dimensional (2D) and three-dimensional (3D) numerical model that analyses the heat transfer mechanism and fluid flow through porous media. Later, a one-plus-one-dimensional (1+1D) model is developed to reduce the computational cost and time.

In the beginning, a literature review that discusses step-by-step information included in the thesis is presented. The review highlighted the numerical methods of heat transfer and fluid flow start from a general concept of the governing equations until developing a reduced-order model. This was followed by an overview of the heat transfer mechanism and fluid flow through porous media, particularly in the MVN and GHE systems.

The following chapter discusses the airflow through the broken rock-filled drawpoint in an underground mine. This was accomplished by comparing the results from 1D-MVN software compiled with the novel friction factor correlation for porous media against the 3D CFD solver. The comparison between both models indicates a good agreement was made between both models and was considered verified. Thus, using the novel analytical friction factor to analyze the flow through porous media in 1D-MVN software is feasible. This result may assist mine ventilation engineers to model airflow through broken rock formation inside the underground mine efficiently.

The next chapter discussed the utilization of the porous media in enhancing the performance of the double-pipe geothermal heat exchanger (DPGHE) system. This study proposed the concept of novel semi closed-loop DPGHE with a fractured zone at the bottom of the well. By hydraulic fracturing the zone below the DPGHE, a tree-like fractal

network model is formed as a fractured zone below the well. With the proposed model, the heat performance of a DPGHE system is significantly increased due to the additional heat transfer mechanism in the fractured zone. The results suggest that by comparing the proposed model with the traditional closed-loop heat exchange, the heat extraction rate might increase by 48-144% and the pumping power elevated by 25-35% based on the fractured zone configurations.

A solution for the heavy computational requirement from the two previous works in the later chapter is provided. On the DPGHE application, a reduced-order 1+1D model is developed. A thermal superposition algorithm is also coupled to extend the single borehole solution into double and multiple boreholes solutions. Using a space marching algorithm to reduce the 2D axisymmetric model into several 1D gridlines resulted in a more simplified model. Thus, the computational time of the proposed model is 99% faster to simulate than the 3D CFD while keeping a similar accuracy. A wide range of parametric analyses for design optimization with the proposed model could be done more easily.

6.2 Recommendations for future work

Geothermal heat as renewable energy has many benefits and has to be utilized as effectively as possible; therefore, the continuation of studies on this topic is essential. For further work, an experimental investigation of lab- or field-scale may be undertaken to analyze the feasibility and the techno-economics of the proposed DPGHE model which was discussed in Chapter 4. By setting up the experimental facility, a variety of analyses could be done experimentally. Additionally, with the proposed computationally-efficient 1+1D model introduced in Chapter 5, both methods could work mutually. Moreover, the 1+1D model could be coupled with solar thermal models for further energy utilization.

Bibliography

- [1] PH Agson-Gani, L Amiri, SA Ghoreishi Madiseh, S Poncet, FP Hassani, and AP Sasmito. Integration of conjugate porous media model into mine ventilation network software. In *Mine Ventilation*, pages 47–55. CRC Press, 2021.
- [2] Ekkehard O Holzbecher. *Modeling density-driven flow in porous media: principles, numerics, software*. Springer Science & Business Media, 1998.
- [3] Koji Morita, Warren S Bollmeier, and Husanobu Mizogami. An experiment to prove the concept of the downhole coaxial heat exchanger (dche) in hawaii. 1992.
- [4] Koji Morita, Warren S Bollmeier, and Husanobu Mizogami. Analysis of the results from the downhole coaxial heat exchanger (dche) experiment in hawaii. 1992.
- [5] Suhas V Patankar. *Numerical heat transfer and fluid flow*. CRC press, 2018.
- [6] V. Masson-Delmotte, P. Zhai, A. Pirani, S. L. Connors, C. Péan, S. Berger, N. Caud, Y. Chen, L. Goldfarb, M. I. Gomis, M. Huang, K. Leitzell, E. Lonnoy, J. B. R. Matthews, T. K. Maycock, T. Waterfield, O. Yelekçi, R. Yu, and B. Zhou (eds.). *Climate change 2021: The physical science basis. contribution of working group 1 to the sixth assessment report of the intergovernmental panel on climate change*. 2021.
- [7] Chao Li, Yanling Guan, Ruitao Yang, Xiong Lu, Wenxue Xiong, and Anjie Long. Effect of inner pipe type on the heat transfer performance of deep-buried coaxial double-pipe heat exchangers. *Renewable Energy*, 145:1049–1060, 2020.

- [8] Sharon WY Cheng, Jundika C Kurnia, Seyed Ali Ghoreishi-Madiseh, and Agus P Sasmito. Optimization of geothermal energy extraction from abandoned oil well with a novel well bottom curvature design utilizing taguchi method. *Energy*, 188:116098, 2019.
- [9] Theo Renaud, Patrick Verdin, and Gioia Falcone. Numerical simulation of a deep borehole heat exchanger in the krafla geothermal system. *International Journal of Heat and Mass Transfer*, 143:118496, 2019.
- [10] Xincheng Hu, Jonathan Banks, Linping Wu, and Wei Victor Liu. Numerical modeling of a coaxial borehole heat exchanger to exploit geothermal energy from abandoned petroleum wells in hinton, alberta. *Renewable Energy*, 148:1110–1123, 2020.
- [11] Liang Fang, Nairen Diao, Zhukun Shao, Ke Zhu, and Zhaohong Fang. A computationally efficient numerical model for heat transfer simulation of deep borehole heat exchangers. *Energy and Buildings*, 167:79–88, 2018.
- [12] Xiaohui Yu, Hongwei Li, Sheng Yao, Vilhjalmur Nielsen, and Alfred Heller. Development of an efficient numerical model and analysis of heat transfer performance for borehole heat exchanger. *Renewable Energy*, 152:189–197, 2020.
- [13] Ahmad F Zueter, Minghan Xu, Mahmoud A Alzoubi, and Agus P Sasmito. Development of conjugate reduced-order models for selective artificial ground freezing: Thermal and computational analysis. *Applied Thermal Engineering*, 190:116782, 2021.
- [14] Henry Darcy. *Les fontaines publiques de la ville de Dijon: exposition et application...* Victor Dalmont, 1856.
- [15] Donald A Nield, Adrian Bejan, et al. *Convection in porous media*, volume 3. Springer, 2006.

- [16] R Rhodes Trussell and Melissa Chang. Review of flow through porous media as applied to head loss in water filters. *Journal of Environmental Engineering*, 125(11):998–1006, 1999.
- [17] Maasoud Kaviany. *Principles of heat transfer in porous media*. Springer Science & Business Media, 2012.
- [18] NeT Burdine. Relative permeability calculations from pore size distribution data. *Journal of Petroleum Technology*, 5(03):71–78, 1953.
- [19] Philipp Forchheimer. Wasserbewegung durch boden. *Z. Ver. Deutsch, Ing.*, 45:1782–1788, 1901.
- [20] S Majid Hassanizadeh and William G Gray. High velocity flow in porous media. *Transport in porous media*, 2(6):521–531, 1987.
- [21] Jacob Bear. *Dynamics of fluids in porous media*. Courier Corporation, 2013.
- [22] Jules Dupuit. *Études théoriques et pratiques sur le mouvement des eaux dans les canaux découverts et à travers les terrains perméables: avec des considérations relatives au régime des grandes eaux, au débouché à leur donner, et à la marche des alluvions dans les rivières à fond mobile*. Dunod, 1863.
- [23] Nihad Dukhan, Özer Bağcı, and Mustafa Özdemir. Experimental flow in various porous media and reconciliation of forchheimer and ergun relations. *Experimental Thermal and Fluid Science*, 57:425–433, 2014.
- [24] M King Hubbert. Darcy’s law and the field equations of the flow of underground fluids. *Transactions of the AIME*, 207(01):222–239, 1956.
- [25] Stephen Whitaker. Simultaneous heat, mass, and momentum transfer in porous media: a theory of drying. In *Advances in heat transfer*, volume 13, pages 119–203. Elsevier, 1977.

- [26] Kambiz Vafai and Chang L Tien. Boundary and inertia effects on flow and heat transfer in porous media. *International Journal of Heat and Mass Transfer*, 24(2):195–203, 1981.
- [27] M Quintard, M Kaviany, and S Whitaker. Two-medium treatment of heat transfer in porous media: numerical results for effective properties. *Advances in water resources*, 20(2-3):77–94, 1997.
- [28] C Özgen Karacan. Modeling and prediction of ventilation methane emissions of us longwall mines using supervised artificial neural networks. *International Journal of Coal Geology*, 73(3-4):371–387, 2008.
- [29] Malcolm J McPherson. *Subsurface ventilation and environmental engineering*. Springer Science & Business Media, 2012.
- [30] Lu Yueze, Saad Akhtar, Agus P Sasmito, and Jundika C Kurnia. Prediction of air flow, methane, and coal dust dispersion in a room and pillar mining face. *International Journal of Mining Science and Technology*, 27(4):657–662, 2017.
- [31] Dong Ma, Botao Qin, Lin Li, Ang Gao, and Yuan Gao. Study on the methane explosion regions induced by spontaneous combustion of coal in longwall gobs using a scaled-down experiment set-up. *Fuel*, 254:115547, 2019.
- [32] Michel J-G Sylvestre. Heating and ventilation study of inco’s creighton mine. 1999.
- [33] Seyed Ali Ghoreishi-Madiseh, Agus P Sasmito, Ferri P Hassani, and Leyla Amiri. Performance evaluation of large scale rock-pit seasonal thermal energy storage for application in underground mine ventilation. *Applied Energy*, 185:1940–1947, 2017.
- [34] Leyla Amiri, Seyed Ali Ghoreishi-Madiseh, Ferri P Hassani, and Agus P Sasmito. Friction factor correlation for airflow through broken rocks and its applications in mine ventilation. *International Journal of Mining Science and Technology*, 30(4):455–462, 2020.

- [35] SA Ghoreishi-Madiseh, FP Hassani, A Mohammadian, and PH Radziszewski. A transient natural convection heat transfer model for geothermal borehole heat exchangers. *Journal of Renewable and Sustainable Energy*, 5(4):043104, 2013.
- [36] LL Sloss. Assessing and managing spontaneous combustion of coal. *IEA Clean Coal Centre*, 2015.
- [37] Leyla Amiri, Seyed Ali Ghoreishi-Madiseh, Ferri P Hassani, and Agus P Sasmito. Estimating pressure drop and ergun/forchheimer parameters of flow through packed bed of spheres with large particle diameters. *Powder Technology*, 356:310–324, 2019.
- [38] Jarosław Brodny and Magdalena Tutak. Applying computational fluid dynamics in research on ventilation safety during underground hard coal mining: A systematic literature review. *Process Safety and Environmental Protection*, 2021.
- [39] Ting Xiang Ren and JS Edwards. Three-dimensional computational fluid dynamics modelling of methane flow through permeable strata around a longwall face. *Mining technology*, 109(1):41–48, 2000.
- [40] Liming Yuan and Alex C Smith. Numerical study on effects of coal properties on spontaneous heating in longwall gob areas. *Fuel*, 87(15-16):3409–3419, 2008.
- [41] Jian-rang Zhang, Chun-qiao Wang, and Ding-wen Dong. Numerical simulation study of gob air leakage field and gas migration regularity in downlink ventilation. *Journal of Coal Science and Engineering (China)*, 17(3):316–320, 2011.
- [42] Yunzhuo Li, Hetao Su, Huaijun Ji, and Wuyi Cheng. Numerical simulation to determine the gas explosion risk in longwall goaf areas: A case study of xutuan colliery. *International Journal of Mining Science and Technology*, 30(6):875–882, 2020.
- [43] Jian Zhang, Jingyu An, Zhihui Wen, Kaixuan Zhang, Rongkun Pan, and Nahid Akter Al Mamun. Numerical investigation of coal self-heating in longwall goaf consid-

- ering airflow leakage from mining induced crack. *Process Safety and Environmental Protection*, 134:353–370, 2020.
- [44] Saqib Ahmad Saki, Jürgen F Brune, and Muhammad Usman Khan. Optimization of gob ventilation boreholes design in longwall mining. *International Journal of Mining Science and Technology*, 30(6):811–817, 2020.
- [45] Gabriel S Esterhuizen and C Ozgen Karacan. A methodology for determining gob permeability distributions and its application to reservoir modeling of coal mine longwalls. 2007.
- [46] Jian Zhang, Hongtu Zhang, Ting Ren, Jianping Wei, and Yuntao Liang. Proactive inertisation in longwall goaf for coal spontaneous combustion control-a CFD approach. *Safety science*, 113:445–460, 2019.
- [47] Rao Balusu, Patrick Humpries, Paul Harrington, Michael Wendt, and Sheng Xue. Optimum inertisation strategies. *The QCO/DME Coal Industry Safety Conference*, page 7, 2002.
- [48] Ting Xiang Ren, Rao Balusu, and Patrick Humphries. Development of innovative goaf inertisation practices to improve coal mine safety. 2005.
- [49] Ting Xiang Ren and Rao Balusu. Proactive goaf inertisation for controlling longwall goaf heatings. *Procedia Earth and Planetary Science*, 1(1):309–315, 2009.
- [50] Ting Ren and Rao Balusu. The use of CFD modelling as a tool for solving mining health and safety problems. 2010.
- [51] Yingke Liu, Sihua Shao, Xinxin Wang, Lipeng Chang, Guanglei Cui, and Fubao Zhou. Gas flow analysis for the impact of gob gas ventholes on coalbed methane drainage from a longwall gob. *Journal of Natural Gas Science and Engineering*, 36:1312–1325, 2016.

- [52] Xiaowei Li, Chaojie Wang, Yujia Chen, Jun Tang, and Yawei Li. Design of gas drainage modes based on gas emission rate in a gob: a simulation study. *Arabian Journal of Geosciences*, 11(16):1–12, 2018.
- [53] Ting Xiang Ren. CFD modelling of longwall goaf gas flow to improve gas capture and prevent goaf self-heating. *Journal of Coal Science and Engineering (China)*, 15(3):225–228, 2009.
- [54] Kayode M Ajayi, Khosro Shahbazi, Purushotham Tukkaraja, and Kurt Katzenstein. Prediction of airway resistance in panel cave mines using a discrete and continuum model. *International Journal of Mining Science and Technology*, 29(5):781–784, 2019.
- [55] Zhongwei Wang, Ting Ren, Liqiang Ma, and Jian Zhang. Investigations of ventilation airflow characteristics on a longwall face—a computational approach. *Energies*, 11(6):1564, 2018.
- [56] Y Pan, R Bhargava, A Jha, P Tukkaraja, K Shahbazi, K Katzenstein, and D Loring. An investigation of the effects of particle size, porosity, and cave size on the airflow resistance of a block/panel cave. In *Proceedings of the 11th International Mine Ventilation Congress*, pages 82–91. Springer, 2019.
- [57] Ang Liu, Shimin Liu, Gang Wang, and Derek Elsworth. Predicting fugitive gas emissions from gob-to-face in longwall coal mines: Coupled analytical and numerical modeling. *International Journal of Heat and Mass Transfer*, 150:119392, 2020.
- [58] Monique De Moel, Peter M Bach, Abdelmalek Bouazza, Rao M Singh, and JingLiang O Sun. Technological advances and applications of geothermal energy pile foundations and their feasibility in australia. *Renewable and Sustainable Energy Reviews*, 14(9):2683–2696, 2010.
- [59] Baldur Lindal. Industrial and other applications of geothermal energy. *Geothermal energy*, pages 135–148, 1973.

- [60] Tomasz Kujawa, Wladyslaw Nowak, and Aleksander A Stachel. Utilization of existing deep geological wells for acquisitions of geothermal energy. In *Thermal Sciences 2004. Proceedings of the ASME-ZSIS International Thermal Science Seminar II*. Begel House Inc., 2004.
- [61] JD Templeton, SA Ghoreishi-Madiseh, F Hassani, and MJ Al-Khawaja. Abandoned petroleum wells as sustainable sources of geothermal energy. *Energy*, 70:366–373, 2014.
- [62] Xianbiao Bu, Weibin Ma, and Huashan Li. Geothermal energy production utilizing abandoned oil and gas wells. *Renewable energy*, 41:80–85, 2012.
- [63] Seyed Ali Ghoreishi-Madiseh, Ali Fahrettin Kuyuk, and Marco Antonio Rodrigues de Brito. An analytical model for transient heat transfer in ground-coupled heat exchangers of closed-loop geothermal systems. *Applied Thermal Engineering*, 150:696–705, 2019.
- [64] MK Alkam and MA Al-Nimr. Improving the performance of double-pipe heat exchangers by using porous substrates. *International Journal of Heat and Mass Transfer*, 42(19):3609–3618, 1999.
- [65] Jiliang Chen and Fangming Jiang. Designing multi-well layout for enhanced geothermal system to better exploit hot dry rock geothermal energy. *Renewable Energy*, 74:37–48, 2015.
- [66] P Olasolo, MC Juárez, MP Morales, IA Liarte, et al. Enhanced geothermal systems (egs): A review. *Renewable and Sustainable Energy Reviews*, 56:133–144, 2016.
- [67] Shyi-Min Lu. A global review of enhanced geothermal system (egs). *Renewable and Sustainable Energy Reviews*, 81:2902–2921, 2018.
- [68] Mohamad Omid, Mousa Farhadi, and Mohamad Jafari. A comprehensive review on double pipe heat exchangers. *Applied Thermal Engineering*, 110:1075–1090, 2017.

- [69] Hannes Hofmann, Guido Blöcher, Nele Börsing, Nico Maronde, Nicole Pastrik, and Günter Zimmermann. Potential for enhanced geothermal systems in low permeability limestones—stimulation strategies for the western malm karst (bavaria). *Geothermics*, 51:351–367, 2014.
- [70] Xianzhi Song, Yu Shi, Gensheng Li, Ruiyue Yang, Gaosheng Wang, Rui Zheng, Jiacheng Li, and Zehao Lyu. Numerical simulation of heat extraction performance in enhanced geothermal system with multilateral wells. *Applied energy*, 218:325–337, 2018.
- [71] Gaosheng Wang, Xianzhi Song, Yu Shi, Ruiyue Yang, Feixue Yulong, Rui Zheng, and Jiacheng Li. Heat extraction analysis of a novel multilateral-well coaxial closed-loop geothermal system. *Renewable Energy*, 163:974–986, 2021.
- [72] Yu Shi, Xianzhi Song, Gaosheng Wang, Jiacheng Li, Lidong Geng, and Xiaojiang Li. Numerical study on heat extraction performance of a multilateral-well enhanced geothermal system considering complex hydraulic and natural fractures. *Renewable Energy*, 141:950–963, 2019.
- [73] Boming Yu. Analysis of flow in fractal porous media. *Applied Mechanics Reviews*, 61(5), 2008.
- [74] Jianchao Cai, Liehui Zhang, and Wei Wei. *Modelling of flow and transport in fractal porous media*. Elsevier, 2021.
- [75] Boming Yu and Jianhua Li. Some fractal characters of porous media. *Fractals*, 9(03):365–372, 2001.
- [76] Jinsui Wu and Boming Yu. A fractal resistance model for flow through porous media. *International journal of heat and mass transfer*, 50(19-20):3925–3932, 2007.
- [77] Jinsui Wu, Boming Yu, and Meijuan Yun. A resistance model for flow through porous media. *Transport in Porous Media*, 71(3):331–343, 2008.

- [78] GA Ledezma, A Bejan, and MR Errera. Constructal tree networks for heat transfer. *Journal of Applied Physics*, 82(1):89–100, 1997.
- [79] Adrian Bejan. *Shape and structure, from engineering to nature*. Cambridge university press, 2000.
- [80] Peng Xu, Agus Pulung Sasmito, Boming Yu, and Arun Sadashiv Mujumdar. Transport phenomena and properties in treelike networks. *Applied Mechanics Reviews*, 68(4), 2016.
- [81] Peng Xu, Boming Yu, Shuxia Qiu, and Jianchao Cai. An analysis of the radial flow in the heterogeneous porous media based on fractal and constructal tree networks. *Physica A: Statistical Mechanics and its Applications*, 387(26):6471–6483, 2008.
- [82] Tongjun Miao, Shanshan Yang, Zhangcai Long, and Boming Yu. Fractal analysis of permeability of dual-porosity media embedded with random fractures. *International Journal of Heat and Mass Transfer*, 88:814–821, 2015.
- [83] Peng Xu, Cuihong Li, Shuxia Qiu, and Agus Pulung Sasmito. A fractal network model for fractured porous media. *Fractals*, 24(02):1650018, 2016.
- [84] Maciej Z Lukawski, Rachel L Silverman, and Jefferson W Tester. Uncertainty analysis of geothermal well drilling and completion costs. *Geothermics*, 64:382–391, 2016.
- [85] Agus P Sasmito, Erik Birgersson, Hung C Ly, and Arun S Mujumdar. Some approaches to improve ventilation system in underground coal mines environment—a computational fluid dynamic study. *Tunnelling and Underground Space Technology*, 34:82–95, 2013.
- [86] Ahmad Zueter, Aurelien Nie-Rouquette, Mahmoud A Alzoubi, and Agus P Sasmito. Thermal and hydraulic analysis of selective artificial ground freezing using air insulation: Experiment and modeling. *Computers and Geotechnics*, 120:103416, 2020.

- [87] John A Wheeler and Eugene H Wissler. The friction factor–reynolds number relation for the steady flow of pseudoplastic fluids through rectangular ducts. part i. theory. *AIChE Journal*, 11(2):207–212, 1965.
- [88] Jin Luo, Haifeng Zhao, Jia Jia, Wei Xiang, Joachim Rohn, and Philipp Blum. Study on operation management of borehole heat exchangers for a large-scale hybrid ground source heat pump system in china. *Energy*, 123:340–352, 2017.
- [89] Tomislav Kurevija, Domagoj Vulin, and Vedrana Krapec. Effect of borehole array geometry and thermal interferences on geothermal heat pump system. *Energy Conversion and Management*, 60:134–142, 2012.
- [90] Ahmet Gultekin, Murat Aydin, and Altug Sisman. Thermal performance analysis of multiple borehole heat exchangers. *Energy Conversion and Management*, 122:544–551, 2016.
- [91] Guang Jin, Zheng Li, Shaopeng Guo, Xuan Wu, Wenfei Wu, and Kai Zhang. Thermal performance analysis of multiple borehole heat exchangers in multilayer geotechnical media. *Energy*, 209:118236, 2020.